Abnormality Detection Methods for Utility Equipment Condition Monitoring

by

Benzhe Li

A thesis submitted in partial fulfillment of the requirements for the degree of

Master of Science

in

Energy Systems

Department of Electrical and Computer Engineering

University of Alberta

Abstract

The wide spread use of power quality monitoring tools in recent years has enabled utility companies to extract non-power-quality information from the power quality monitoring data. A high potential use of such data is the equipment condition monitoring. General purpose detection method for waveform abnormality is considered as an important step for data analytics based equipment condition monitoring.

Two general purpose detection methods are proposed in this thesis. The first one is a modified detection method based on existing scheme, where segment RMS values of differential waveform and half-cycle refreshed RMS values of original waveform are used as features for the detection. The second method is based on statistical characteristics of current signals, where abnormalities are detected by comparing the statistical distributions of waveform variations with and without disturbances. Current waveform is used for the detection since they are more sensitive to equipment conditions than voltage waveform. An automatic threshold selection scheme is adopted in the detection method. In addition, as hard binary detection can sometimes lead to large error especially for boundary situations, a soft detection scheme is proposed which returns soft detection results. The soft detection scheme can reduce the number of missing

events compared with binary detection methods. Moreover, the detection value provides reference for severity of a certain abnormal event.

Preface

This thesis makes contributions in the area of abnormality detection for equipment condition monitoring.

After summarizing the signatures of equipment failures and existing methods for abnormality detection, a novel statistics based generic abnormality detection method is proposed. This statistics based method in Chapter 3 has been published as: Benzhe Li, Yindi Jing, and Wilsun Xu, "A Generic Waveform Abnormality Detection Method for Utility Equipment Condition Monitoring," *IEEE Transactions on Power Delivery*, DOI: 10.1109/TPWRD.2016.2580663, 2016. With the general detection idea proposed by Prof. Yindi Jing, I further developed the method, carried out the data analysis, verification and drafted the manuscript. Prof. Yindi Jing and Prof. Wilsun Xu further revised the manuscript and supervised the whole work.

Acknowledgements

I really appreciate Professor Wilsun Xu and Professor Yindi Jing for their guidance and help during my MSc program. The knowledge and attitude toward research I have learned from them will significantly benefit my future careers.

Many thanks to all the students in PDS-Lab for their help and company: Yu Tian, Qingxin Shi, Pengfei Gao, Tianyu Ding, Yang Wang, Xin Li, Bing Xia, Kunlong Chen, Wenhai Zhang, Yaxiang Zhou, Juncheng Wang, Wenrui Wu, and Tianyi Hou.

I want to express my gratitude to my parents Mr. Daru Li and Ms. Shunying Fu. Their love and support really means a lot to me.

Contents

1 Introduction **1**

1.1 Overview of Power Quality Data Analytics Based Equipment Condition Monitoring 2

1.2 Signatures of Power Quality Disturbances 3

1.3 Signatures of Equipment Failure Disturbances 6

1.3.1 Cable Failures 7

1.3.2 Overhead Line Failures 14

1.3.3 Transformer Failures 18

1.3.4 Circuit Breaker Failures 20

1.3.5 Capacitor Failures 23

1.3.6 Lightning and Surge Arrester Failures 26

1.3.7 Summary and Motivation 27

1.4 Thesis Contribution and Organization 31

2 Existing Methods to Detect Waveform Abnormality and Proposed Modification **34**

2.1 Current Signature Based Methods 35

2.1.1 Fault Component Methods 35

2.1.2 Wavelet Analysis Methods 38

2.1.3 Fundamental Frequency Component Method 40

2.2 Voltage Signature Based Methods 41

2.2.1 Waveform Methods 42

2.2.2 Wavelet Analysis Method 43
2.3 Composite Method 44
2.4 Proposed Improved Method 45
2.4.1 Description of the Method 46
2.4.2 Test Results 53

3 Generic Waveform Abnormality Detection Method Based on Statistical Distribution 60

3.1 Hypothesis Testing Model for General Abnormality Detection . 62
3.1.1 Steady-State Components Estimation 64
3.1.2 Modelling of the Noise Component 67
3.2 Generic Abnormality Detection Scheme 69
3.2.1 Abnormality Detection Rule and Threshold Selection . . 69
3.2.2 Summary of the Proposed Detection Method 75
3.3 Performance of the Proposed Method 77
3.3.1 Discussions on Parameter Values 81
3.3.2 Performance of the Proposed Method With Field Data . 83
3.3.3 Performance of the Proposed Method With Simulated Data 86
3.3.4 Strength and Limitations of the Proposed Method 89
3.4 Summary 90

4 Soft Detection of Waveform Abnormality 92

4.1 Motivations for Soft Detection and Existing Literature 92
4.1.1 Motivations for Soft Detection 92
4.1.2 Review of Existing Literature on Soft Detection 93
4.2 Proposed Soft Detection Scheme 94
4.2.1 Selection of Membership Function 95
4.2.2 Determination of the Parameters of the S-shaped Function 97
4.2.3 Proposed Soft Detection Algorithm and Test Results . . 100
4.3 Summary and Discussion 102

5 Conclusions and Future Work **104**

5.1 Conclusions 104

5.2 Suggestion for Future Work 105

Bibliography **107**

A Positive-Going Zero Crossing Point Detection and Frequency Variation Correction **114**

A.1 Positive-Going Zero Crossing Point Detection 114

A.2 Frequency Variation Correction 115

B Sensitive Study and Performance Comparison Using Phase-B and Phase-C of Field Data **120**

List of Tables

1.1 Classification of power quality disturbances. 4

1.2 Basic indices to characterize power quality disturbances. 6

1.3 Two applications of disturbance data 30

2.1 Typical parameter values. 53

2.2 Measurement setup. 54

2.3 Thresholds used for abnormality detection. 54

2.4 Number of disturbances captured by using different features. . . 55

3.1 List of symbols used in algorithm description 62

3.2 Numbers of detected events per day. 85

3.3 Numbers of false alarms. 86

3.4 Simulation setup. 88

4.1 Number of missing events under soft and binary detection scheme.102

A.1 List of symbols used in frequency variation correction 117

List of Figures

1.1 Self-clearing incipient cable faults that lead to a permanent fault [4]. . . . 3
1.2 Signatures of voltage transients. . . . 4
1.3 Signatures of short variation disturbances (voltage signals). . . . 5
1.4 Waveform distortion and harmonics. . . . 5
1.5 Two instances of self-clearing incipient faults. . . . 8
1.6 Single incipient single-line-to-ground fault [6]. . . . 8
1.7 Multiple incipient single-line-to-ground fault [6]. . . . 9
1.8 Multiple incipient single-line-to-ground fault [9]. . . . 9
1.9 Self-clearing incipient cable fault lasting one and a half cycles [6]. 9
1.10 Incipients faults followed by a permanent fault [4]. . . . 10
1.11 Incipient and permanent faults of an underground cable [13]. . . 10
1.12 Incipient fault followed by a multi-cycle fault [6]. . . . 11
1.13 Underground cable failure incipient fault [6]. . . . 11
1.14 Voltage and current waveforms during an evolving cable failure [6]. . . . 12
1.15 Electrical waveforms during an underground PILC cable failure [6]. . . . 12
1.16 Incipient cable joint fault [6]. . . . 13
1.17 Incipient cable joint failure single-line-to-ground fault [6]. . . . 13
1.18 Underground cable joint failure waveform [6]. . . . 14
1.19 Underground cable termination failure [6]. . . . 14

1.20 First episode of a series of tree contact events from data of [14]. 15
1.21 Second episode of a series of tree contact events from data of [14]. 15
1.22 Third episode of a series of tree contact events from data of [14]. 16
1.23 Tree contact fault lasting for about one cycle [18]. 16
1.24 An arcing fault caused by tree contact [6]. 16
1.25 Fault caused by tree falling into customer triplex service [6]. . . 17
1.26 Tree contact causes primary to burn down [6]. 17
1.27 Zero current during load tap changer failure [19]. 18
1.28 RMS trends during recurrent faults [20]. 19
1.29 Example transformer bushing failure [6]. 20
1.30 Another example of transformer bushing failure [6]. 20
1.31 Electrical signatures during and after temporary faults [20]. . . . 21
1.32 Current waveform during arcing of a capacitor bank [6]. 22
1.33 Electrical waveforms of a capacitor de-energizing with restrike [24]. 23
1.34 Phase-A capacitor short circuit [25]. 24
1.35 Electrical signatures during Phase-B switch failure [25]. 25
1.36 Waveforms of a capacitor energized using synchronous closing control [24]. 25
1.37 Electrical signatures during Phase-B switch failure [26]. 27
1.38 Surge arrester failure fault waveform [6]. 27
1.39 A possible path for general-purpose condition monitoring scheme. 30

2.1 Illustration of the fundamental fault component method [8]. . . 37
2.2 Illustration of instantaneous fault component method. 38
2.3 Illustration of wavelet analysis method [9]. 40
2.4 Illustration of fundamental component method. 41
2.5 Wavelet transform of voltage transients [29]. 44
2.6 Detailed process of the proposed improved method. 46
2.7 Illustration of the proposed method to derive differential waveform. 48

2.8 Illustration of detection using waveform abnormality for the proposed method. 49
2.9 Illustration of detection using RMS value abnormality for the proposed method. 50
2.10 Output of disturbance detection procedure for the proposed method. 52
2.11 Measurement point and measured parameters. 54
2.12 Percentage of disturbances detected by using different features. . 55
2.13 Distribution of disturbances at different time. 55
2.14 Transients-case 1. 56
2.15 Transients-case 2. 56
2.16 Overcurrent-case 1. 57
2.17 Overcurrent-case 2. 57
2.18 Low-level current variation-case 1. 58
2.19 Low-level current variation-case 2. 58
2.20 Increase of current waveform distortion-case 1. 59
2.21 Increase of current waveform distortion-case 2. 59

3.1 Residuals under different cases. 67
3.2 Illustration of the proposed detection rule. 70
3.3 Comparison between histogram and kernel density estimation. . 72
3.4 False alarm probability v.s. different threshold values for the field test data. 75
3.5 Detection procedure. 76
3.6 Examples of abnormal events. 80
3.7 A typical normal event. 80
3.8 Detection performance for different N_d. 81
3.9 Detection performance for different N_G. 82
3.10 Detection performance for different N_h. 83

3.11 Performance comparison of the proposed method with the differential waveform RMS method and the MAVSA method with extracted events. 84
3.12 Results after applying the three methods to different signals. . . 85
3.13 An example of AMR signals. 86
3.14 Performance comparison of proposed method and differential waveform RMS method under different sampling frequencies. . . 88
3.15 Performance comparison of proposed method and MAVSA method under different sampling frequencies. 89

4.1 Detection flow chart for the soft detection in [44]. 93
4.2 General structure of the proposed soft detection scheme. 95
4.3 An illustrative example of membership function. 95
4.4 Typical membership functions [47][48]. 96
4.5 A linear membership function. 97
4.6 False alarm probability v.s. different threshold values for soft detection. 99
4.7 Procedure of the proposed soft detection scheme. 101
4.8 Two examples of missing events. 102
4.9 An example with severe abnormality. 102

A.1 Impact of frequency variation on sample locations 115
A.2 Parameters for frequency variation correction 116
A.3 Determining the value of $x'_{ref}(k)$ 119

B.1 Detection performance for different N_d derived with Phase-B and Phase-C data. 121
B.2 Detection performance for different N_G derived with Phase-B and Phase-C data. 121
B.3 Detection performance for different N_H derived with Phase-B and Phase-C data. 121

B.4 Detection performance comparison derived with Phase-B and Phase-C data. 122

List of Abbreviations

CT	current transformer
FFT	fast Fourier transform
KLD	Kullback-Leibler divergence
pdf	probability density function
PT	potential transformer
RMS	root-mean-square

Chapter 1

Introduction

In recent years, the wide use of power quality monitors and research advancements in power quality disturbance analysis has resulted in a new research field named power quality data analytics. Power quality data analytics targets at collecting waveform data in power systems, extracting useful information from it, and solving various power system problems based on the information. Utility equipment condition monitoring is an important branch of this field [1]. By detecting and identifying incipient failures or abnormal operations from voltage and current data, unhealthy condition of power equipment can be discovered and condition-based maintenance can be conducted in time to avoid catastrophic equipment failures. Some recent work on using power disturbance data for equipment condition monitoring can be found in [2, 3, 4, 5].

In this chapter, the background of power quality data analytics based utility equipment condition monitoring is provided. Then, the signatures of power equipment failures are discussed in comparison with those of the power quality disturbances. In addition, research needs for power quality data analytics based equipment condition monitoring are identified. Among these needs, a general purpose method to detect waveform abnormality is an important step. Finally, the thesis contributions and organization are presented.

1.1 Overview of Power Quality Data Analytics Based Equipment Condition Monitoring

Many equipment failures such as the arcing of a cable joint, restrike of a capacitor switch, and tree-contact by a power line can produce unique electrical signatures [4, 6]. These signatures can be observed from the voltage and current waveforms associated with the equipment. In recent years, engineers and researchers in the field of power quality, power system protection, and equipment testing have realized that useful information can be extracted from the waveforms for the purpose of equipment condition monitoring [1, 7]. In the field of power quality, for example, power quality monitors routinely collect power disturbance data. Some of the data do not indicate the existence of a power quality problem but they have been used to detect the presence of abnormal equipment operation in the system. Example incipient failure signatures of a cable is shown in the Figure 1.1[4].

How to analyze the waveform-type power disturbance data and extract information for purposes such as equipment condition monitoring have attracted a good interest from industry and academia recently [6, 7, 8, 9]. In view of the wide availability of power quality monitors and advancements in power quality disturbance analysis methods, the IEEE Power Quality Subcommittee formed a Working Group in 2013 to prompt the research, development and application of power quality data for purposes beyond traditional power quality concerns. The working group is named "Power Quality Data Analytics". Detecting equipment failures is one of the areas with significant potentials for power quality data analytics.

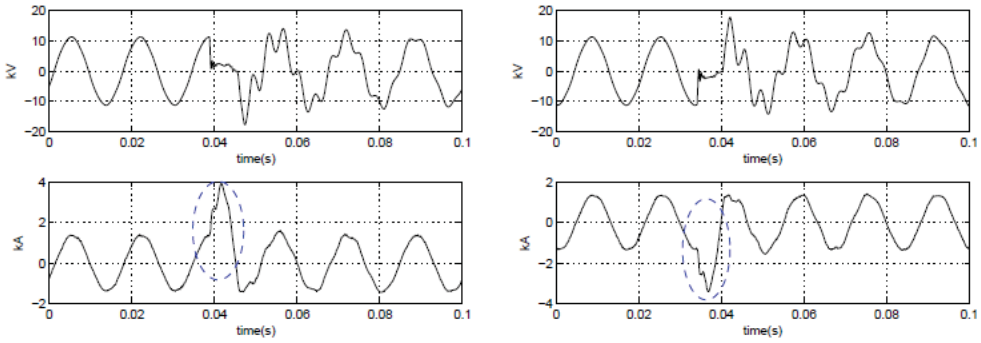

(a) Self-Clearing Fault on 2008-11-12 at 19:40 (b) Self-Clearing Fault on 2008-11-12 at 21:11

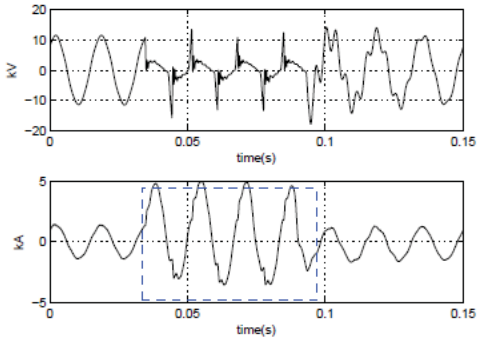

(c) Permanent Fault on 2008-11-14 at 15:51

Figure 1.1: Self-clearing incipient cable faults that lead to a permanent fault [4].

1.2 Signatures of Power Quality Disturbances

Before presenting the signatures of equipment failures, it is useful to have a brief overview of the signatures of power quality disturbances. Power quality disturbances are those electrical disturbances that lead to power quality problems. Equipment failure may or may not result in a disturbance of concern from the power quality perspective. The comparison of power quality disturbances and equipment failure disturbances can help us get a better understanding about challenges in detecting, characterizing and extracting useful information from the equipment failure disturbances.

Over the past 30 years, significant progresses have been made in the power

quality field [10]. There are consensus on definitions, characteristics, and indices of various power quality disturbances [10, 11]. Standards for disturbance detection and characterization have also been established. According to IEEE 1159-1995, power quality disturbances are classified as shown in Table 1.1. Sample signatures of the most common power quality disturbances are shown in Figure 1.2 to Figure 1.4.

Table 1.1: Classification of power quality disturbances.

Categories	Typical spectral content	Typical duration	Typical magnitude
1. Transients			
Impulsive Oscillatory	 0.5 MHz - 5 kHz	1 ns - 1 ms plus 5 us -50 ms	 0 - 8 pu
2. Short duration variations			
Interruptions Sags Swells		0.5 cycle- 1 min 0.5 cycle- 1 min 0.5 cycle- 1 min	< 0.1 pu 0.1 - 0.9 pu 1.1 - 1.8 pu
3. Long duration variations			
Sustained interruptions Under-voltages Over-voltages		>1 min >1 min >1 min	0.0 pu 0.8 - 0.9 pu 1.1 - 1.2 pu
4. Voltage fluctuations	<25Hz	Intermittent	0.1 - 7%
5. Power frequency variations		<10s	
6. Voltage imbalances		Steady state	0.5 - 2%
7. Waveform distortions	0 - 50th harmonics	Steady State	0 - 20%

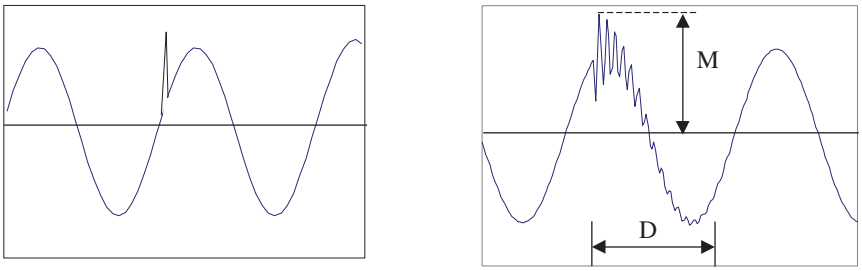

(a) Impulsive transients. (b) Oscillatory transients.

Figure 1.2: Signatures of voltage transients.

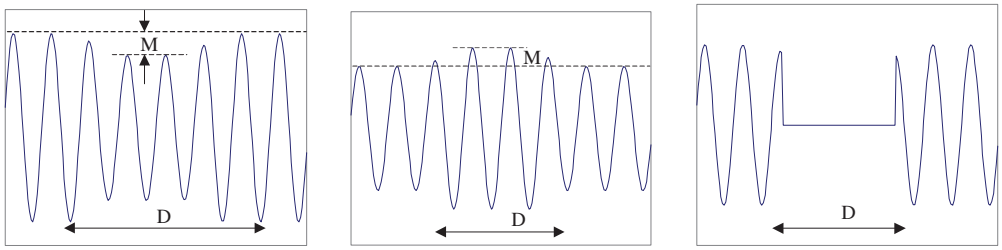

(a) Sag. (b) Swell. (c) Interuption.

Figure 1.3: Signatures of short variation disturbances (voltage signals).

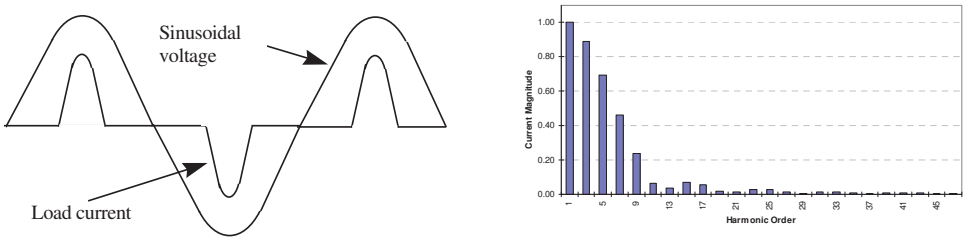

(a) Waveforms of voltage and current. (b) Harmonic spectrum of current waveform.

Figure 1.4: Waveform distortion and harmonics.

Power quality disturbances are characterized using indices that focus on the severity of a disturbance (see Table 1.2). For disturbances that occur as individual events (called transient disturbances in Table 1.2), the indices are magnitude and duration. For steady-state disturbances such as harmonics and voltage unbalance, magnitude is recognized as the only index. Disturbances that occur intermittently such as voltage flicker, the frequency of occurrence has been used as another severity index.

It is very important to note that the majority of power quality disturbances manifests as changes to the voltage waveforms. As a result, power quality indices are developed mainly for the voltage waveforms. As will be seen in the next section, signatures of equipment failures are mainly observed from current waveforms. They exhibit a wide variety of characteristics.

Table 1.2: Basic indices to characterize power quality disturbances.

Disturbance Group	**Transient Disturbances**	**Steady- state Disturbances**
Disturbance Types	• Impulsive transients • Oscillatory transients • Interruptions • Sags • Swells	• Over- voltages • Under- voltages • Imbalances • Flicker • Waveform distortions
Severity indices	• Magnitude • Duration	• Magnitude
Graphic illustration of disturbance severity (4 events are used as an example)	Magnitude ~ duration plot 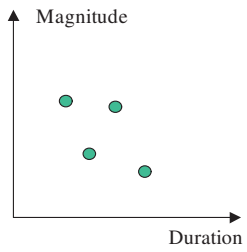	Magnitude bar chart 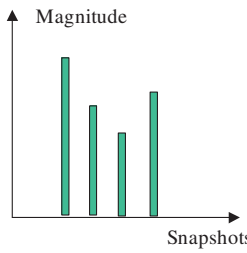

1.3 Signatures of Equipment Failure Disturbances

This section presents the electrical signatures of various utility equipment failures, including waveforms and root-mean-square (RMS) plots of the voltages and currents. The data and charts are collected from various literatures such as [6, 12, 13, 14] and they are fully acknowledged. All data shown here are collected from substation-based feeder current transformers (CT) and bus potential transformers (PT) unless mentioned otherwise. Generally speaking, substation is the most feasible location for data collection in power quality data analytics based equipment condition monitoring. It should be noted that most of the cases presented in this section are located in the medium-voltage distribution system, electrical behaviors of equipment in low-voltage network such as photovoltaic inverter and other equipment in secondary side [15, 16, 17] are not shown here.

1.3.1 Cable Failures

Most utilities possess a lot of power cables. Since many of current cable systems are aging, failures are getting more and more common. Medium voltage underground cables may show signs of incipient faults before permanent failures occur. Incipient faults show one or more current pulses whose magnitude depends on the location of the fault and the location on the voltage waveform when the fault starts [6]. Incipient faults typically do not require the operation of protective devices as they are usually self-clearing. But they indicate the cable is deteriorating, thus their detection is important for monitoring the cable health condition. A common cause of such fault type is the cable insulation breakdown caused by moisture penetration into cable splices. The self-clearing nature of such faults is associated with the fact that, once an arc is produced (insulation breakdown), water is evaporated and the resulting high pressure vapors extinguish the arc. Electrical trees, chemical reaction and partial discharge are other common causes of incipient faults [8].

(1) Incipient Faults on Primary Cable

Cases of sub-cycle incipient faults, multi-cycle incipient faults and sub-cycle faults followed by multi-cycle faults are presented and analyzed below. Figure 1.5 shows two instances of self-clearing incipient fault, whose durations are less than one cycle.

The current waveform during a single-phase incipient fault on Phase-C of a 13.8 kV underground feeder is shown in Figure 1.6. This fault originated from an incipient failure of an XLPE cable, and lasted a half cycle, with a 2.7 kA peak fault current.

The current waveform during multiple single-phase incipient faults on Phase-B of a 27 kV feeder is shown in Figure 1.7. These faults originated from an XLPE cable failure, and lasted a half cycle each, with roughly 3.1 kA peak

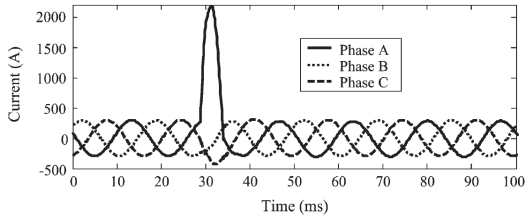

(a) Self-clearing fault lasting about one-quarter cycle [9].

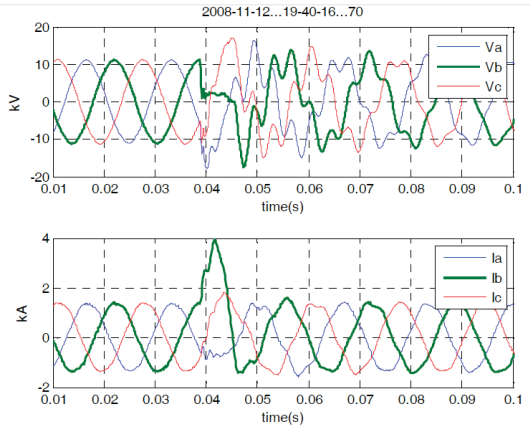

(b) Self-clearing fault lasting about one-half cycle [12].

Figure 1.5: Two instances of self-clearing incipient faults.

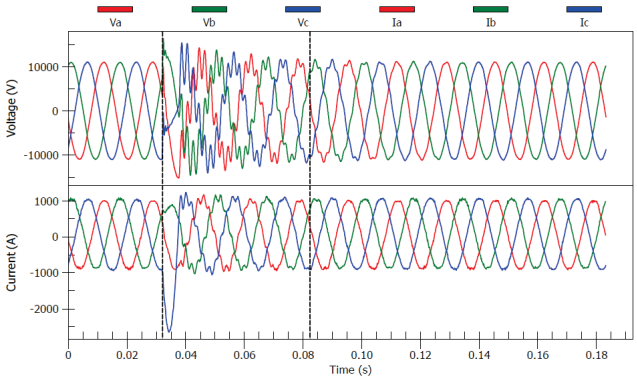

Figure 1.6: Single incipient single-line-to-ground fault [6].

fault currents.

Unlike the examples in Figure 1.5 to Figure 1.7, Figure 1.8 shows a multi-cycle incipient fault which is also a single phase fault and lasted about two and a half cycles.

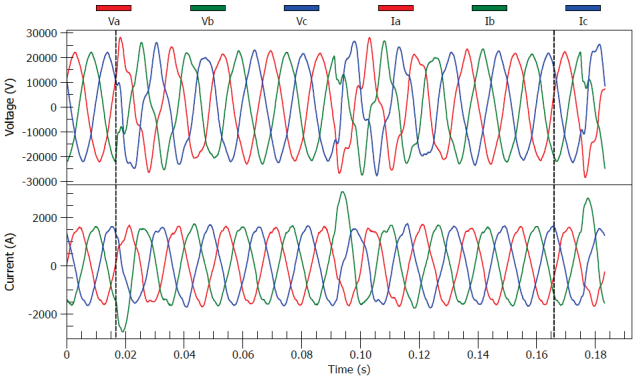

Figure 1.7: Multiple incipient single-line-to-ground fault [6].

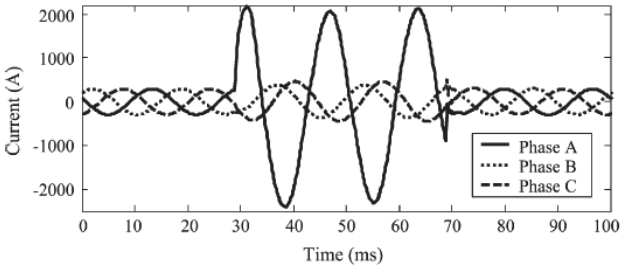

Figure 1.8: Multiple incipient single-line-to-ground fault [9].

The current waveform during a single-phase self-clearing fault on Phase-C of a 13.8 kV underground feeder is shown in Figure 1.9. This fault lasted one and a half cycles, with 6.3 kA peak fault current on Phase-B.

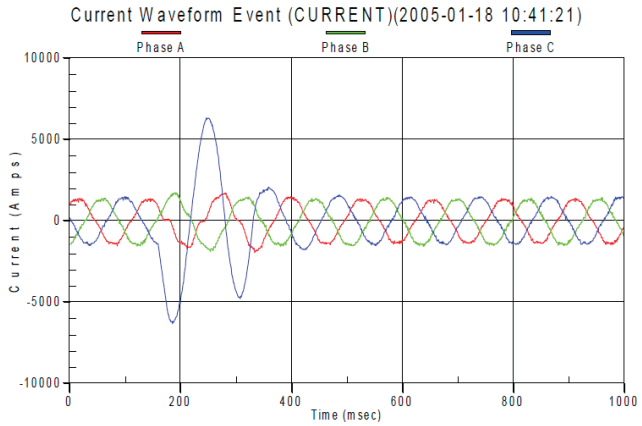

Figure 1.9: Self-clearing incipient cable fault lasting one and a half cycles [6].

After a number of such events during several months, the incipient faults may turn permanent, causing overcurrent protective devices to operate [4].

Figure 1.10 presents a very interesting event. This figure illustrates the last phases of the cable failure process, where the frequency of incipient faults had increased. After the first three incipient faults, a permanent fault occurred. Durations of the incipient faults are all between half and one cycle, while the duration of the permanent fault is about two cycles [4]. Figure 1.11 shows another incipient fault and corresponding permanent fault of an underground cable.

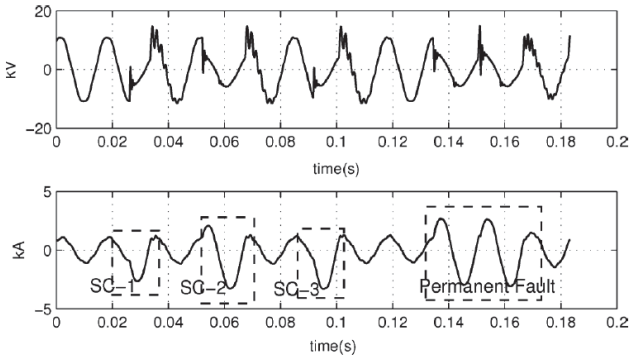

Figure 1.10: Incipients faults followed by a permanent fault [4].

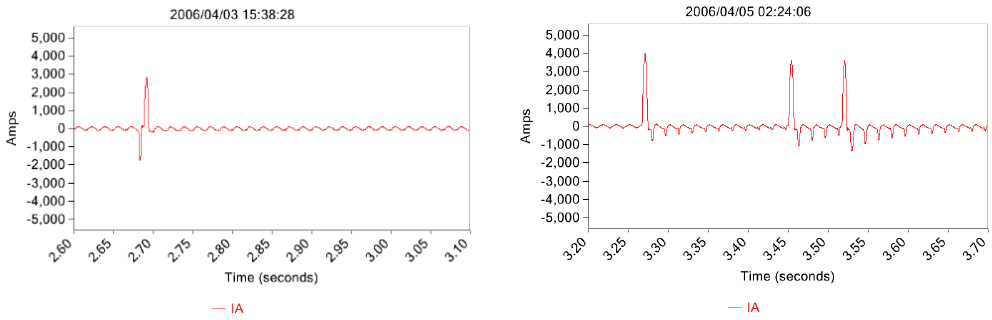

(a) Incipient fault. (b) Permanent fault.

Figure 1.11: Incipient and permanent faults of an underground cable [13].

The voltage and current waveforms shown in Figure 1.12 outline the occurrence of an incipient fault on Phase-A of a 27 kV underground feeder, followed by a second fault due to PILC cable failure. Both faults durations and magnitudes are a half cycle and 3.0 kA, followed by 3 cycles and 3.7 kA.

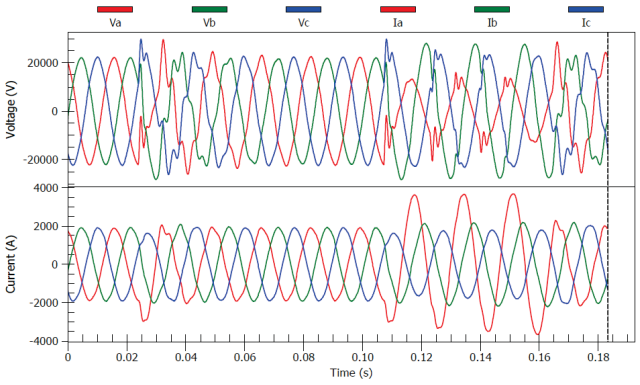

Figure 1.12: Incipient fault followed by a multi-cycle fault [6].

The current waveform shown in Figure 1.13 outlines the occurrence of an incipient fault on a 12 kV feeder, followed by a second fault resulting from an underground cable failure. Both faults durations and magnitudes are a half cycle and 5.7 kA, followed by two and a half cycles and 5.4 kA.

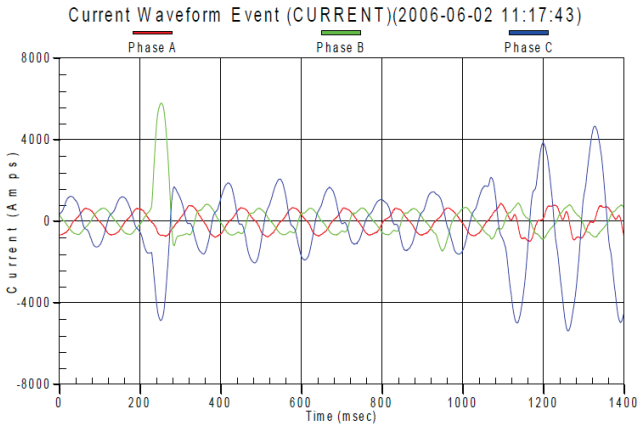

Figure 1.13: Underground cable failure incipient fault [6].

The voltage and current waveforms shown in Figure 1.14 outline an evolving cable failure fault on a 13.8 kV feeder. Initially, one can observe a two-and-a-half cycle single-phase fault on Phase-A, with 3.3 kA magnitude. This fault then evolved to a 5 cycle phase-to-phase fault between Phases A and C, with 5.3 kA magnitude.

The current and voltage waveforms during a sequence of two events on a 27 kV feeder are shown in Figure 1.15. It outlines an incipient fault on Phase-A,

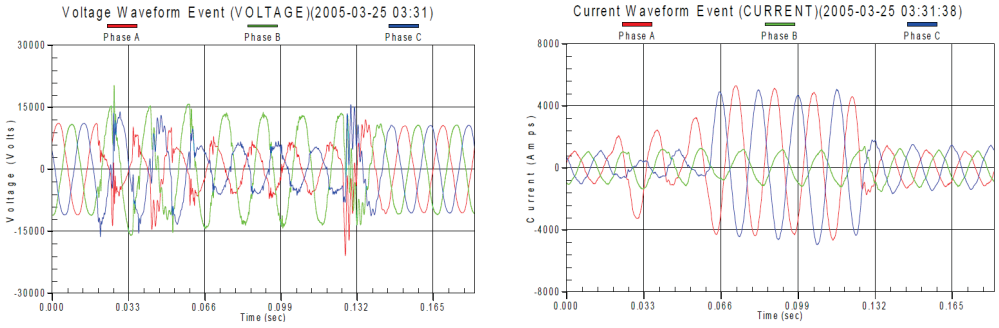

(a) Voltage waveforms. (b) Current waveforms.

Figure 1.14: Voltage and current waveforms during an evolving cable failure [6].

followed by a second fault due to XLPE cable failure. The faults durations and magnitudes are a half cycle and 2.2 kA, followed by three and a half cycles and 2.6 kA.

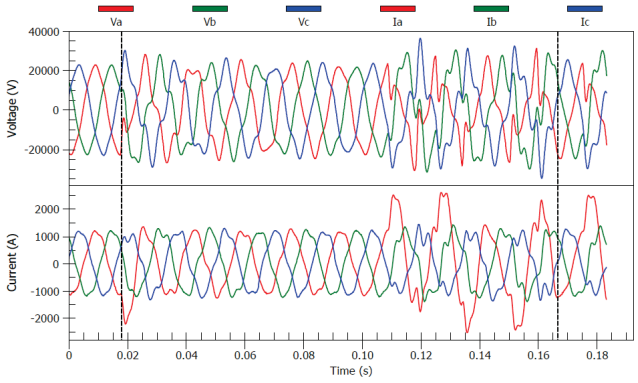

Figure 1.15: Electrical waveforms during an underground PILC cable failure [6].

(2) Incipient Faults on Primary Cable Joint

The current waveform during a self-clearing fault on a 27 kV underground system is shown in Figure 1.16. This fault originated from excessive moisture in cable joint, and lasted a half cycle, with a 3.8 kA peak magnitude on Phase-B.

The voltage and current waveforms during an incipient fault on Phase-A of

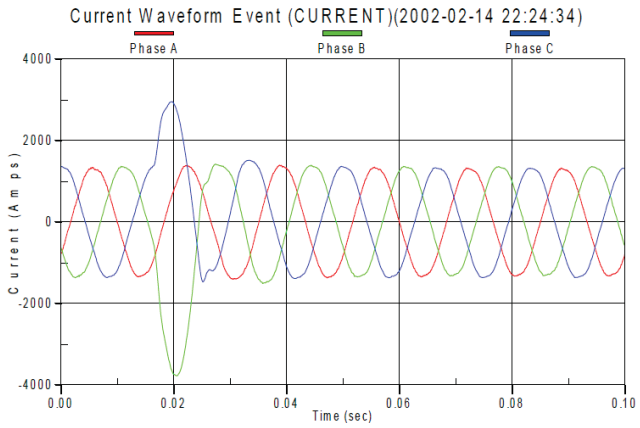

Figure 1.16: Incipient cable joint fault [6].

a 27 kV feeder is shown in Figure 1.17. This fault originated from a XLPE-to-EPR cable joint failure, and lasted a half cycle, with a 2.3 kA peak current.

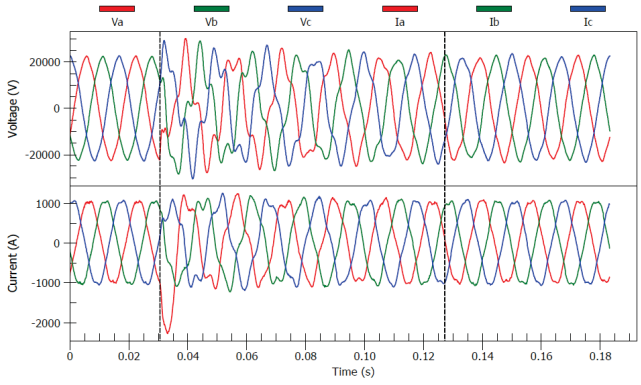

Figure 1.17: Incipient cable joint failure single-line-to-ground fault [6].

The voltage and current waveforms during a fault on Phase-A of a 27 kV underground feeder is shown in Figure 1.18. This fault originated from a PILC-to-XLPE cable joint failure, causing a circuit breaker to trip. The fault lasted three and a half cycles. Although this event is classified as a permanent failure, the signatures can also be considered as the "final version" of an incipient fault signature.

(3) Faults on Primary Cable Termination

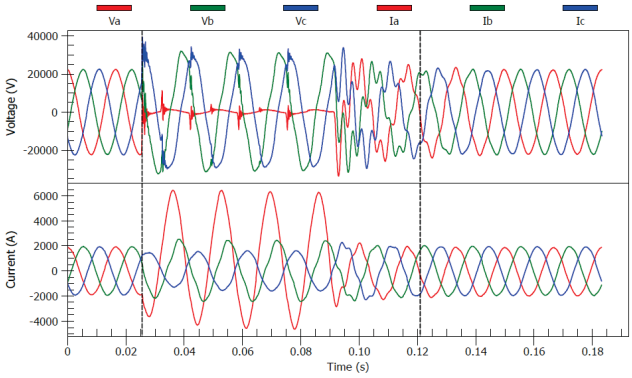

Figure 1.18: Underground cable joint failure waveform [6].

The voltage and current waveforms during a fault on Phase-C of a 13.8 kV underground feeder is shown in Figure 1.19. This fault originated from a PILC cable termination failure, and lasted 5 cycles, before cleared by a breaker opening. The peak current was 7.8 kA. This event is classified as a permanent failure. However, the signatures can also be considered as the "final version" of an incipient fault signature, the same as the example in Figure 1.18.

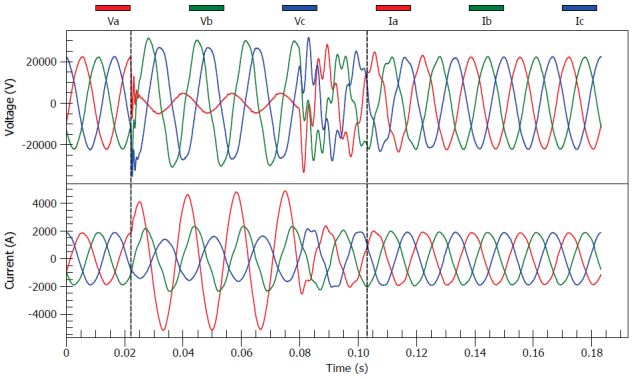

Figure 1.19: Underground cable termination failure [6].

Additional example signatures of cable failures including those of service cables can be found in [7].

1.3.2 Overhead Line Failures

There are many causes for overhead line "failures" which are defined as a short-circuit condition here. Some of the failures such as a conductor contacting a

tree branch can have certain signatures. Their identification before the failure evolves into a major outage is highly desirable.

Figure 1.20 to Figure 1.22 show a series of faults caused by tree contact. In about half an hour, three faults occurred and each fault caused a recloser to trip and reclose, but no sustained outage resulted. Such temporary overcurrent faults can cause damage to overhead lines and has the potential to burn the overhead line down if the underlying problem is not addressed properly.

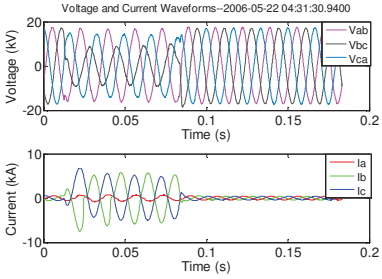

(a) Voltage and current waveforms.

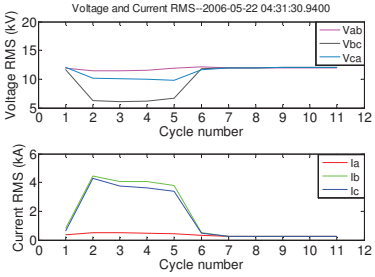

(b) Voltage and current RMS values.

Figure 1.20: First episode of a series of tree contact events from data of [14].

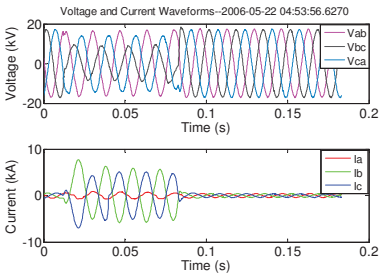

(a) Voltage and current waveforms.

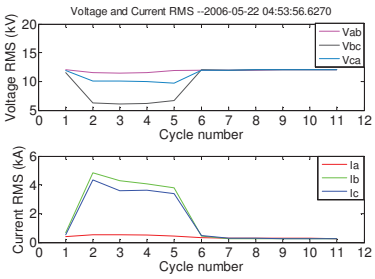

(b) Voltage and current RMS values.

Figure 1.21: Second episode of a series of tree contact events from data of [14].

The voltage and current waveforms during a tree contact event are shown in Figure 1.23. In this case, the resulting fault caused the tree branch to burn and fall to the ground. As a result, this fault cleared itself without the operation of any protective devices.

Voltage and current waveforms collected during an arcing fault on a 13.8 kV feeder are presented in Figure 1.24. This figure shows the instant when a

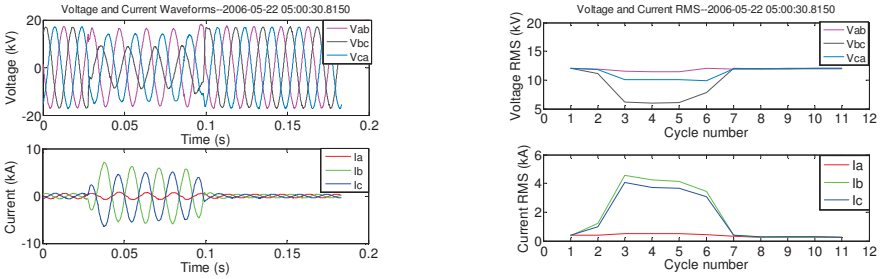

(a) Voltage and current waveforms. (b) Voltage and current RMS values.

Figure 1.22: Third episode of a series of tree contact events from data of [14].

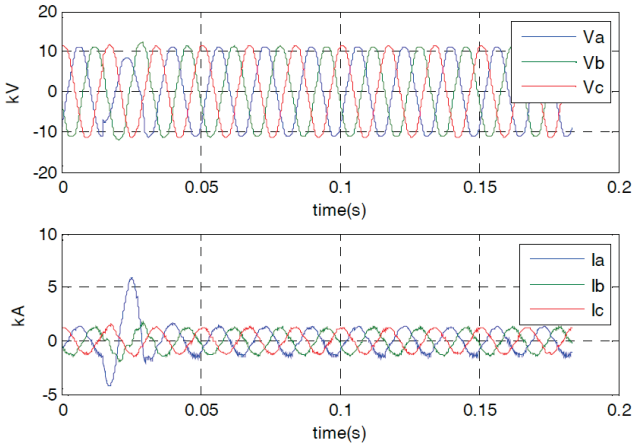

Figure 1.23: Tree contact fault lasting for about one cycle [18].

tree limb touched the overhead distribution line during a storm, causing the single-phase fault. The feeder circuit breaker cleared the single-phase fault in about 5 cycles.

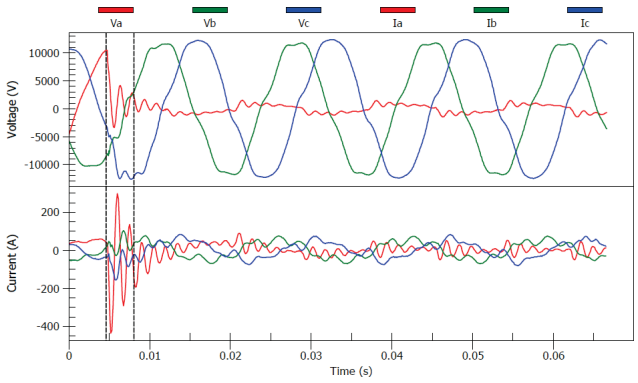

Figure 1.24: An arcing fault caused by tree contact [6].

The current waveform during a single-phase fault on Phase-B of a 25 kV system is shown in Figure 1.25. This fault originated from a tree falling into a customers triplex service due to windy weather conditions, and lasted three and a half cycles, with a 1.1 kA magnitude.

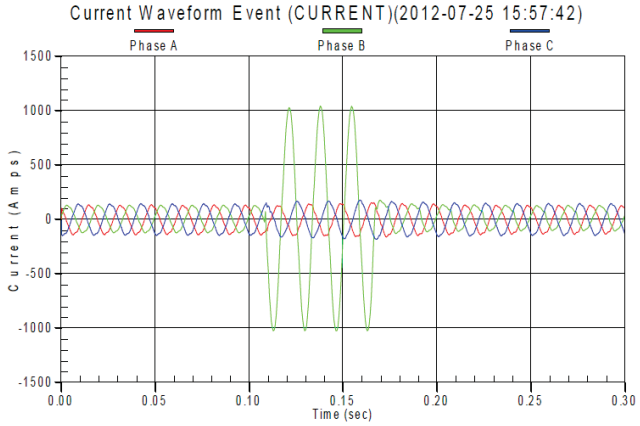

Figure 1.25: Fault caused by tree falling into customer triplex service [6].

The current waveform during a single-phase fault on Phase-C of the 25 kV system is shown in Figure 1.26. This fault originated from tree contact that caused primary to burn down, and lasted three and a half cycles, with a 1.5 kA magnitude. Although this event is classified as a permanent failure, the signatures can be considered as the "final version" of an incipient fault signature.

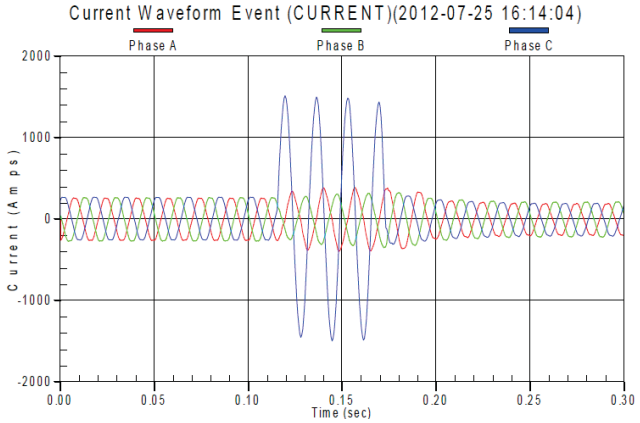

Figure 1.26: Tree contact causes primary to burn down [6].

1.3.3 Transformer Failures

Transformers are made of several components. Each component can experience failure. The corresponding signatures are different.

(1) Load Tap Changer Failures

Figure 1.27 illustrates a case of load tap changer failure. Initially, system reported 0 current value on one phase for less than one cycle. The issue happened several times each day. Over the following several days, the duration of such anomaly increased to just over 1 cycle. The utility company scheduled a maintenance outage and sent technicians to investigate the root cause of such anomaly. The technicians found a pin which was shearing and resulting in arcing when the load tap changer moved. After the planned maintenance, it was believed that a catastrophic transformer failure would have occurred within two weeks if the arcing had not been detected and addressed properly [19].

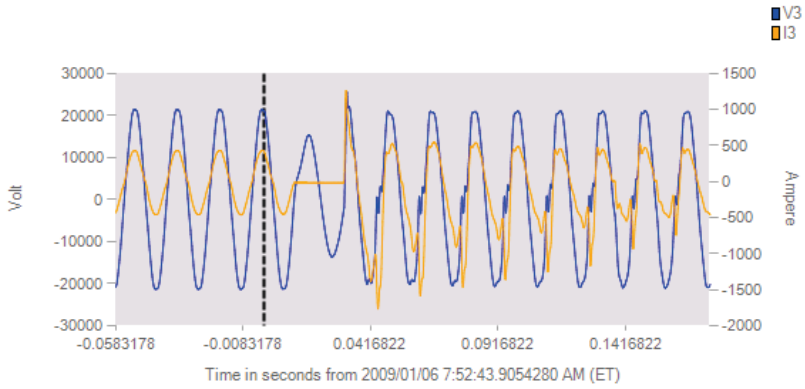

Figure 1.27: Zero current during load tap changer failure [19].

(2) Transformer Bushing Failures

Bushing failures may occur when the dielectric degrades, which can cause

significant damage to the transformer and other equipment connected nearby. When a bushing failure occurs, corrective actions should be undertaken to avoid internal arcing and subsequent violent failures [6]. In this subsection, three cases of transformer bushing failures are presented and discussed.

In the first case, a recloser tripped and reclosed (due to a single-phase fault) several weeks prior to the final failure. In total, there were six single-phase faults before the permanent outage. The last of these six faults (the one that caused the permanent outage) occurred seven weeks after the first fault. Figure 1.28 shows the third episode and the final fault. After the permanent outage occurrence, utility investigation showed that the first fault event happened due to an animal crossing the primary bushing. This damaged the bushing, leading to the subsequent faults and permanent outage [20].

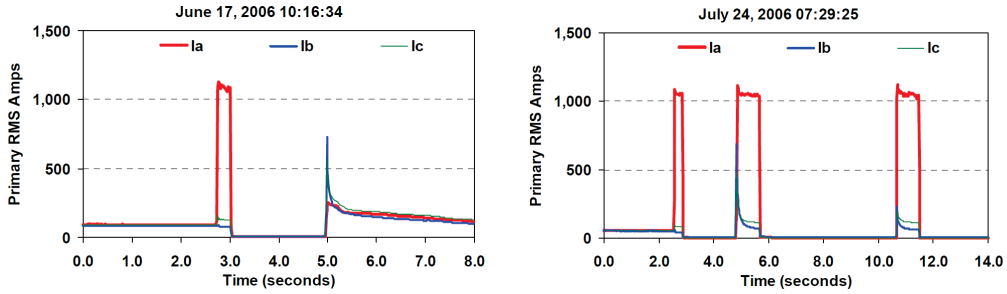

(a) Third episode.

(b) Final episode.

Figure 1.28: RMS trends during recurrent faults [20].

In the second case, voltage and current waveforms during an arcing fault on a 12.47 kV feeder are presented in Figure 1.29. It happened due to a bushing failure on transformer primary winding, resulting in a sustained arc to ground. A recloser cleared the fault in about 2 cycles.

The current waveform behavior during an arcing fault on a 4.4 kV distribution feeder is presented in Figure 1.30. The event happened during a bushing failure of a distribution transformer, and was cleared in 5 cycles by a recloser.

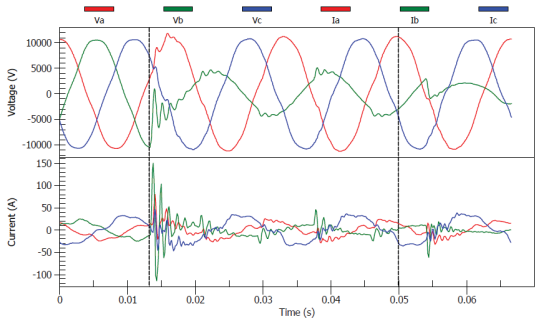

Figure 1.29: Example transformer bushing failure [6].

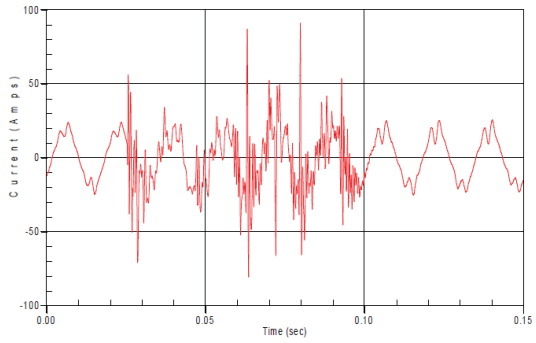

Figure 1.30: Another example of transformer bushing failure [6].

1.3.4 Circuit Breaker Failures

Due to the high power typically passing through circuit breakers (under normal or faulty conditions), arcing usually occurs between the moving and fixed breaker contacts during maneuvers. As a result, circuit breakers are prone to failures after experiencing sufficient wear and tear over time. This section presents several failure modes of circuit breakers.

(1) Line Switch Failure Triggered by Temporary Overcurrent Faults

Reference [20] presents an example of line switch failure. It can be described as follows. Firstly, an overcurrent fault occurred, leading substation breaker to trip and reclose twice. The fault was cleared without the need for a permanent service outage. This sequence of events was in accordance with a usual

fault and protection sequence, except for the behavior of Phase-A current after fault clearance. Such current presented an irregular behavior, different from the other two phases and from fluctuations caused by regular load variations. The fault and post-fault currents are shown in Figure 1.31. Overcurrent temporary faults continued happening multiple times after the initial fault, with the post-fault behavior becoming more irregular and occurring for longer times. Finally, a permanent fault occurred, causing the substation breaker to trip to lockout. Utility investigation determined a main line switch failure, outside the substation.

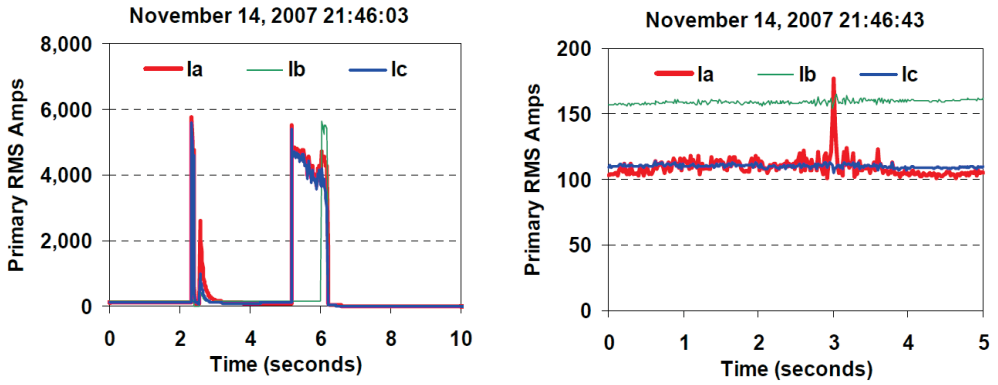

(a) Temporary overcurrent fault. (b) Erratic signlas after temporary fault.

Figure 1.31: Electrical signatures during and after temporary faults [20].

It was believed that multiple overcurrent faults that occurred over a period of a month deteriorated the switch conditions. Series arcing happened and finally burned its contacts open, causing flashover between the switch and supporting hardware.

(2) Arcing Capacitor Bank Switch

The current waveform for an arcing capacitor bank switch during energizing of a capacitor bank is presented in Figure 1.32 [6]. Repetitive transients can be observed in this figure. The possible underlying cause of the transients

is a phenomenon called "multiple prestrike". When closing a switch, a prestrike can occur if the electric field strength exceeds the dielectric strength of the contacts gap. Inrush current with high-frequency and high-amplitude flows through the circuit breaker. Then the prestrike arc may be interrupted at or near a zero-crossing point, which is dependent on the rate of change of current. If interruption does happen, the dielectric strength will recover. Prestrike may reoccur if the voltage across the contacts exceeds again the dielectric strength of the gap [21]. This process may repeat several times until the contacts touch, and a number of high frequency current zeros can occur as shown in Figure 1.32. The inrush current may lead to contact welding which can further result in damage to the contact surfaces [22]. The cumulative damage may lead to final failure of a circuit breaker which is connected to a capacitor bank.

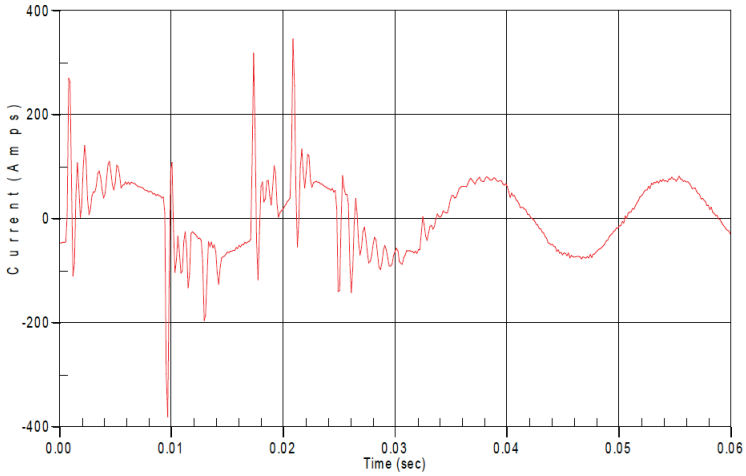

Figure 1.32: Current waveform during arcing of a capacitor bank [6].

(4) Restrikes during Capacitor De-Energizing

Restrike has been defined as "A resumption of current through a switching device during an opening operation after zero current lasts 1/4 cycle at power frequency or longer" [23]. A capacitor switch may restrike during de-energizing when the switch contacts are contaminated or faulty. Rough contacts surface

lead to higher electrical stress as contacts open. When the electric field strength exceeds the dielectric strength of the contact gap, a restrike can occur. Unlike a normal capacitor de-energizing event which does not produce any significant switching transients, obvious transients can be observed during capacitor de-energizing with restrikes. Figure 1.33 shows the three-phase voltage and current waveforms measured at a substation during a capacitor de-energizing event with restrikes. Restrikes further degrade the breaker and may lead to failure of the breaker eventually.

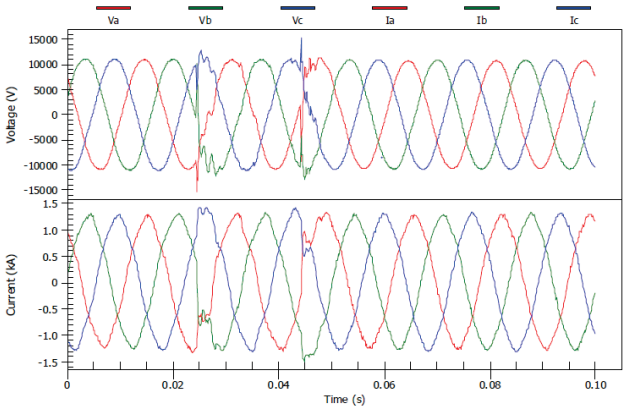

Figure 1.33: Electrical waveforms of a capacitor de-energizing with restrike [24].

1.3.5 Capacitor Failures

Capacitors are typically energized using circuit breakers or switches. The voltage and current waveform measured during capacitor bank switching can contain unique signatures (e.g., oscillatory transient frequency, high transient energy, etc.) that can be useful for determining which capacitor on the feeder switched as well as diagnosing capacitor problems. Three instances of capacitor problems are described and discussed below.

(1) Capacitor Failure Caused by Misoperation of Controller

A capacitor bank usually switches on and off one or two times during one day. Excessive operations over short period of time would probably lead to capacitor bank failures. Reference [25] presents such a case whose underlying cause was believed to be the misoperation of capacitor bank controller. Initially, the capacitor bank experienced excessive switching operations. Shortly after that, Phase-A capacitor experienced a short-circuit fault. Three-phase current waveforms during Phase-A short circuit are shown in Figure 1.34.

Phase B and C still switched frequently after the Phase-A capacitor failure. After about two weeks, the contacts of the switch for the Phase-B capacitor started to fail. Figure 1.35(a) illustrates the RMS current signals as the switch began to fail. Figure 1.35(b) illustrates several cycles of the phase voltage and current shortly after the instance shown in Figure 1.35(a). The transients are obvious. After Phase-B switch began to fail, the controller still operated the switch frequently. After another four days, the Phase-B switch only made sporadic contact, leading to the effective disconnection of Phase-B capacitor from the grid [25]. According to [25], it was almost certain that the misoperation of capacitor controller caused this series of failures.

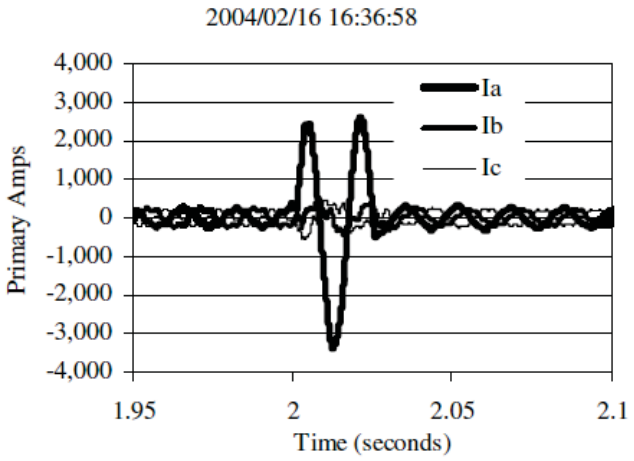

Figure 1.34: Phase-A capacitor short circuit [25].

(2) Unsuccessful Synchronous Closing Control

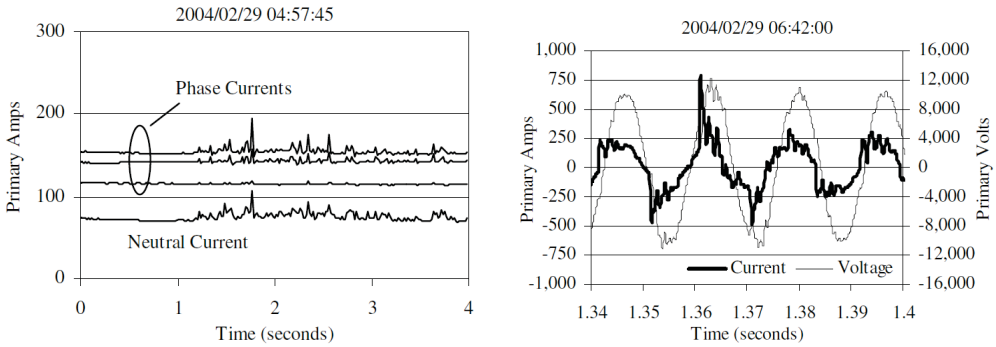

(a) RMS currents as the Phase-B switch began to fail.

(b) Voltage and current waveforms in the process of switch failure.

Figure 1.35: Electrical signatures during Phase-B switch failure [25].

Generally speaking, by switching on a capacitor at or near voltage zero, capacitor switching transients can be minimized. Such kind of accurately timed switching operation can be accomplished with a synchronous closing control. Figure 1.36 shows the voltage and current waveforms during the energizing of a three-phase capacitor bank using synchronous closing control. It is obvious that switching transients happened away from a voltage zero, which means that the closing control did not work as designed [24].

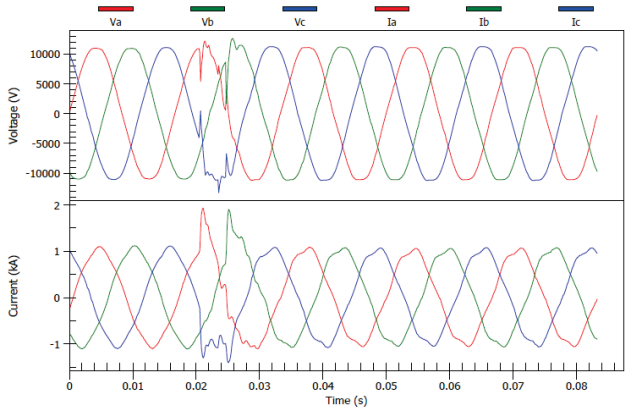

Figure 1.36: Waveforms of a capacitor energized using synchronous closing control [24].

1.3.6 Lightning and Surge Arrester Failures

A lightning arrester is usually used to protect the conductors and insulation of power systems or telecommunication systems from the damaging effects of lightning. In most situations, current from a lightning surge can be diverted through a nearby lightning arrester, to earth. A surge arrester is a similar device to protect electrical equipment from over-voltage transients which are caused by internal (switching) or external (lightning) events. In this subsection, one instance of lightning arrester and one instance of surge arrester are presented and discussed below.

(1) Lightning Arrester Failure

Reference [26] presents one instance of lightning arrester failure. Small arc bursts can be observed prior to the permanent arrester failure, as illustrated in Figure 1.37(a). In this figure, however, the arc fault is not obvious due to its small current (if compared to the load current). It occurs approximately in the middle of the measurement window, where one shall observe a slightly larger current peak. An extended measurement window (about 60 seconds) of the RMS current is shown in Figure 1.37(b). The observed current spikes correspond to arc bursts [26]. Figure 1.37(c) presents the final burst, where a current of about 3800 A is added to the load current for over 20 cycles. In this event, the substation breaker tripped. Further investigation reveals that a lightning arrester destroyed itself.

(2) Surge Arrester Failure

Many gapped silicon carbide (SiC) surge arresters contain a number of spark gaps in series with blocks of silicon carbide material which shows a nonlinear voltage/current characteristic. The spark gaps can degrade over time. As a

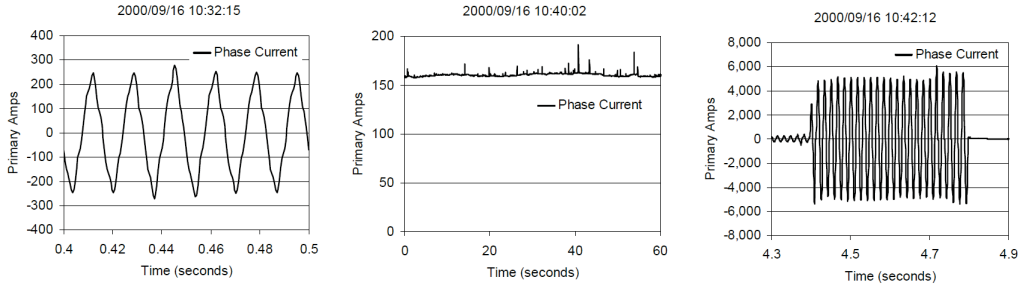

(a) One burst of intermittent arc current.

(b) RMS of multiple arc bursts.

(c) Final failure.

Figure 1.37: Electrical signatures during Phase-B switch failure [26].

result, power frequency currents can flow through the SiC arrester blocks. Such condition can overheat the arrester and cause it to fail very quickly [6].

The voltage and current waveforms during a SiC arrester failure are shown in Figure 1.38. A recloser cleared the fault in approximately 0.2 seconds.

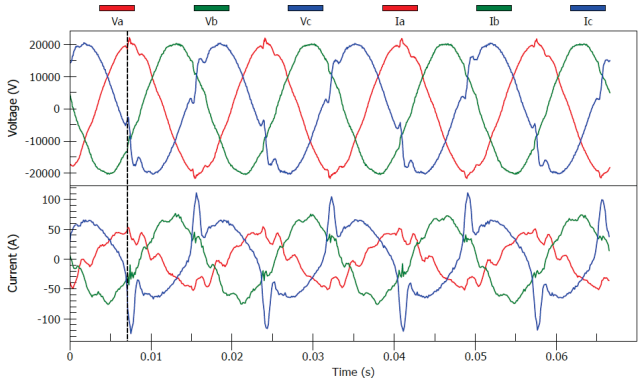

Figure 1.38: Surge arrester failure fault waveform [6].

1.3.7 Summary and Motivation

The results in this section have clearly shown that the signatures of equipment failures are quite diverse and are very different from those of the power quality disturbances. The main characteristics of equipment failure signatures may be summarized as follows.

- Abnormal current response. The signatures of equipment failures are of-

ten more visible in the current waveforms as oppose to the voltage waveforms. Many equipment failures exhibit a short-duration current increase or repetitive current pulses. Low-level variations of current can also be observed. Such characteristics are especially evident when examining the RMS values of the current waveforms.

- Diverse time scale. Some equipment failures can only be identified from the waveforms. Examples are breaker restrike and asynchronous capacitor closing. There are also equipment failures that are most visible from a longer time scale such as RMS value variations in several seconds or minutes.

- Complexity in characterization. Severity of a disturbance is the main concern for power quality disturbances. As a result, power quality disturbances are characterized using severity parameters. For equipment condition monitoring, however, the goal is to identify the existence of incipient failures or abnormal operations. Severity-oriented indices may not be the best candidate to characterize the signatures of equipment failures. It is not clear at present what indices are appropriate to characterize equipment failure signatures.

- Challenge in detection. Due to the diverse signatures of equipment failures, methods developed to detect power quality disturbances are not adequate for equipment condition monitoring. New methods to detect waveform abnormality associated with equipment operation are needed.

The task to identify equipment failures from their electric signatures seems to be quite daunting. However, if we study the history of power quality monitoring many similarities can be found. The need to monitor power quality was identified in early 1980's. At that time, the signatures of power quality disturbances were not well understood. The data recording capability of power

quality monitors were very poor. There were no indices to characterize the disturbances. It was a big challenge to monitor and study power quality at that time. But the situation also represented a great opportunity for research and product commercialization. Intensive research on power quality monitoring started in early 1990's. Through over 20 years of efforts, power quality monitoring has become a "routine" exercise for utility engineers. The disturbance signatures and indices have become so "obvious". In comparison, equipment condition monitoring is a relatively new field. So it is natural to encounter many unknowns and uncertainties. They represent challenges as well as opportunities. In view of the development trajectory of power quality monitoring, we can safely state that it is just a matter of time that equipment condition monitoring will become as well developed as the power quality monitoring.

There is also a larger trend to support the use of electrical signatures for equipment condition monitoring. One of the main characteristics of the future power systems, the smart grids, is the extensive presence of sensors, meters and other monitoring devices. Massive amount of field data will be collected. The most granular data that can be collected are the waveform-type disturbance-related data. Such data contain unique information about the behavior and characteristics of the power system and equipment involved. With advancement on data acquisition hardware and substation automation, it is just a matter of time that system-wide synchronized waveform data will be made widely available to utility companies. However, the mere availability of such data does not make a power system more efficient or reliable. How to extract useful information from the data and apply it to support power system planning and operation are a new challenge as well as a new opportunity facing our industry. Equipment condition monitoring, as one area of power quality data analytics, represents a highly attractive direction to push the boundary of data analytics in the smart grid era.

An application scenario is used to illustrate the future of power quality

data analytics for equipment condition monitoring, as shown in Table 1.3. The scenario is compared with that of power quality oriented applications. One can see that a power quality monitor can function as an "equipment doctor" if it is added with data analytics capabilities. It should be noted that the V & I responses in this table means voltage and current responses.

Finally, a possible path for general-purpose condition monitoring scheme is presented in Figure 1.39. It involves several steps. The first step is to detect the existence of waveform abnormality. The second step is to extract the waveforms associated with the abnormality. The third step is to analyze the extracted waveforms to determine the cause of abnormality and if equipment failure is involved. The fourth step is to determine the characteristics of equipment failure such as the location of a fault.

Table 1.3: Two applications of disturbance data

Type of Applications	**Power Quality (Current Practice)**	**Condition Monitoring (Future Practice)**
Illustrative problem	A customer complains repeated trips of its variable frequency drives	A utility company needs to determine if an aging underground cable needs to be replaced
Solution steps	1) A power quality monitor is used to record disturbances experienced by the customer 2) The data are then analyzed to find the cause of the drive trips	1) A power quality monitor is used to record voltage and current responses of the cable during its operation 2) The data are then analyzed to check if the cable exhibits abnormal V& I responses such as partial discharges. The frequency & severity of abnormal responses may be compared with those collected from various cables
Outcomes	Methods to mitigate the PQ problem are recommended	Decision on if the cable needs to be replaced is made
Nature of monitoring	Diagnostic monitoring	Preventive monitoring
Medical analogy	Find the causes and damages of a heart attack after it has occurred	Determine if a patient has the risk of heart attack

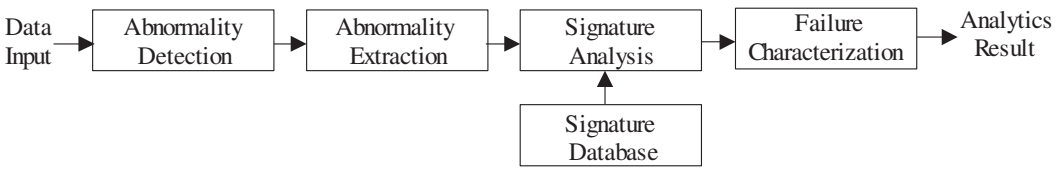

Figure 1.39: A possible path for general-purpose condition monitoring scheme.

This thesis aims to develop new methods to detect generic waveform ab-

normality for equipment condition monitoring. The motivation of developing generic detection method instead of any specific abnormality detection method is that we still do not have a complete knowledge of the specific signatures of various equipment failure abnormalities. Under such situation, it is impossible to monitor equipment conditions by specific methods. Instead, we can detect and capture generic waveform abnormalities to narrow down the search range. By analyzing the captured abnormal events and conduct field investigation if possible, we will be able to monitor the health condition of equipment.

1.4 Thesis Contribution and Organization

In developing reliable and sensitive methods for waveform abnormality detection, four directions are taken in the research.

The first is on extensive survey on the electrical signatures of various equipment failures. The summarization of equipment failure signatures lay the foundation for the whole research presented in this thesis, for the goal of this thesis is to develop robust and efficient methods to detect generic waveform abnormalities, especially those associated with equipment failures.

The second direction is on the development of an improved traditional method which is a modification based on several existing methods. The used features for detection are segment RMS values of differential waveform and half-cycle refreshed RMS values of original waveform. The signals used here include both phase voltage and phase current waveforms. Illustrative examples of detection results are presented to show main types of abnormalities to be detected and the effectiveness of the method.

To overcome the disadvantages of existing detection methods, the third direction is on robust and flexible detection of generic waveform abnormalities, which has the following objectives.

- The developed method should be able to detect generic abnormalities

associated with power equipment failures, instead of a certain type of abnormality.

- In traditional detection methods, threshold selection relies heavily on experience. A systematic and analytical threshold selection scheme is highly desired to overcome the difficulty to set proper threshold due to large variations of current waveforms.

The fourth direction is on soft detection of waveform abnormalities. Instead of returning binary detection results (i.e. an abnormality either exists or does not exist), soft detection scheme which can return a numerical value in unit interval [0,1] for the data of interest is desired to reflect the credibility that the data contain waveform abnormality and to decrease the average detection error.

The rest of the thesis is organized as follows.

Chapter 2 reviews existing traditional methods for the detection of waveform abnormalities. Then a modified detection method based on existing schemes is proposed. Segment RMS values of differential waveform and half-cycle refreshed RMS values of original waveform are used as features for the detection. Illustrative examples of detection results are provided to show the effectiveness of this method.

Chapter 3 presents a novel statistics-based detection method for the detection of generic waveform abnormalities. It uses the probability density function of residual data which is derived by removing steady-state components from the measured current signal as the feature for detection and the KLD between distributions as abnormality measure. The proposed method is tested with field and computer simulation data. Results show that it can effectively detect abnormality-containing data, and at the same time reduce false alarms due to small load changes.

Chapter 4 provides a soft detection scheme based on fuzzy set theory. The

scheme is easy to implement and its output for a certain period of data is a numerical value in the real unit interval $[0, 1]$ which reflects the degree or credibility for the data being abnormal. Illustrative examples and statistical results are used to show advantages of the soft detection scheme over the proposed binary detection method in Chapter 3.

Chapter 5 concludes this thesis and provides suggestions for future research.

Appendix A describes positive-going zero crossing point detection and frequency variation correction, which are used in the improved traditional detection method proposed in Chapter 2.

Appendix B presents the parameter selection results and performance evaluation for the proposed statistics-based binary detection method with phase-B and phase-C data.

Chapter 2

Existing Methods to Detect Waveform Abnormality and Proposed Modification

The first step to identify equipment failure or malfunction is to detect abnormality in voltage and current waveforms. Once an abnormality is detected, the waveforms and RMS values associated with the period of abnormality can then be extracted for detailed analysis. This may include signature evaluation, pattern recognition, statistical analysis and other types of assessments. Eventually equipment condition can be determined from the results.

As a result, the first problem that needs to be solved is the detection of waveform abnormality. As discussed earlier, there is a wide variety of equipment failure signatures and many of them are not well understood. Alos, methods to detect power quality disturbances are usually not applicable. A proper approach to solving the problem is, therefore, to create new general methods that can detect all types of abnormalities for equipment failures.

Some research has been conducted in this direction for a few types of equipment failures. We first provide a brief review of existing literature, then presents an improved general purpose waveform abnormality detection method which

combines the advantages of several existing detection methods. The proposed method is applied to real field data and the detection results are presented.

2.1 Current Signature Based Methods

Disturbances associated with equipment failures usually results in abnormalities in current signals. As a result, most of the published detection methods use current waveforms or RMS trends. In this subsection, existing traditional current-based methods are reviewed.

2.1.1 Fault Component Methods

Superimposed fault component is the current signal from which normal load component has been removed. According to References [8] and [9], superimposed fault component can be derived with the following equation:

$$i_F(k) = i(k) - i(k - N_M) \tag{2.1}$$

where i is the instantaneous current value of a certain phase (A, B or C); i_F represents the superimposed fault component of the phase; k is a sample index; N_M is an integer multiple of N_1 which represents the number of samples per power cycle.

Fault components are very small under steady state conditions. During faults and other switching events, the above signals will be relatively bigger [8]. If the fault components exceed normal limits, a disturbance can be considered to occur. There are two different methods to determine if the fault components exceed normal limits, as follows.

(1) Magnitude of Fundamental Frequency Fault Component

After superimposed fault components have been calculated, the magnitudes of fundamental frequency component can be derived with fast Fourier transform (FFT). Let I_{FA_MAG}, I_{FB_MAG}, I_{FC_MAG} stand for the magnitudes of fundamental frequency component of Phase A, B and C respectively and I_{A_thre}, I_{B_thre}, I_{C_thre} stand for thresholds for three phases. If any of the three-phase magnitudes of fundamental frequency component exceeds a certain threshold, a disturbance is detected. In other words, if any of the following three equations is satisfied,

$$I_{FA\_MAG} > I_{A\_thre}, \tag{2.2}$$

$$I_{FB\_MAG} > I_{B\_thre}, \tag{2.3}$$

$$I_{FC\_MAG} > I_{C\_thre}, \tag{2.4}$$

a disturbance is detected. The thresholds can be predefined, or be estimated by analyzing previous cycles of current signals.

Both References [8] and [9] propose such a method, but there is some difference between them. The main difference is as follows: in [9], the fundamental components are derived with full cycle Fourier analysis; while in [8], half cycle Fourier analysis is used.

Figure 2.1 illustrates the process of this method. In Figure 2.1(c), IRBMag stands for the fundamental component magnitude of Phase-B fault current. User pickup stands for the threshold defined by user. From Figure 2.1(c), we can know that this method successfully detects the disturbance shown in Figure 2.1(a).

(2) Instantaneous Superimposed Fault Components

Reference [27] proposes a method to detect arcing events. Instantaneous superimposed fault current is used to detect disturbances. Detailed algorithm

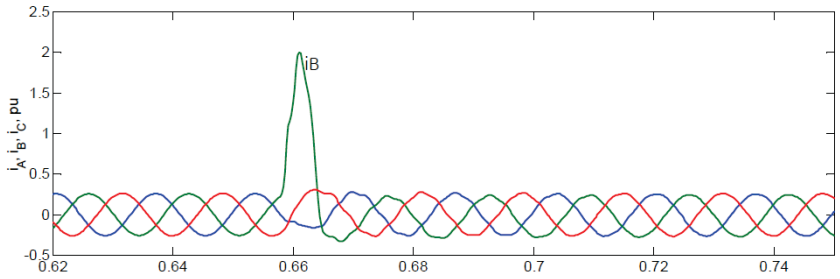

(a) Three-phase current waveforms.

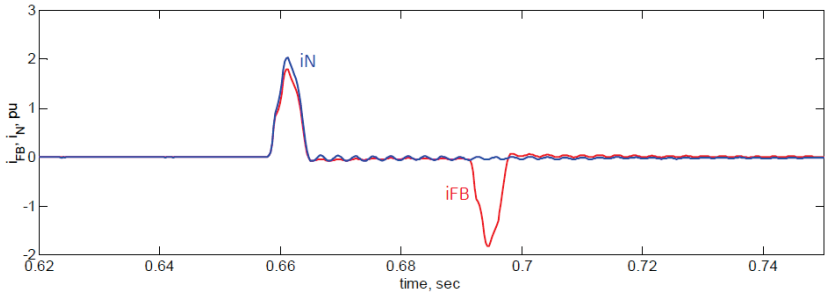

(b) Fault components of phase B and neutral current.

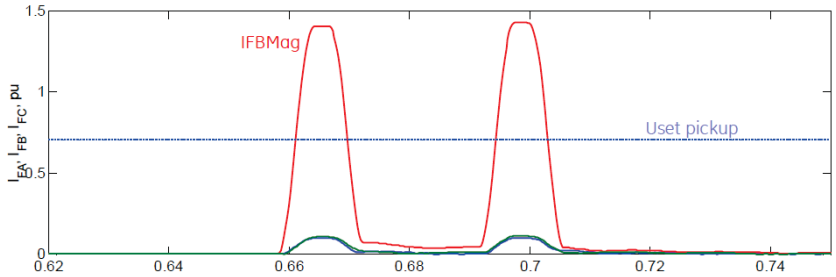

(c) Fundamental components of fault component.

Figure 2.1: Illustration of the fundamental fault component method [8].

can be explained as follows: first, superimposed fault currents are derived; if the maximum value of the fault current exceeds a certain threshold during a predefined time interval, then a disturbance is detected. Let $|i_{FA}(k)|$, $|i_{FB}(k)|$, $|i_{FC}(k)|$ stand for the absolute values of fault components in Phase A, B and C, and i_{A_thre}, i_{B_thre}, i_{C_thre} stand for the threshold of Phase A, B and C. During a predefined interval, if any of the following three equations is satisfied,

$$|i_{FA}(k)| > i_{A\_thre}, \tag{2.5}$$

$$|i_{FB}(k)| > i_{B\_thre}, \tag{2.6}$$

$$|i_{FC}(k)| > i_{C\_thre}, \tag{2.7}$$

a disturbance is detected. The thresholds can be predefined, or estimated by analyzing previous cycles of current signals.

Figure 2.2 illustrates this method. It should be noted that the current waveform is not from field measurement, but from synthetic signals with MATLAB simulation. Reference [27] does not provide a detailed method to derive the fault component. In order to illustrate this method, (2.1) is used to derive the fault component. It is apparent that there is a disturbance in the original waveform and this method successfully detects the disturbance.

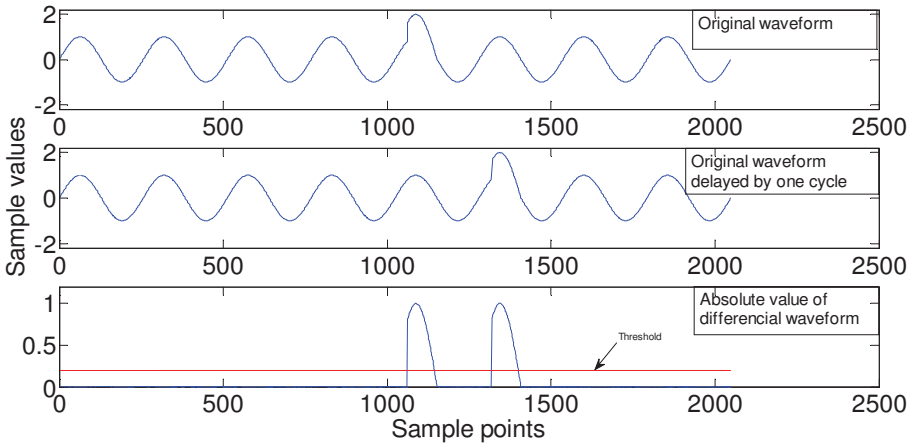

Figure 2.2: Illustration of instantaneous fault component method.

2.1.2 Wavelet Analysis Methods

In [9], wavelet analysis method is used to detect incipient failures in underground cables. Incipient failures are usually self-clearing faults which have

short durations (less than 3 cycles) and are generally extinguished before utility protective devices have time to operate. In order to identify incipient failures, an algorithm based on wavelet analysis is developed.

More specifically, with wavelet analysis, the measured signal can be decomposed into the low frequency approximation coefficients and the high frequency detail coefficients. The low frequency approximation coefficients can represent the fundamental frequency component, while the high frequency detail coefficients can represent the transient state [9]. The detection method involves two rules, and if either one is triggered, a disturbance is detected.

(1) Detection Based on Approximation Coefficients

The approximation coefficients in the frequency band of 0-240 Hz are utilized in this detection rule. This rule is less related to the high frequency components. A disturbance is detected if Equation (2.8) is satisfied.

$$RMSCR = \frac{RMS_{latest\ half\ cycle} - RMS_{one\ cycle\ before}}{RMS_{one\ cycle\ before}} > threshold \qquad (2.8)$$

where RMS is the root mean square value, $RMSCR$ is a derived parameter. The second subfigure of Figure 2.3 illustrates this detection rule. The disturbance shown in the first subfigure can be detected with this rule. It is insensitive to heavy noise because it is not related to the high frequency components. It also includes a short detection delay.

(2) Detection Based on Detail Coefficients

In this rule, the detail coefficients in the frequency band of 240-960 Hz are utilized for detection. It is less related to the fundamental frequency. A

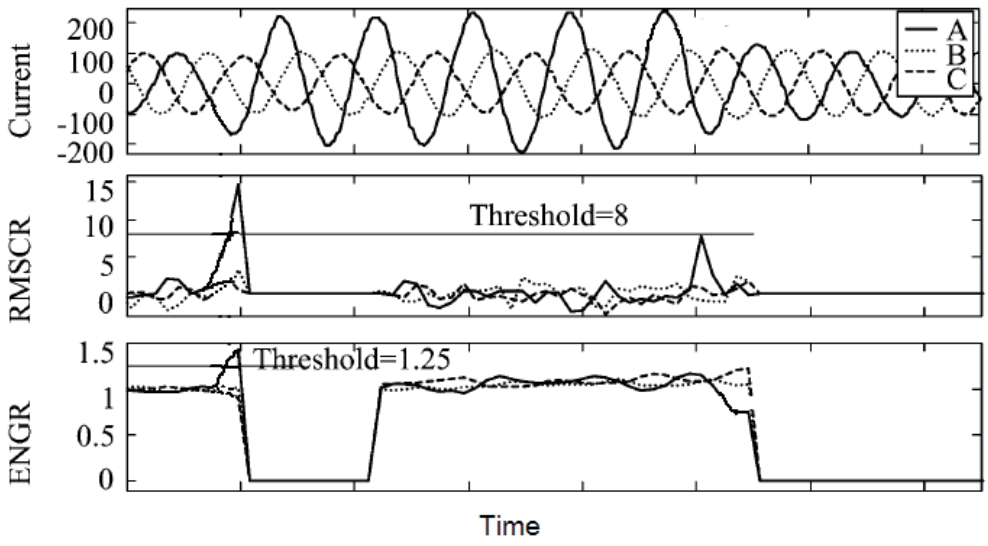

Figure 2.3: Illustration of wavelet analysis method [9].

disturbance is considered to be detected when Equation (2.9) is satisfied.

$$ENGR = \frac{Energy_{latest} - MEAN(Energy_{past})}{STD(Energy_{past})} > threshold \qquad (2.9)$$

where $Energy_{latest}$ stands for the energy of the latest detail coefficients; $Energy_{latest}$ stands for an array of the energy of the past detail coefficients; $MEAN$ stands for the average function; STD stands for the standard deviation function.

The third subfigure of Figure 2.3 illustrates this detection rule. The disturbance shown in the first subfigure can be detected with this rule. It has good performance in low noise environment. Since it does not consider the low frequency component, it is insensitive to slow change of fundamental frequency component.

2.1.3 Fundamental Frequency Component Method

In [28], a method is proposed to detect incipient faults in medium voltage circuits using the fundamental frequency components. Its detection process can be explained as follows: first, the fundamental component of actual current wave-

form is calculated with discrete Fourier transform (DFT); if the fundamental component magnitude exceeds a certain threshold, a disturbance is detected. Then, more detailed analysis is made to determine if a cable fault occurs.

Let N_1 be the number of samples in one power frequency cycle. In order to get fundamental component magnitude, half cycle DFT is done every one eighth of a cycle which means for every Fourier analysis, one eighth of N_1 new samples are moved in and one eighth of N_1 old samples are moved out.

There are two different modes for the calculation of the threshold: (1) fixed threshold, i.e. predefined threshold; (2) dynamic threshold, where the average value of several previous cycles' fundamental component magnitude is calculated first; and the threshold can be derived by multiplying the average value by a coefficient larger than 1. Figure 2.4 illustrates the process of this method. A fixed threshold is used in this case.

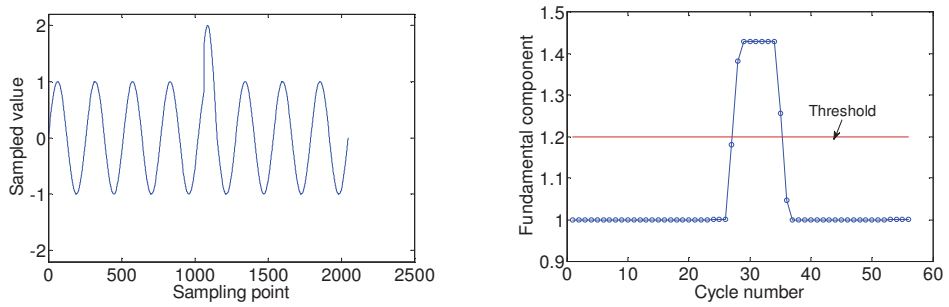

(a) Original waveform (b) Detection process

Figure 2.4: Illustration of fundamental component method.

2.2 Voltage Signature Based Methods

Most disturbances in voltage waveforms are power quality disturbances. There have been extensive research on those disturbances. There are also many commercial devices for the detection of power quality disturbances. Reference [11] has provided comprehensive techniques for the detection and characteriza-

tion of power quality disturbances, including short duration voltage variations (voltage sag, swell and interruption) and steady state disturbances (harmonics, inter-harmonics and voltage flicker). However, there is little discussion on the detection of voltage transients. Voltage transient is a special kind of disturbance. It not only causes power quality problems but also carries valuable information about utility equipment conditions, such as capacitor restrike. Thus, this section presents existing methods for the detection of voltage transients.

2.2.1 Waveform Methods

The main idea of waveform detection methods is to detect disturbances by comparing two consecutive cycles. Since there are different ways to compare two cycles of waveforms, there are some subtle differences among the various adaptations of the method. Three representative versions of the method are summarized as follows.

1. Two consecutive cycles of a waveform are compared sample-by-sample. A disturbance is detected if the comparison shows that the difference exceeds a user supplied magnitude threshold and lasts longer than a user-supplied minimum duration.

2. The two consecutive cycles of the waveform are first squared. Point-by-point differences are calculated on the squared values. The absolute values of the differences are summed over the comparison cycle to form a mean absolute variation in squared amplitude (MAVSA) value. If the value exceeds a threshold, a disturbance is detected.

3. The two consecutive cycles of the waveform are subtracted point by point. The RMS value of the differential waveform is then calculated. It represents the distance between the two cycles. A percentage distance is then calculated by dividing the RMS value of the differential cycle by that of a

healthy cycle. If the percentage value exceeds a threshold, a disturbance is detected.

The advantages and disadvantages of above methods are analyzed. The first method is the most flexible one. For users who are not experienced in selecting threshold values, the method may catch a lot of inconsequential disturbances or miss important disturbances. The third method is simpler since only one percentage threshold is needed. Since it compares an entire cycle, disturbances that last a fraction of a cycle have a high probability to be missed. The second method also compares one whole cycle and has the shortcoming of the third method. Furthermore, its square operation lacks theoretical foundation and physical meaning.

2.2.2 Wavelet Analysis Method

Reference [29] presents a wavelet analysis method to detect voltage transients. The method can be explained as follows: time-frequency plane is first computed; then the behavior of fundamental frequency and high frequency components is analyzed to detect the presence of voltage transients. Figure 2.5 illustrates an example of voltage transients. In this case, the fundamental frequency of the voltage signal is 50 Hz.

Figure 2.5(a) represents the voltage waveform. Figure 2.5(b)-(e) represent the profile at 50Hz, 350Hz, 650Hz and 1500Hz, respectively. In this case, high frequency peaks and sharp changes in the signal appear almost simultaneously. Peaks in the high frequency profiles are compared with threshold values to detect transients. A part of the signal which is assumed to be disturbance-free, is used to derive the threshold values. It should be noted that voltage sags also show abnormal behavior in high frequency components. In order to differentiate voltage transients and sags, the duration and number of peaks exceeding threshold values are important parameters that can be used [29].

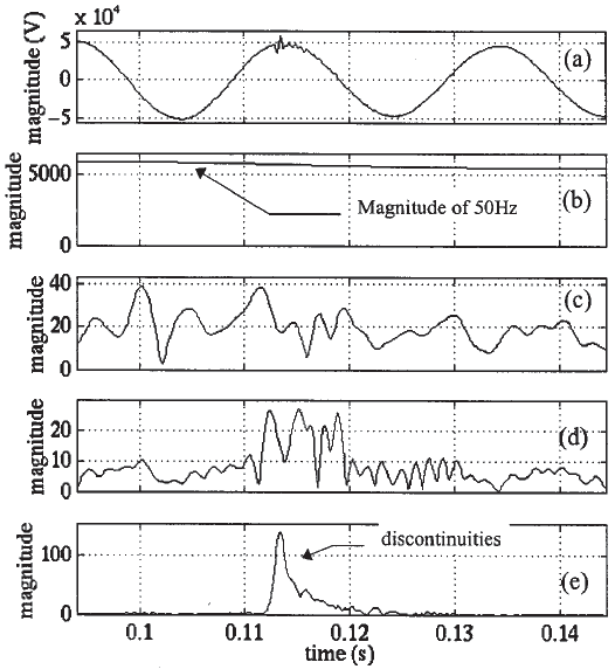

Figure 2.5: Wavelet transform of voltage transients [29].

2.3 Composite Method

Reference [30] presents a composite method to detect disturbances. Multiple parameters are computed using voltage and current signals.

- Harmonic and non-harmonic components below 16th harmonic are computed for each current input. The calculation is conducted one time for every period of two cycles.
- Current and voltage RMS values are computed. One RMS value is derived for every two-cycle data from each input.
- The real, reactive, and apparent power are computed one time for every period of two cycles.
- Energy is computed for high-frequency current channels.

A running average is derived for each parameter. For each parameter shown above, this method uses the running average to calculate two trigger thresholds;

one upper threshold and one lower threshold. For every two-cycle interval, each parameter is compared with the corresponding thresholds. If any of the above parameters falls beyond the range set by the upper and lower thresholds, a disturbance is detected, as shown in (2.10).

$$X(i) > \alpha X_{mean} \qquad or \qquad X(i) < \beta X_{mean} \tag{2.10}$$

where $X(i)$ represents the ith value of any of above parameters; X_{mean} represents the running average; α is the coefficient (larger than 1) corresponding to the upper threshold; β is the coefficient (less than 1) corresponding to the lower threshold.

The use of each parameter in this composite method is actually similar to the current fundamental component method illustrated in Section 2.1.3. Figure 2.4 can help readers to understand the detailed process of this composite method.

2.4 Proposed Improved Method

By combining the strength of various known methods with our research experiences, an improved abnormally detection method is developed for testing and demonstration. This method is illustrated here for the purpose of revealing the main issues that need to be considered when developing abnormality detection methods. The main characteristics of the illustrative method are that 1) both voltage and current signals are used and 2) both the variations of waveforms as well as RMS values are used. The overall flowchart of the method is shown in Figure 2.6.

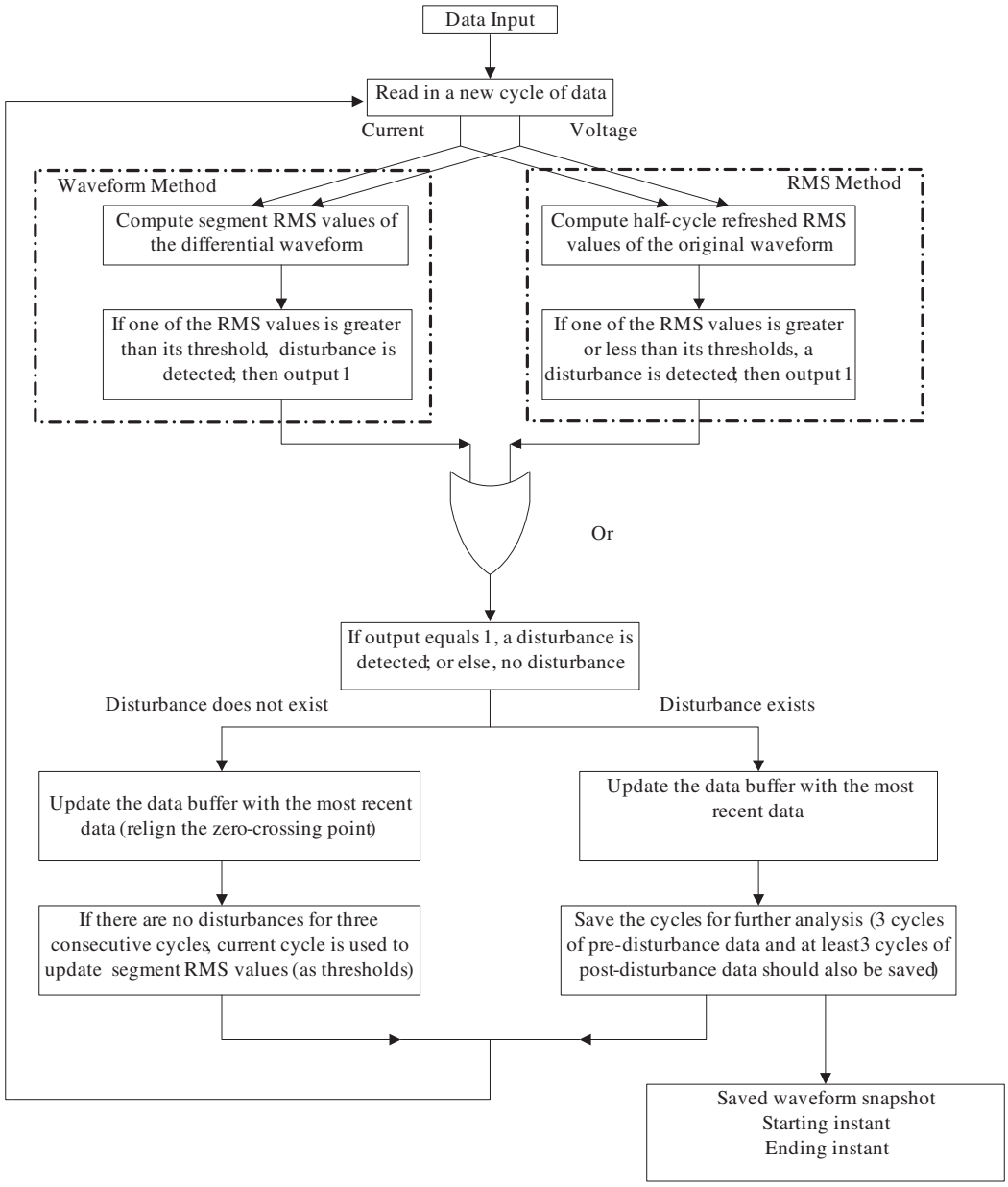

Figure 2.6: Detailed process of the proposed improved method.

2.4.1 Description of the Method

Due to the diverse signatures of equipment failures, both the waveform abnormality and RMS value abnormality in voltage and current signals are used in this method in order to detect all types of associated abnormalities. In other

words, four different features are applied concurrently for disturbance detection. The detailed steps of detection using waveform abnormality and detection using RMS value abnormality are illustrated below.

(1) Detection Using Waveform Abnormality

Waveform method detects the presence of disturbances by comparing consecutive cycles of waveform data. When the difference between two consecutive cycles exceeds a certain threshold, a disturbance is detected. Since there are different ways to compare two cycles of waveforms, there are some subtle differences among the various adaptations of the method. Three representative versions of waveform method have been summarized in Section 2.2.1. A new waveform detection method is proposed by combining the advantages and avoiding the disadvantages of the three methods.

The new waveform method can be explained as follows. The differential waveform between two consecutive cycles is computed first. The waveform is then divided into M segments (for example M=8). RMS value is calculated for each segment. If one of the segment RMS values is greater than a threshold, a disturbance is detected. This criterion is described using the following equation.

$$\Delta X_{RMS}(i) > \alpha X_{RMS}(i) \qquad i = 1, ..., M \tag{2.11}$$

where $\Delta X_{RMS}(i)$ is the root-mean-square value of the ith segment of the differential waveform $\Delta x(t)$; $X_{RMS}(i)$ is the root-mean-square value of the ith segment of the pre-disturbance (or reference) waveform $x(t)$; α is the threshold value supplied by user.

$\Delta X_{RMS}(i)$ and $X_{RMS}(i)$ can be calculated using the following equations:

$$\Delta X_{RMS}(i) = \sqrt{\frac{\sum_{k \in i} \Delta x^2(k)}{\frac{N}{M}}} \qquad i = 1, ..., M \tag{2.12}$$

$$X_{RMS}(i) = \sqrt{\frac{\sum\limits_{k \in i} x^2(k)}{\frac{N}{M}}} \qquad i = 1, ..., M \tag{2.13}$$

where N is the number of samples in one power cycle; $\Delta x(k)$ is the kth point in differential waveform; $x(k)$ is the kth point in the reference waveform.

This proposed waveform detection method is illustrated in Figure 2.7 and Figure 2.8. This method is simple to implement and can successfully detect disturbances which last only a section of one cycle.

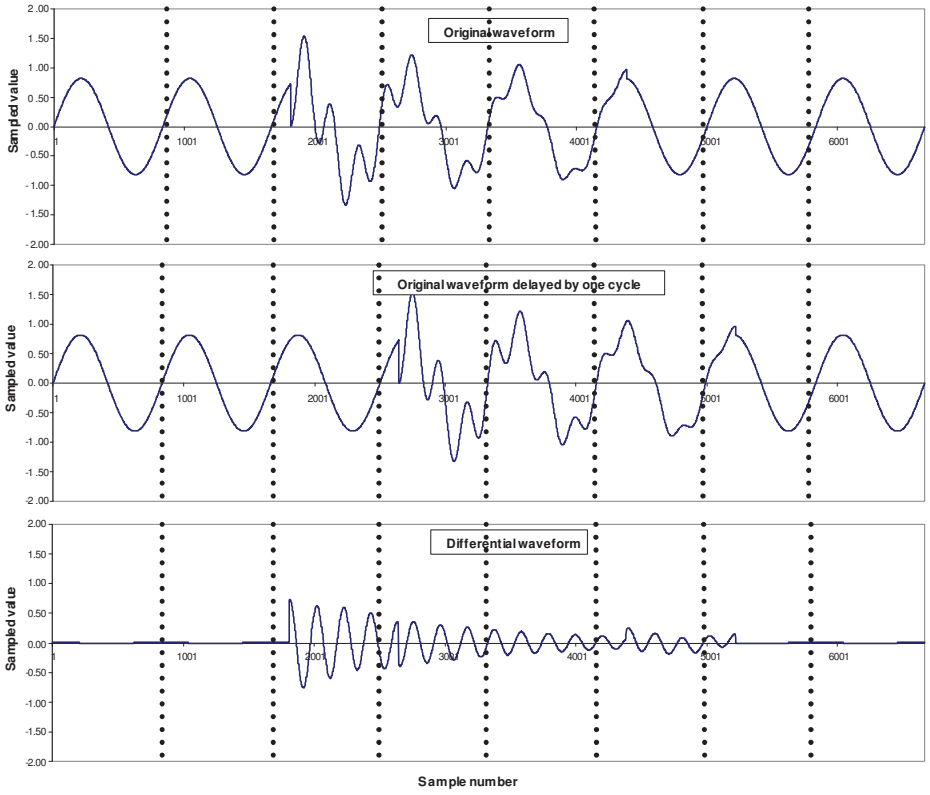

Figure 2.7: Illustration of the proposed method to derive differential waveform.

The reference cycle is a healthy cycle which is disturbance-free. When there are no disturbances in three consecutive cycles, the current cycle is used as a reference cycle and its segment RMS values are calculated from (2.13). Thresholds are updated with the new segment RMS values. If any cycle of last three consecutive cycles contains disturbances, the thresholds will not be updated.

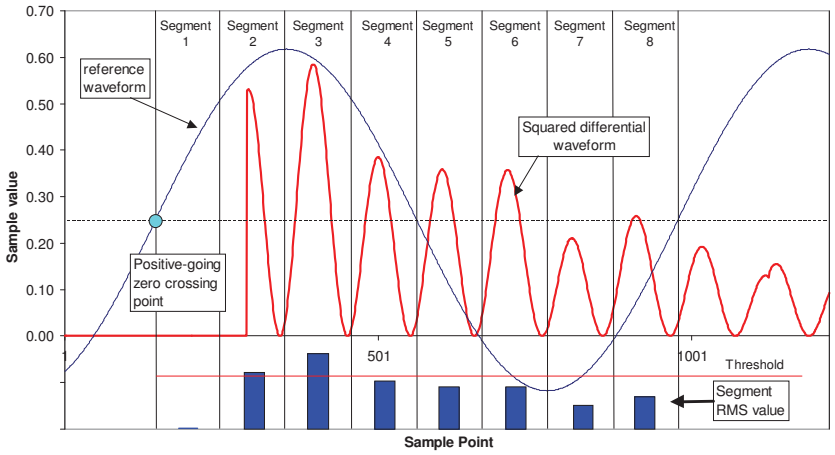

Figure 2.8: Illustration of detection using waveform abnormality for the proposed method.

This detection method using waveform abnormality is an adapted version of the third waveform method in Section 2.2.1. The novelty of this adapted method is that instead of using the RMS value of a whole cycle of differential waveform, this adaption detects abnormality using small segment (part of one cycle) RMS value of differential waveform. This can increase the sensitivity in detecting abnormalities that last only a fraction of one cycle.

When using the proposed waveform method, there are two practical issues to consider. First, when doing subtraction calculation for two consecutive cycles, positive going zero crossing point needs to be checked if the first cycle is disturbance-free. The comparison of two consecutive cycles starts from the positive going zero crossing point. Second, the real frequency of a power system usually fluctuates in a small range near the nominal value, which will result in phase difference between the corresponding points in two consecutive cycles. Thus, frequency variation correction is needed. Detailed methods for zero crossing point detection and frequency variation correction is provided in Appendix A. It should be noted that though the two operations are useful add-on, they are not necessary, especially when the waveform distortion level is big. In the presence of high waveform distortion, these two operations may increase

false alarms due to the possible error in getting the differential waveform and the ratios of segment RMS values of differential waveform to those of reference waveform.

(2) Detection Using RMS Value Abnormality

The basic idea of the proposed RMS method is to detect disturbances by evaluating the RMS values of current and voltage signals. Every half cycle, this method calculates RMS values using one-cycle data. If any RMS value exceeds the range defined by the upper and lower limits, a disturbance is detected. Compared with detection methods which utilize RMS values updated every whole cycle, this half-cycle refreshed method has better time resolution. The reason why we use both the RMS value abnormality and waveform abnormality is that we can avoid the situation when one disturbance that contains several cycles of similar waveform is detected as two disturbances if only using the waveform method, such as the voltage sag caused by motor starting [31]. Figure 2.9 illustrates the detailed process of this RMS method.

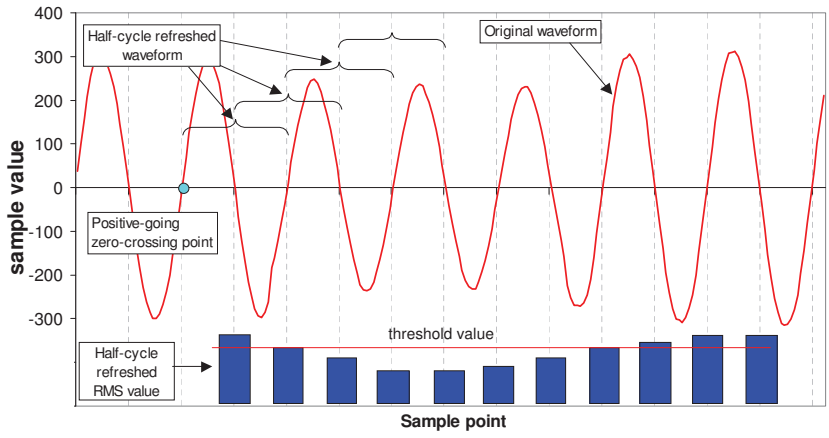

Figure 2.9: Illustration of detection using RMS value abnormality for the proposed method.

Half-cycle refreshed RMS value refers to the RMS value calculated for a

one-cycle sliding window that refreshes every half-cycle. In other words, half of the data used for calculating a RMS value is fresh data. When the data of a new cycle arrive, two RMS values need to be calculated. One is $X'_{RMS(1/2)}$ which is the RMS value calculated using the last half samples in the previous cycle and the first half samples in the current cycle. The other one is $X_{RMS(1/2)}$ which is the RMS value of the current cycle. It should be noted that the RMS value is calculated for the original waveform, not for the differential waveform. Besides, if the previous cycle is disturbance free, its zero crossing point needs to be checked. If one of the half-cycle refreshed RMS values is greater than or less than certain thresholds, a disturbance is detected. The criteria are described using the following equations.

$$X'_{RMS(1/2)} < \beta_{sag} X_{RMS} \qquad or \qquad X_{RMS(1/2)} < \beta_{sag} X_{RMS} \tag{2.14}$$

$$X'_{RMS(1/2)} > \beta_{swell} X_{RMS} \qquad or \qquad X_{RMS(1/2)} > \beta_{swell} X_{RMS} \tag{2.15}$$

where X_{RMS} is the nominal RMS value of the original waveform $x(t)$; β_{sag} and β_{swell} are the threshold values supplied by user.

X_{RMS} can also be calculated with the following equation.

$$X_{RMS}(n) = 0.9967 X_R MS(n-1) + 0.0033 X_1 2RMS, \tag{2.16}$$

where $X_{RMS}(n)$ is the current reference RMS value; $X_{RMS}(n-1)$ is the previous reference RMS value; X_{12RMS} is the RMS value calculated by the latest 12 healthy cycles.

If all equations in (2.17)-(2.19) are satisfied for three consecutive cycles, a disturbance can be considered to have ended.

$$\Delta X_{RMS}(i) < \alpha X_{RMS}(i) \qquad i = 1, ..., M \tag{2.17}$$

$$\begin{cases} X'_{RMS(1/2)} > (\beta_{sag} + \beta_{hysteresis}) X_{RMS} \\ X_{RMS(1/2)} > (\beta_{sag} + \beta_{hysteresis}) X_{RMS} \end{cases} \tag{2.18}$$

$$\begin{cases} X'_{RMS(1/2)} < (\beta_{swell} - \beta_{hysteresis}) X_{RMS} \\ X_{RMS(1/2)} < (\beta_{swell} + \beta_{hysteresis}) X_{RMS} \end{cases} \tag{2.19}$$

where $\beta_{hysteresis}$ stands for hysteresis value and its typical value is 2%.

The results of the disturbance detection procedure are listed below.

- Starting time of the disturbance (in the unit of sample number)
- Ending time of the disturbance (in the unit of sample number)
- Disturbance waveform including three or more cycles of pre-disturbance data and at least three cycles of post-disturbance data

Figure 2.10 illustrates the output of the proposed disturbance detection procedure.

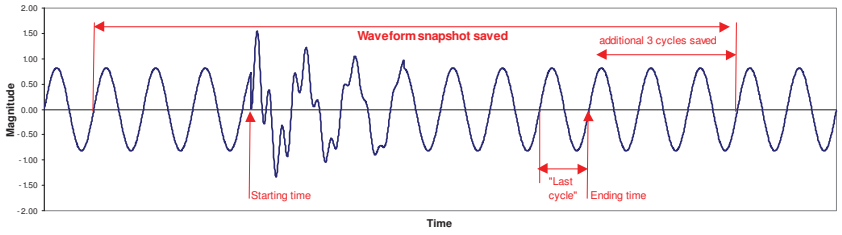

Figure 2.10: Output of disturbance detection procedure for the proposed method.

(3) Threshold Values

The setting of threshold values is very important for the accuracy of disturbance detection. For the proposed method in previous sections, critical parameters whose values need to be set are M, α, β_{sag} and β_{swell}. Typical values used for detection of voltage disturbances are shown in Table 2.1.

Table 2.1: Typical parameter values.

Level of capability	M	α	β_{sag}	β_{swell}
1	8 or 16	7% - 20%	70% - 90%	110%
2	16 or 32	7% - 20%	70% - 90%	110%
3	3000 to 4000	7% - 20%	70% - 90%	110%
4	Specialized instruments have their own methods for disturbance detection			

Since current signals are more prone to various disturbances than voltage signals, these parameters need to be reset when used for detection of current disturbances. In normal conditions, variations in current RMS values are relatively bigger than variations in voltage RMS values. However, the difference is not significant. Thus, the typical values of β_{sag}, β_{swell} and M in Table 2.1 can be adopted for the detection of current disturbances as well. In normal conditions, the waveform distortion of current signals is much more serious than that of voltage signals. If similar values are used for the detection of current disturbances, many inconsequential disturbances may be captured. Thus, these values need to be reset. After applying different values to a large amount of field measurement data, we recommend to adopt the values between 27% and 40%.

2.4.2 Test Results

The proposed method is applied to a multi-day field record and the main results are shown in this section. The purpose is to demonstrate the type of abnormalities in the waveforms. Table 2.2 shows the measurement setup. Figure 2.11 shows the metering point in the substation. The parameters used for threshold setting are shown in Table 2.3.

Table 2.2: Measurement setup.

Measured signals	Substation three-phase bus voltages and feeder currents
Measurement duration	Two weeks
Sample points per cycle	64
Sampling mode	Continuous (i.e. no gap in the data)
PT ratio	14.1:0.12
CT ratio	1200:5

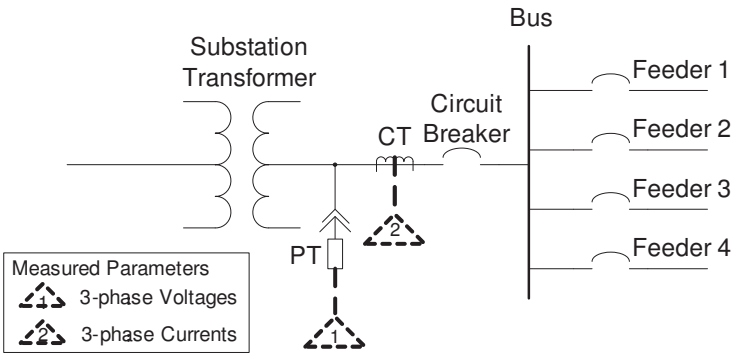

Figure 2.11: Measurement point and measured parameters.

Table 2.3: Thresholds used for abnormality detection.

	M	α	β_{sag}	β_{swell}
I	8	36%	90%	110%
V	8	17%	90%	110%

The number of abnormalities or disturbances captured by different features is shown in Table 2.4 and in Figure 2.12. Since some disturbances can be detected by two or more algorithms, the summation of the four percentage values is larger than 1. Figure 2.13 shows the distribution of disturbances at different hours captured by using different features.

Table 2.4: Number of disturbances captured by using different features.

	Voltages	Currents
RMS method	4	41
Waveform method	24	89

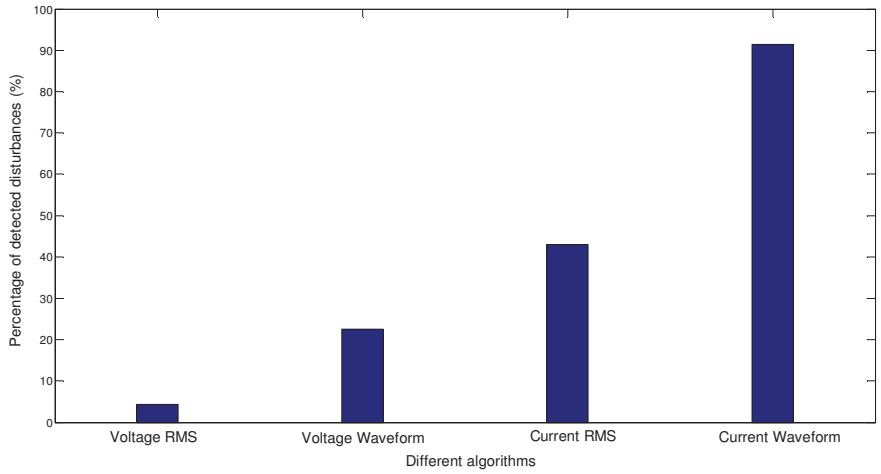

Figure 2.12: Percentage of disturbances detected by using different features.

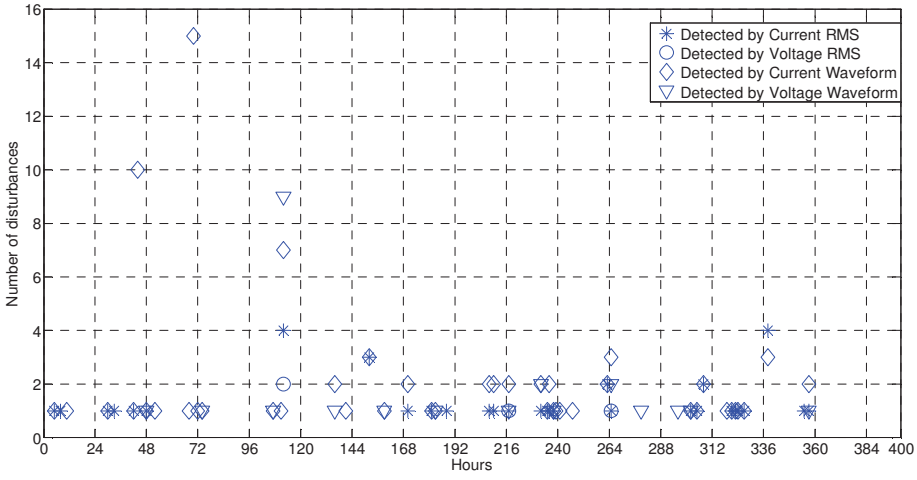

Figure 2.13: Distribution of disturbances at different time.

The detection results include disturbances of the following categories: (1) transients; (2) overcurrent; (3) low-level current variations; (4) increase of current waveform distortion. Disturbances of these different categories are pre-

sented in Figure 2.14 to Figure 2.21.

(1) Transients.

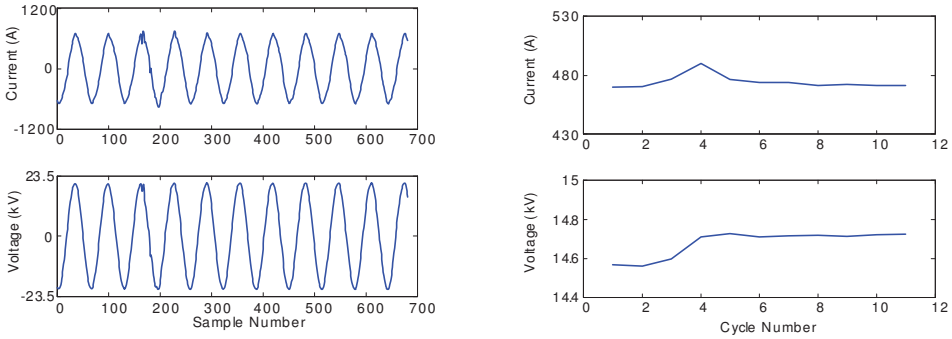

(a) Waveforms. (b) RMS trends.

Figure 2.14: Transients-case 1.

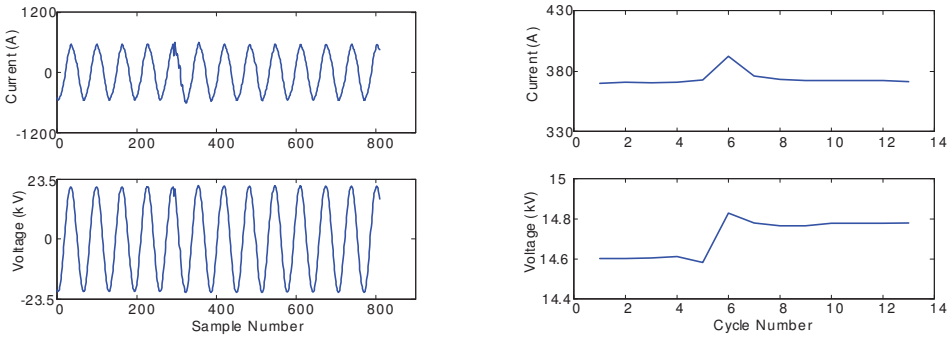

(a) Waveforms. (b) RMS trends.

Figure 2.15: Transients-case 2.

(2) Overcurrent.

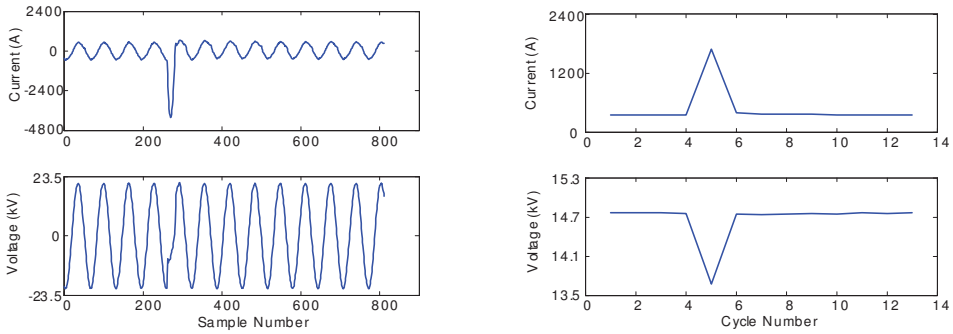

(a) Waveforms. (b) RMS trends.

Figure 2.16: Overcurrent-case 1.

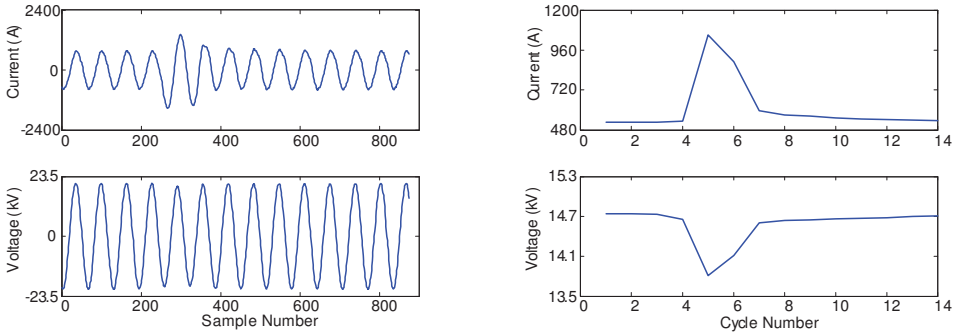

(a) Waveforms. (b) RMS trends.

Figure 2.17: Overcurrent-case 2.

(3) Low-level current variations.

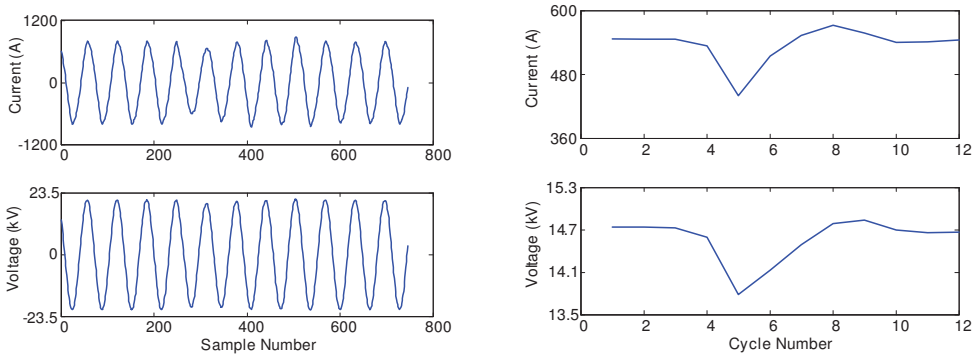

(a) Waveforms. (b) RMS trends.

Figure 2.18: Low-level current variation-case 1.

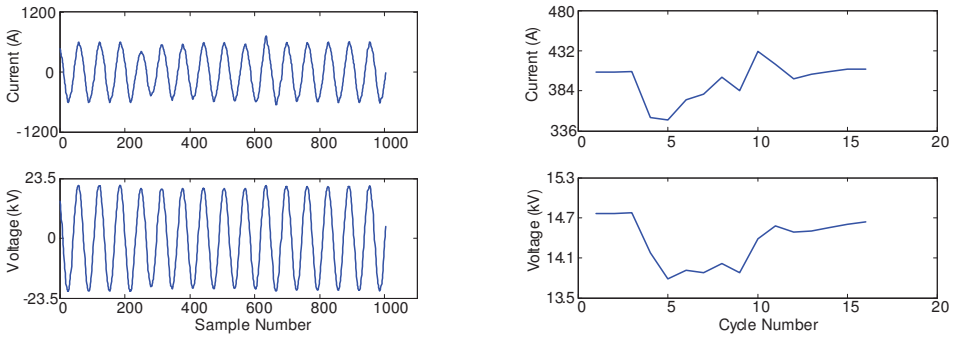

(a) Waveforms. (b) RMS trends.

Figure 2.19: Low-level current variation-case 2.

(4) Increase of current waveform distortion.

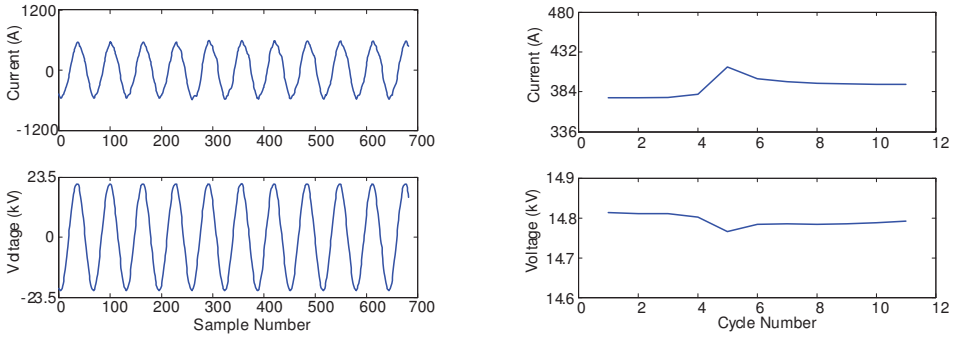

(a) Waveforms. (b) RMS trends.

Figure 2.20: Increase of current waveform distortion-case 1.

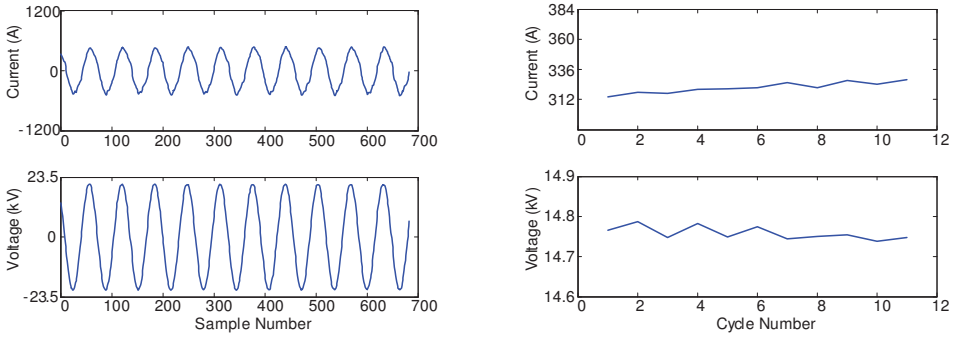

(a) Waveforms. (b) RMS trends.

Figure 2.21: Increase of current waveform distortion-case 2.

Chapter 3

Generic Waveform Abnormality Detection Method Based on Statistical Distribution

As shown in the last chapter, there are several studies on the detection of waveform abnormalities for utility equipment condition monitoring [8, 9, 27, 28, 29]. But they are all focused on the detection of waveform abnormality associated with certain specific types of incipient failures. For example, the work in [8, 9, 28] are for underground cable failures. Although the improved traditional method we proposed in Section 2.4 combines the advantages of existing abnormality detection methods, there are some limitations for the method in detecting generic waveform abnormalities due to the fact that it still follows traditional methods for abnormality detection and that waveform abnormalities that are associated with utility equipment failures are less explicit in voltage and current magnitudes, RMS values, etc. Furthermore, with existing schemes, the detection thresholds are usually selected by experiences and largely vary for different scenarios, which impede their use in general setups.

In this chapter, a new detection framework based on the distribution of the power signals is proposed. We formulate the detection problem as a binary hy-

pothesis test to differentiate normal situation and abnormal situation. Under normal situation, the residual data which is extracted by removing the steady-state components of the waveforms are modeled as Gaussian samples. Under abnormal situation, however, the residual data deviate largely from Gaussian samples. The Kullback-Leibler divergence (KLD) is then applied to quantify the deviation. An abnormality is detected if the KLD is larger than a threshold. In contrast to the power quality disturbance detection which mainly uses voltage waveforms, the proposed method is based on current waveforms as they are more sensitive to equipment condition. The challenge associated with the large deviations of currents due to load changes is overcome through the adoption of KLD as the distance measure and a proposed systematic threshold selection scheme that maximizes the detection probability for a given false alarm probability.

The remaining of the chapter is organized as follows. Section 3.1 presents the detection problem formulation, the current residual data extraction, and the modelling of the residual data. The detection rule, the threshold selection, and the summarized detection procedure are provided in Section 3.2. The test results and comparison with existing work are shown in Section 3.3. Finally, a brief summary is presented in Section 3.4. To help the presentation, we list the important symbols used in this chapter and their meanings in Table 3.1.

Table 3.1: List of symbols used in algorithm description

Symbol	Meaning
t	time instant
$i(t)$	measured current signal
$\hat{h}(t)$	steady-state components
f_n	nominal power frequency
f_r	operating power frequency
$\tilde{i}(t)$	residual signal
N_G	window size for Gaussian estimation
N_H	window size for steady-state components estimation
N_d	window size for detection
N_0	number of sampling points in one cycle
$\hat{m}$	estimated mean of Gaussian distribution
$\hat{\sigma}^2$	estimated variance of Gaussian distribution
$f_n(x)$	pdf of Gaussian distribution
$\hat{f}(x)$	estimated pdf of residual data
D_{th}	detection threshold

3.1 Hypothesis Testing Model for General Abnormality Detection

The goal of this work is to detect generic waveform abnormalities related to conditions of utility equipments, including overhead lines, cables, transformers, capacitors, circuit breakers, and lightning arresters, etc. The detailed signatures of various equipment failures can be found in the Chapter 2. Abnormalities related to equipment conditions often show asymmetric and sporadic current signatures with diverse time scales, and they are often more visible in current waveforms as opposed to voltage waveforms. Thus, we study the current signal measured at the feeder. The abnormality detection problem is naturally a binary hypothesis test where the two hypotheses are H_0 : there is no abnormality and H_1 : there is an abnormality.

Under normal situation (Hypothesis H_0), the current signal contains nor-

mal load component and random noise/fluctuations caused by random load behavior and data acquisition devices. When an abnormality exists (Hypothesis H_1), a fault component is superimposed on the normal current signal. Thus, the hypothesis test problem can be formulated as follows.

$$H_0 : i(t) = \sum_{k=0}^{K} A_k \cos\left(2\pi k f_r t + \varphi_k\right) + n(t), \tag{3.1}$$

$$H_1 : i(t) = \sum_{k=0}^{K} A_k \cos\left(2\pi k f_r t + \varphi_k\right) + n(t) + a(t), \tag{3.2}$$

where the t is the time instant, $i(t)$ is the current signal measured at the substation, A_k and φ_k are the magnitude and phase angle of the kth harmonic component, K is the highest harmonic order, f_r is the fundamental operating frequency, $n(t)$ represents the random noise, and $a(t)$ represents the fault component. Ideally, $f_r = f_n$ where f_n is the nominal frequency, e.g. 60Hz in North America. But in reality, the operating frequency fluctuates slightly around the nominal frequency and may change from cycle to cycle. In real applications, discrete-time samples of the feeder current are measured, thus t takes discrete values $t = n\Delta t$ for $n = 1, 2, \cdots$, where Δt is the sampling time.

The steady-state components in the current signal, $\sum_{k=0}^{K} A_k \cos(2\pi k f_r t + \varphi_k)$, is common for both hypotheses, thus contain no useful information for the abnormality detection. We propose to estimate the steady-state components and subtract them from the current signal to reveal the residue. Also, since our goal is to detect general abnormality instead of any specific type of equipment failure, $a(t)$ is unknown and can take a large variety of forms. Thus we can only rely on signatures of the normal situation for detection. In this work, we propose to detect the abnormality based on how well the observed current signal matches the H_0 hypothesis. For this to be possible, the noise $n(t)$ needs to be understood and modelled.

In the following subsections, we solve the aforementioned two issues in our

detection model: the estimation of the steady-state components and the modeling of the noise.

3.1.1 Steady-State Components Estimation

Since within the period of a few cycles, the steady-state components are approximately the same, we estimate the steady-state components of the current cycle from the previous one or several cycles, which we refer to as the reference cycles. Let N_H be the number of reference cycles used for the steady-state components estimation. The effect of N_H on the detection performance will be discussed in Section 3.3.1.

By applying FFT on the current samples of the reference cycles, estimations of the magnitudes and phase angles of the steady-state components can be obtained, which are denote as $\hat{A}_k$ and $\hat{\varphi}_k$, for $k = 0, 1, ..., K$. Under the ideal assumption that there is no fluctuation in the operating frequency, the steady-state components of the current cycle can be estimated as

$$\hat{h}(t) = \sum_{k=0}^{K} \hat{A}_k \cos(2\pi k f_n t + \hat{\varphi}_k).$$

But in reality, operating frequency fluctuation always exists. To accommodate this for better detection performance, we first estimate the operating frequency via a one-dimensional searching. Let f_r be the operating frequency of the current cycle. Usually its value is within a small range around f_n. Denote its possible range as $[f_{\min}, f_{\max}]$. We conduct a grid search over the range to find the frequency that leads to the best match with the signal of the current cycle in the sense of energy. In other words, the error signal, which is the signal of the current cycle subtracted by the estimated steady-state components, has the smallest energy, or equivalently, the smallest RMS. The motivation behind the method is that the energy of the current signal is dominated by its steady-state components.

Without loss of generality, let the time origin $t = 0$ be the time instant the cycle of interest starts. Denote the total number of samples of one cycle as N_0. Thus, the samples of the cycle of interest are $i(l\Delta t)$ for $l = 1, \cdots, N_0$. Define

$$E(f) = \sum_{l=0}^{N_0} \left[i(l\Delta t) - \sum_{k=0}^{K} \hat{A}_k \cos(2\pi k l f \Delta t + \hat{\varphi}_k) \right]^2,$$

which is the energy of the error signal if the operating fundamental frequency is f. The operating fundamental frequency search can be mathematically represented as:

$$\hat{f}_r = \arg \min_{f \in [f_{\min}, f_{\max}]} E(f). \tag{3.3}$$

Thus the following estimation of the steady-state components can be obtained:

$$\hat{h}(t) = \sum_{k=0}^{K} \hat{A}_k \cos(2\pi k \hat{f}_r t + \hat{\varphi}_k). \tag{3.4}$$

By subtracting the steady-state components, the residual signal is obtained as

$$\tilde{i}(t) = i(t) - \hat{h}(t). \tag{3.5}$$

The hypothesis test in (3.1)-(3.2) is simplified into the following:

$$H_0 : \tilde{i}(t) = n(t), \tag{3.6}$$

$$H_1 : \tilde{i}(t) = n(t) + a(t). \tag{3.7}$$

We should note that if the steady-state components estimation is precise, the $n(t)$ in (3.6)-(3.7) is the same as the $n(t)$ in (3.1)-(3.2). If the estimation is with error, the $n(t)$ in (3.6)-(3.7) contains both the random noise and the estimation error. It models the overall random component in the residual signal.

Theoretically, variations in both the power system frequency and the sam-

pling frequency can impact the estimation of steady-state components. However, the impact of the power system frequency variation is usually much stronger. Thus in this work we only consider the impact of system frequency and neglect the variation of the sampling frequency. We have conducted the following studies to show this.

Using one-hour field data, we calculate the trends of both the power system frequency and the sampling frequency (using GPS clock). Results show that the largest deviation from the nominal power system frequency is 0.05Hz, and the largest deviation from the nominal sampling frequency is 0.52Hz. Based on these parameters, we use synthesized data (i.e. simulation in Matlab) to analyze the effect of the two kinds of variations on the estimation of the steady-state components. The following model is used:

$$x(n) = \sum_{k=1,3,5,7,9} a_k \cos\left(2\pi n k \frac{f_r}{f_s} + \varphi_k\right) + \omega(n), \tag{3.8}$$

where n is the sample index, f_r is the fundamental frequency, f_s is the sampling frequency. φ_k is the phase angle of the kth harmonic, and $\omega(n)$ is the white Gaussian noise. We set $a_1 = 1$, $a_3 = 0.02$, $a_5 = 0.03$, $a_7 = 0.01$, $a_9 = 0.02$, $SNR = 50dB$. Without loss of generality, φ_k are set to be 0. The following three cases are considered: (1) $f_r = 60Hz$, $f_s = 64 \times 60 = 3840Hz$; (2) $f_r = 60.05Hz$, $f_s = 64 \times 60 = 3840Hz$; and (3) $f_r = 60Hz$, $f_s = 64 \times 60 - 0.52 = 3839.48Hz$. Case 1 is the perfect case with no variation, Case 2 has $0.05Hz$ variation in the power system frequency while the sampling frequency is perfect, and Case 3 has $0.52Hz$ variation in the sampling frequency while the power system frequency is perfect.

Since the behavior of estimated residuals can be used to evaluate the quality of the steady-state components, the estimated residuals are shown above in Figure 3.1 in this response. We can see from this figure that the impact of the system frequency variation is much greater than the sampling frequency vari-

ation. Thus in this work we only consider the impact of the system frequency and neglect the variation of the sampling frequency. To avoid the strong effect of the variation in system frequency, frequency variation correction is proposed in this chapter. With the correction, we can see from Figure 3.1 that the error in the residual estimation is greatly reduced.

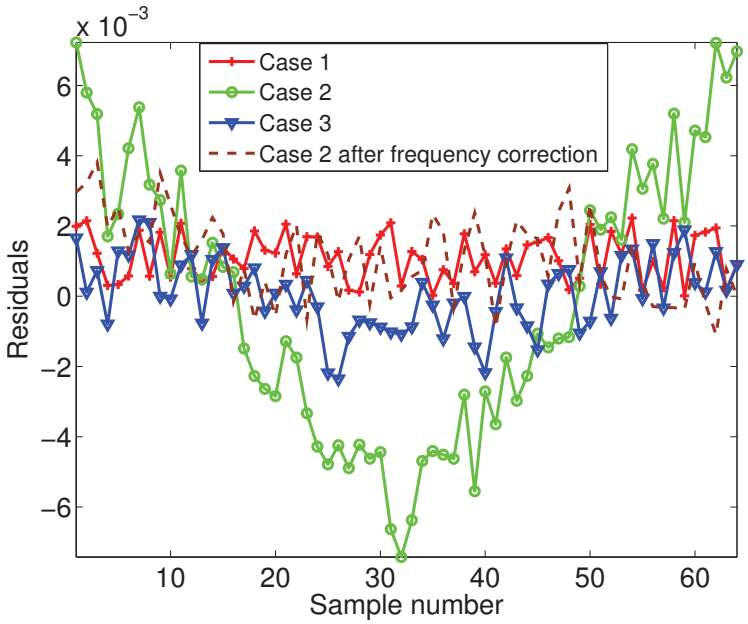

Figure 3.1: Residuals under different cases.

3.1.2 Modelling of the Noise Component

Understanding the noise component $n(t)$ is crucial for the detection problem. The Gaussian model is the most widely used and validated noise model in various areas such as control systems, communications, and signal processing. It is also adopted in power systems [32, 33]. In this work, we assume that $n(t)$ is an ergodic Gaussian random process, thus the discrete-time residual samples $n(l\Delta t)$ follows a Gaussian distribution. To validate the assumption, tests on the field current data are conducted. The data are measured at one end of a transmission cable which is located in a 138kV ring network. The sampling frequency is 3840Hz with the nominal frequency of 60Hz, i.e., 64 points per

cycle. For the tests on the noise distribution, we randomly choose 1000 events, where each event contains 5 cycles of current samples, i.e., 320 sample points. All chosen events are normal ones without abnormality.

For each cycle of the chosen events, the steady-state components are estimated and subtracted using the scheme explained in Section 3.1.1 to obtain the residual signals. To test whether the residual signals follow Gaussian distribution (also called the normality test), several statistical methods are used, including the classic Shapiro-Wilk, Anderson-Darling, and Jarque-Bera tests [34]. If an event passes any of the three tests, the event is considered to pass the normality test. Our experiments on the 1000 events show that the pass rate is 94.4%, which validates the Gaussian assumption.

Under the Gaussian assumption, to fully understand the noise, we only need its mean and variance, which can be estimated from the residual signals. Let N_G be the number of cycles of residual data used for estimating the mean and variance, and recall that N_0 is the number of samples for each cycle. Denote the discrete-time residual data of the N_G cycles as $\tilde{i}_{1,1}, \cdots, \tilde{i}_{l,r}, \cdots, \tilde{i}_{N_G,N_0}$, where $\tilde{i}_{l,r}$ represents the r-th point in the l-th cycle. The unbiased estimates of the mean and variance are [35]

$$\hat{m} = \frac{1}{N_0 N_G} \sum_{l=1}^{N_G} \sum_{r=1}^{N_0} \tilde{i}_{l,r}, \tag{3.9}$$

$$\hat{\sigma}^2 = \frac{1}{N_0 N_G - 1} \sum_{l=1}^{N_G} \sum_{r=1}^{N_0} \left(\tilde{i}_{l,r} - \hat{m}\right)^2. \tag{3.10}$$

The probability density function (pdf) of the Gaussian distribution for the noise is thus

$$f_n(x) = \frac{1}{\sqrt{2\pi\hat{\sigma}^2}} e^{-\frac{(x-\hat{m})^2}{2\hat{\sigma}^2}}. \tag{3.11}$$

The assumption that $n(t)$ is an ergodic Gaussian random process is an ideal

one. In reality, the parameters of the Gaussian model may vary with time. Thus, in real applications, the mean and variance estimates of the Gaussian noise pdf can be updated continuously or periodically to improve the accuracy of the noise modelling.

3.2 Generic Abnormality Detection Scheme

In this section, we present the proposed detection rule and the threshold selection method. Then an algorithm that summarizes the proposed detection scheme is provided.

3.2.1 Abnormality Detection Rule and Threshold Selection

With the modelling in Section 3.1, under Hypothesis H_0 (no abnormality), the current residual samples follow the Gaussian pdf in (3.11). On the other hand, under Hypothesis H_1 (an abnormality exists), the residual samples are expected to largely deviate from the Gaussian pdf in (3.11) but follow the shape of the fault/abnormality $a(t)$. However, since $a(t)$ is unknown and has a large variety, it is impossible to conduct the traditional likelihood-ratio-based detection for binary hypothesis testing, for example, to decide on the hypothesis whose waveform shape is closer to the residual data.

Instead, we propose to detect whether an abnormality exists by comparing the distance between the distribution of the current residual samples and the Gaussian distribution in (3.11) with a threshold. If the distance is smaller than the threshold, the residual samples have a good match with the noise pdf, thus an abnormality does not exist. On the other hand, when it is larger than the threshold, the distribution of the residual samples does not match the Gaussian pdf of the noise and an abnormality exists. The detection idea is illustrated in Figure 3.2.

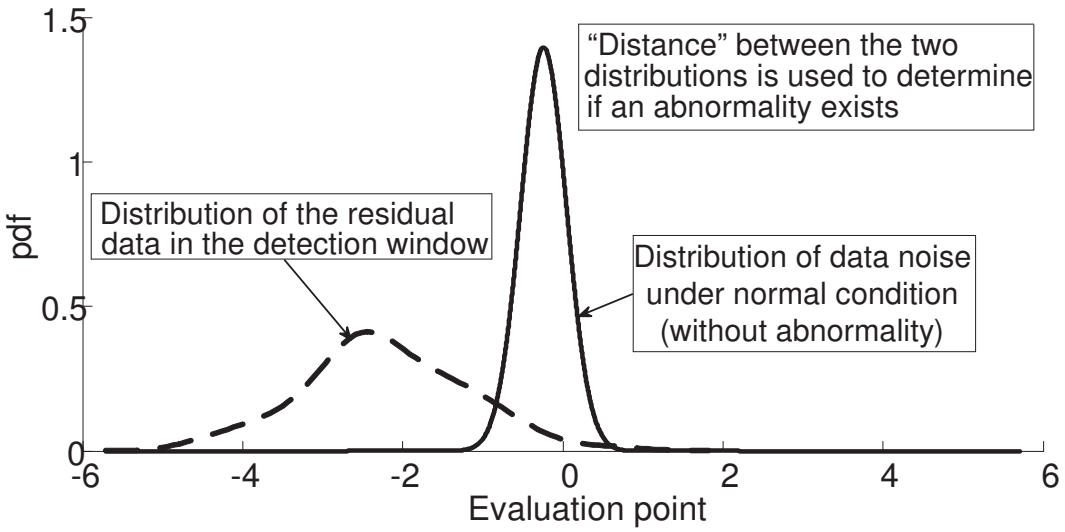

Figure 3.2: Illustration of the proposed detection rule.

To materialize this detection idea, we need to conduct the following three tasks: to generate the distribution of the measurement residual data samples, to calculate the distance between the two distributions, and to select the threshold. In what follows, we explain the three tasks sequentially.

(1) Empirical Residual Distribution Generation

We first explain how the distribution of the measurement residual data is generated. Recall that the residual data are the current samples measured at the feeder subtracted by the estimated steady-state components as given in (3.4) and (3.5). Let N_d be the number of cycles of the current data used for the abnormality detection, thus there are $N_0 N_d$ data points in a detection window. For the simplicity of presentation, denote the residual samples of the detection window as $x_{1,1}, \cdots, x_{l,r}, \cdots, x_{N_d,N_0}$,

$$x_{l,r} = \tilde{i}((l-1)N_0\Delta t + r\Delta t), \tag{3.12}$$

which is the r-th point in the l-th cycle of the residual data. Kernel density

estimation is used to generate the empirical residual pdf. Kernel density estimation is a fundamental method to estimate the pdf of a distribution from a finite set of independent and identically distributed (i.i.d.) samples drawn from this distribution [36]. It has the same basic principle as the histogram but possesses more appealing properties such as the smoothness. Given the discrete samples $x_{1,1}, \cdots, x_{l,r}, \cdots, x_{N_d,N_0}$, kernel density estimation of the pdf of the residual data is:

$$\hat{f}(x) = \frac{1}{N_0 N_d h} \sum_{l=1}^{N_d} \sum_{r=1}^{N_0} K\left(\frac{x - x_{l,r}}{h}\right), \tag{3.13}$$

where $K(x)$ is the kernel function and h is the bandwidth (or smoothing parameter). The kernel function is a zero-mean pdf, implying that it is non-negative and it integrates to 1. Common kernel functions include uniform, triangular, biweight, Epanechnikov, and Gaussian distribution functions. Here, we use the standard Gaussian distribution function due to its convenient mathematical properties. The bandwidth h is a positive parameter. Its value affects the smoothness and precision of the kernel density estimation. For Gaussian random variable, the optimal choice of h has been proved to be [36]:

$$h = \left(\frac{4\sigma^5}{3n}\right)^{\frac{1}{5}} \approx 1.06\sigma n^{-0.2}. \tag{3.14}$$

This result is adopted in our scheme.

It should be noted that the reason why we use kernel density estimation instead of histogram is that the kernel density estimation returns much smoother distribution than the histogram. This can be seen from Figure 3.3(b) which presents the histogram plot and the kernel density estimation of the residual signals in the abnormal cycle in Figure 3.3(a).

(2) Distance Measure

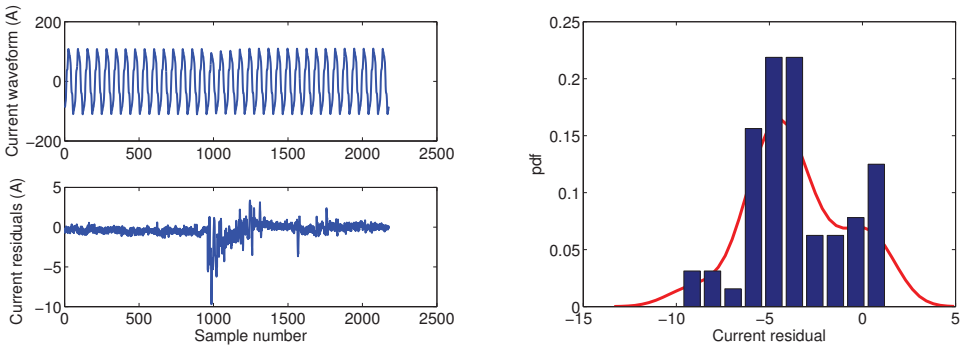

(a) Current and residual waveforms.

(b) Kernel density estimation and histogram of residual waveform.

Figure 3.3: Comparison between histogram and kernel density estimation.

To quantify the distance between the measured data and Hypothesis H_0, we use the KLD from the estimated pdf of the measured residual samples to the theoretical noise pdf under H_0. KLD is widely used in probability theory and information theory [37]. Let $p(x)$ and $q(x)$ be two pdfs. Thus they are both non-negative and integrate to 1. The KLD of q from p, denoted by $D_{KL}(p||q)$, is defined as [37]

$$D_{KL}(p||q) = \int_{-\infty}^{\infty} p(x) \ln \frac{p(x)}{q(x)} dx. \tag{3.15}$$

It provides a quantitative measure for the difference of q from p. It also equals the amount of information loss when using q to approximate p.

In this work, with the model in Section 3.1, under Hypothesis H_0, the theoretical pdf of the residual samples, f, is given in (3.11). Based on the measurement residual data of the detection window, we can obtain the kernel estimate of their pdf, $\hat{f}$, as in (3.13). The distance of the H_0 hypothesis from the observed event is thus $D_{KL}(\hat{f}||f)$. For the numerical integration in the KLD calculation, the midpoint rule is used. In our experiments, the theoretical Gaussian pdf is estimated from previous normal (no abnormality) cycles before the detection window. In calculating the KLD, extra steps containing the RMS normalization and mean shift are conducted. Specifically, the current samples

are scaled so that the one-cycle-RMS values of the data are the same. Another step is to shift the residual data so the kernel estimation has the same mean as the Gaussian distribution estimated with (3.9). This can be realized by the following transformation of the current samples and the residual samples:

$$\hat{i}_{l,r} = i_{l,r}\frac{RMS(1)}{RMS(l)}, \tag{3.16}$$

$$\hat{x}_{l,r} = x_{l,r} - \frac{1}{N_0}\sum_{r=1}^{N_0} x_{l,r} + \hat{m}, \tag{3.17}$$

where the $RMS(l)$ is the RMS value of the l-th cycle, $i_{l,r}$ and $x_{l,r}$ represent the r-th current sample and r-th residue of the l-th cycle, respectively.

The reason behind this extra step is to deal with small load variations. Small load variations are very common and frequent phenomena in power systems. Thus, in this work, we classify small load variations as normal situation to avoid excessive alarm-raising and extra-sensitive detection. The transformation in (3.16) and (3.17) effectively avoids this problem. With the mean-shift and RMS-scaling, the calculated KLD value reflects mainly the shape difference of the two distributions.

(3) Detection Rule and Threshold Selection

Since the abnormality type has a large variety with different shapes and is unknown. For a generic scheme, we detect whether an abnormality exists by comparing the distance of the theoretical Gaussian distribution from the estimated distribution of the residual data with a threshold. The detection rule can be represented as follows:

$$\text{Decide on } H_0 \text{ if } D_{KL}(\hat{f}||f) \leq D_{th}, \tag{3.18}$$

$$\text{Decide on } H_1 \text{ if } D_{KL}(\hat{f}||f) > D_{th}, \tag{3.19}$$

where D_{th} is the threshold.

The selection of the threshold value is an important issue which determines the performance of the proposed scheme. Following detection theory, we choose the threshold to maximize the detection probability given the desired level of the false alarm probability. Denote the pdf of the KLD $D_{KL}(\hat{f}||f)$ as $p(s)$. With an arbitrary threshold value D_{th}, the false alarm probability can be calculated as

$$P_{FA}(D_{th}) = \int_{D_{th}}^{\infty} p(s)ds. \tag{3.20}$$

Let α be the desired false alarm probability. Since both the detection probability and the false alarm probability are non-increasing functions of D_{th}, the threshold value is the smallest value that satisfies $P_{FA}(D_{th}) \leq \alpha$. In other words,

$$D_{th} = \arg \min_{P_{FA}(x) \leq \alpha} x. \tag{3.21}$$

We propose the following steps for the threshold selection. It should be noted that the false alarm rate used to select threshold can be fixed or adaptive based on number of events detected in previous data.

- Step 1: Gather N_{KLD} sets of the residual data of previous cycles, where each set contains N samples.
- Step 2: For each set, calculate the kernel density estimation of the N samples, then calculate the KLD of the kernel estimation with the theoretical Gaussian noise pdf. Each KLD value is a sample of $p(s)$.
- Step 3: From the N_{KLD} KLD values, calculate the density estimation of $p(s)$.
- Step 4: Find the threshold value using (3.21) for the given false alarm rate α.

Figure 3.4 illustrates the false alarm probability as a function of the KLD threshold value D_{th} for a segment of the field data described in Section 3.1.2.

The threshold selection for the desired false alarm rate of 3.5% is shown. Based on (3.21), the corresponding KLD value, which is 13.74, is chosen as the threshold.

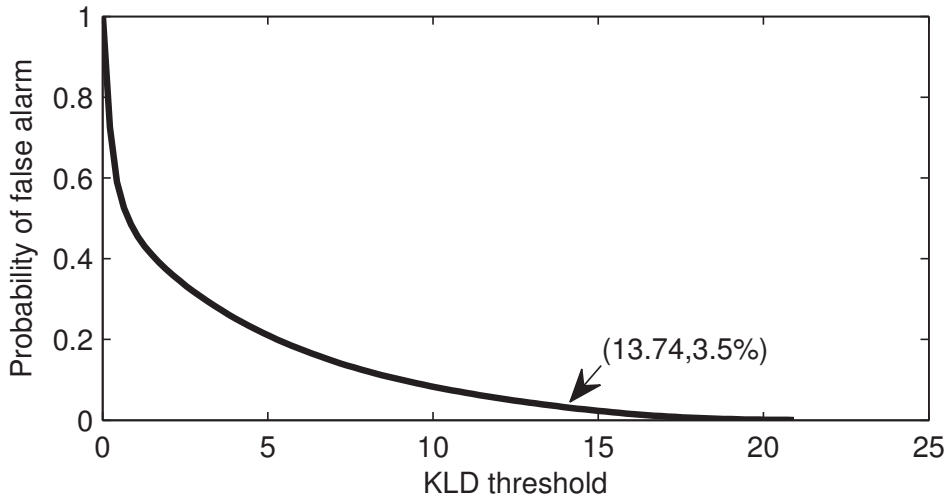

Figure 3.4: False alarm probability v.s. different threshold values for the field test data.

The threshold selection can overcome the difficulty to set proper threshold due to large variations of current values. It can also achieve automatic trigger setting by continuously or periodically updating the pdf of the KLD, $p(s)$. In real applications, we can also update the threshold setting by using a sliding time window prior to the signal that is being detected. The data inside the window can be used as the reference data for threshold selection.

3.2.2 Summary of the Proposed Detection Method

Based on the ideas and schemes discussed in Section 3.1 and Section 3.2.1, the overall procedure of the proposed method is summarized in Figure 3.5. This algorithm allows continuous and adaptive detection of abnormality for a monitoring device installed at a substation. In this procedure, the threshold is updated using a sliding window whose length is N_{KLD}. A buffer stores the most recent N_{KLD} KLD values. When N_{set} newest KLD values are added into the

buffer and N_{set} oldest KLD values are removed from the buffer, the threshold is updated.

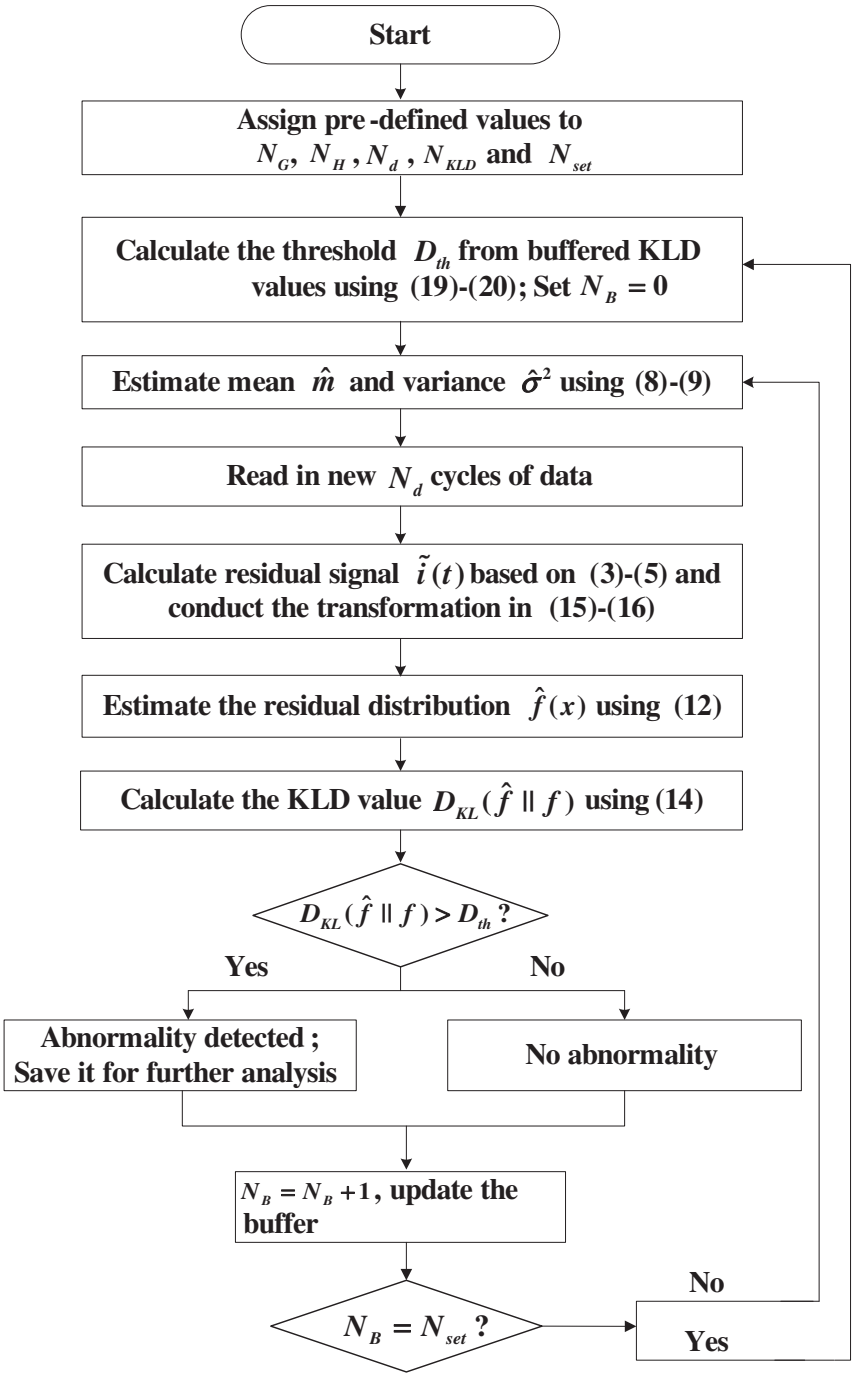

Figure 3.5: Detection procedure.

In the initialization step, values of several implementation parameters are

set. The selection of these values will be discussed in the next section. The threshold D_{th} is derived from N_{KLD} KLD values which are stored in a buffer. A counter N_B is set to be zero. It indicates the number of new-coming KLD values in the buffer after the last update of the threshold. Then, the theoretical Gaussian pdf for the normal situation and pdf of the residual data in the detection window are estimated. The KLD of the two pdfs are calculated and saved into the buffer. The calculation result is compared with the threshold to decide if there is an abnormality. If an abnormality is detected, the abnormal data are saved for further detailed analysis. Then the counter N_B increases by one. The KLD value is stored into the buffer and the oldest one KLD value is removed from the buffer. When $N_B = N_{set}$, i.e. N_{set} newest KLD values are added into the buffer and N_{set} oldest KLD values are removed from the buffer, the threshold D_{th} is updated based on buffered KLD values.

3.3 Performance of the Proposed Method

In this section, the performance of the proposed detection method is shown, where field measured data are used.

In showing the performance, we plot the probability of detection P_D versus the probability of false alarm P_{FA} curve. It is the mostly widely used performance measure for binary hypothesis test, and illustrates the trade-off between the detection performance and the tolerance of false alarm rate as the discrimination threshold varies [38]. For a certain false alarm probability, the bigger the corresponding detection probability is, the better the performance. On the other hand, for a certain detection probability, the smaller the corresponding false alarm probability is, the better the performance.

Comparison with existing methods is also important in validating the proposed method. While there are many work on fault detection of power systems, most of them are for specific kinds of faults with known characteristics. They

cannot be applied in our generic abnormality goal where the fault types are unknown and have a large variety. In [39], several waveform methods that can be used for comparison were mentioned. We use two of them in this work since the other was shown to be inferior.

The first competing method is a differential waveform RMS method, which detects abnormalities based on the segment RMS value of the differential waveform between consecutive cycles. The differential waveform RMS method can be explained as follows. First, the differential current waveform is obtained by subtracting the current values of the previous cycle from those of the current cycle, i.e.,

$$\Delta i(k\Delta t) = i(k\Delta t) - i((k - N_0)\Delta t), \tag{3.22}$$

where N_0 is the number of sample points in one cycle. Then, the differential waveform is seperated into M segments. For each segment, a RMS value is calculated. Ratios of the segment RMS values of the differential waveform to the segment RMS values of the reference waveform are derived as follows,

$$\alpha_{l,r} = \frac{\Delta I_{l,r}}{I_r}, \tag{3.23}$$

where $\alpha_{l,r}$ is the ratio of the r-th segment in the l-th cycle, $\Delta I_{l,r}$ is the segment RMS value of the r-th segment in the l-th cycle of the differential waveform and I_r is the r-th segment RMS value in the reference waveform. The maximum ratio is used to determine if an abnormality exists. The detection rule for the differential waveform RMS method can be represented as follows:

$$\text{Decide on } H_0 \text{ if } \alpha_{max,l} \leq \alpha_{th},$$
$$\text{Decide on } H_1 \text{ if } \alpha_{max,l} > \alpha_{th},$$

where $\alpha_{max,l} = \max_r \alpha_{l,r}$ is the maximum ratio in the l-th cycle and α_{th} is the threshold whose value is usually determined by experiences.

The other competing method is based on the mean absolute variation in squared amplitude (MAVSA). Although developed for the detection of voltage transients, it is sensitive to waveform variations and can be used for generic abnormality detection. With this method, the point-by-point differences of the squared values of two consecutive cycles are calculated first, then the mean absolute value of the differences is derived and compared with a threshold for the detection. In what follows, we explain the field test and show the results on the detection performance. The power system where the data are measured is described in Section 3.1.2. The measurement parameters are also explained in Section 3.1.2. The feeder current data are measured gaplessly for 3 weeks. In order to get the P_D versus P_{FA} curve, a set of waveforms called events need to be selected and identified as normal or abnormal. Then the probability of detection and the probability of false alarm of a given method can be obtained by comparing the detection result with our initial identification. We capture 2991 events by applying the waveform method in Section 4.4.1 of Reference [39] to the 3-week continuous data measured from the system explained in Section 3.1.2. A very small threshold was used in this process, so as to capture as many as events of variations as possible.

Among the 2991 selected events, there are 1069 normal ones and 1922 abnormal ones from the perspective of Phase-A data. Every event contains 150 cycles of current data. For an event that has abnormality, the data contain the 50 cycles before the abnormality and the 100 cycles after the abnormality happens (including the abnormal cycles). Abnormalities existing in these data include but not limited to oscillatory voltage or current transients, multi-cycle over-current events, and low-level current bursts. A few examples of abnormal events are shown in Figure 3.6. A normal event has a form of waveform variation that does not exhibit electromagnetic or electromechanical transient characteristics. An example of normal event is shown in Figure 3.7. In this case, there is a burst of noise-like current variation. Based on our knowledge

of various creditable power disturbances, such a waveform is unlikely to contain useful information. So it is clarified as a normal event. It is noteworthy that pre-screening uses the waveform RMS value, which conceivably favors the differential waveform RMS method that is used as the competing method in this work. As a result, the comparison result in this work is a conservative estimation of the advantage of the proposed method.

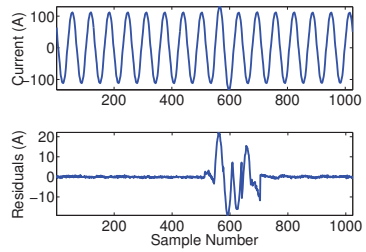

(a) Sub-cycle low-level overcurrent.

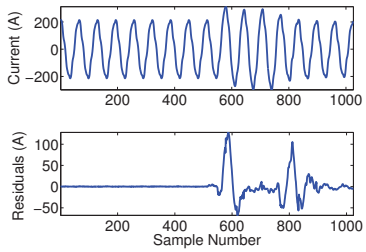

(b) Multi-cycle overcurrent.

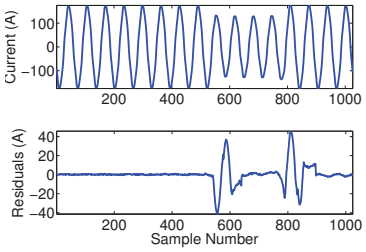

(c) Multi-cycle current sag.

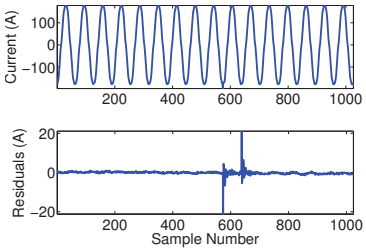

(d) Short-duration current burst.

Figure 3.6: Examples of abnormal events.

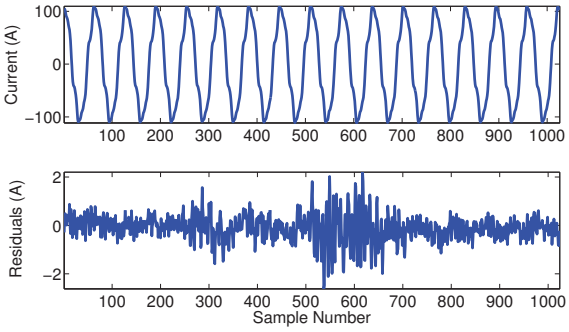

Figure 3.7: A typical normal event.

3.3.1 Discussions on Parameter Values

Notice that N_G, N_H, N_d need to be specified for the proposed scheme. In this subsection, we discuss how to choose the parameter values.

First, recall that N_d is the number of data cycles used to detect abnormality, in other words, the size of the detection window. More specifically, for each detection, the residual data of N_d cycles are used to obtain the kernel estimation of the pdf, which is then compared with the reference pdf to obtain the KLD value for the detection.

For the effect of N_d on the performance, Figure 3.8 shows the P_D v.s. P_{FA} curves of the proposed method with the field data for different N_d ranging from 1 to 5, where $N_G = 10$ and $N_H = 1$. It can be seen that when $P_{FA} < 0.4\%$, $N_d = 1$ performs better than other situations. When $P_{FA} > 0.4\%$, $N_d = 2$ performs the best. Considering the complexity and detection of short duration abnormalities (e.g. one cycle or less), we use $N_d = 1$.

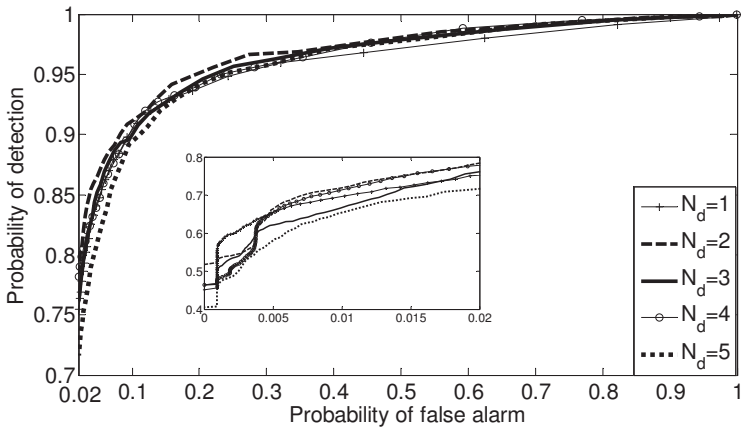

Figure 3.8: Detection performance for different N_d.

For the effect of N_G, Figure 3.9 shows the P_D v.s. P_{FA} curves of the proposed method with the field data for different N_G ranging from 5 to 15, where $N_H = 1$ and $N_d = 1$. N_G represents the number of cycles used to get the underlying pdf of residuals under normal condition. If N_G is too small, it is hard to get a reliable residual pdf because of the limited number of samples.

Meanwhile, if N_G is too big, we can not get accurate estimation of the residual pdf under normal condition since it can vary with time. Based on the results in Figure 3.9 and the normality test of the noise pdf, we chose $N_G = 10$.

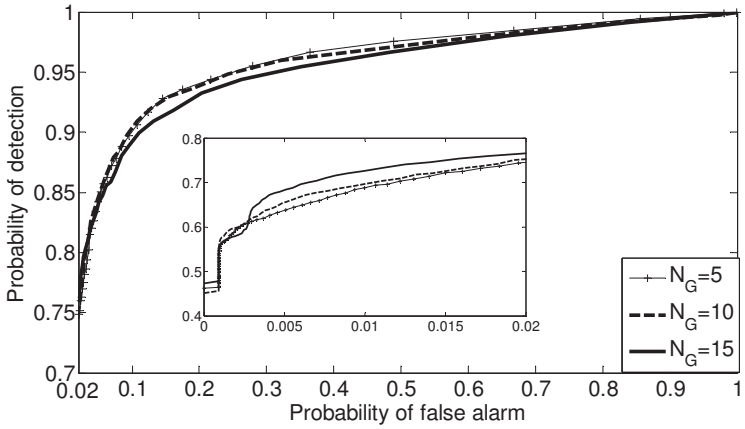

Figure 3.9: Detection performance for different N_G.

Figure 3.10 shows the P_D v.s. P_{FA} curves of the proposed method with the field data for different N_H ranging from 1 to 5, where $N_d = 1$ and $N_G = 10$. N_H is the number of cycles used to estimate the steady-state components. The figure shows that using the previous one cycle of the data is the best. This result is natural since the steady-state components in two consecutive cycles are approximately stable, while they may have non-negligible fluctuation for cycles with further distance. Thus, $N_H = 1$ is chosen.

It should be noted that the results shown in Figure 3.8 to Figure 3.10 are derived with Phase-A data. From the perspective of Phase-B data, there are 931 normal ones and 2060 abnormal ones among those 2991 events; from the perspective of Phase-C data, there are 968 normal ones and 2023 abnormal ones. The results derived with Phase-B and Phase-C data are presented in Appendix C. Results show that the same parameter values can be selected with sensitive study on Phase-B and Phase-C data.

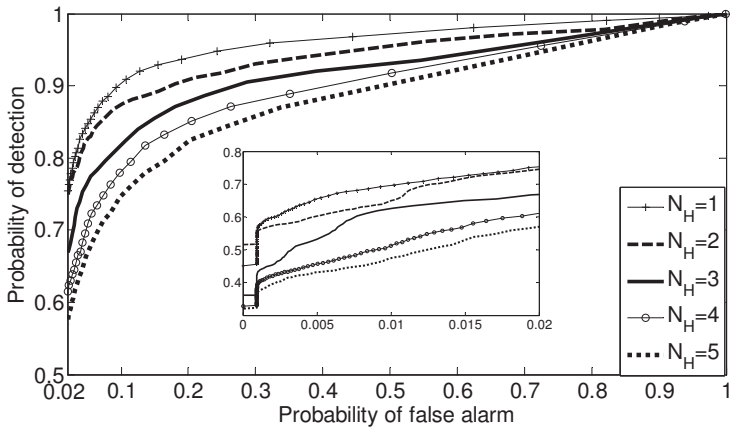

Figure 3.10: Detection performance for different N_h.

3.3.2 Performance of the Proposed Method With Field Data

In this subsection, we show the performance of the proposed method and the comparison with another two existing methods described above. Based on the studies in Section 3.3.1, we set $N_G = 10$, $N_H = 1$, and $N_d = 1$. For the differential waveform RMS method, M is set to be 8 based on the work of [40].

The P_D v.s. P_{FA} curves for the field data are shown in Figure 3.11. We can see that the proposed method has clear advantage over the differential waveform RMS method and the MAVSA method. At the false alarm probability of 2%, our scheme has 74.8% detection rate, while the detection rate of the differential waveform RMS method and the MAVSA method are 59.5% and 27.4%. At the detection probability of 90%, our scheme has 10.7% false alarm rate, while the false alarm rate of the differential waveform RMS method and the MAVSA method are as high as 42.8% and 85.9%, respectively.

The results in Figure 3.11 are derived by applying the three methods to current signals. In reality, these methods can also be applied to voltage signals. After applying the methods to voltage signals, we can get the P_D v.s. P_{FA} curves as shown in Figure 3.12. For the proposed method and the differential waveform RMS method, the performance when applying the methods to both

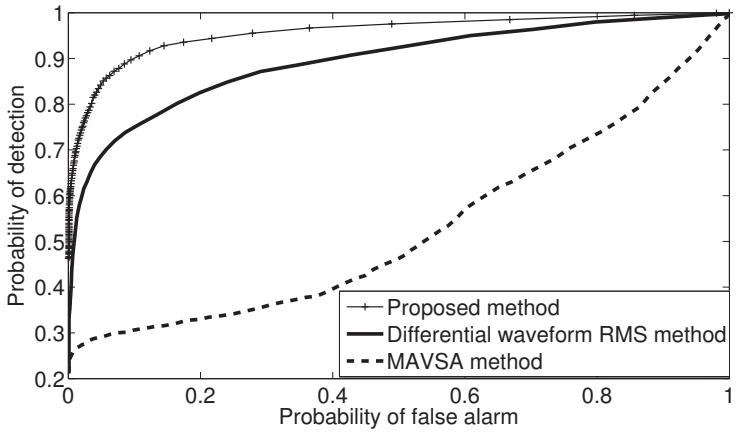

Figure 3.11: Performance comparison of the proposed method with the differential waveform RMS method and the MAVSA method with extracted events.

voltage and current signals is quite close to that when applying the methods to current signals only, and is much better than the performance when only applying the methods to voltage signals. This validates our assumption that the current signal is more sensitive to equipment conditions.

In addition to the performance comparison based on those selected events, experiments are conducted on three datasets each containing 5-day gapless data. Dataset 1 is measured from the system explained in Section 3.1.2. The system where Dataset 2 is measured is described in [41]. The 25 kV substation data described in [39] is used as Dataset 3. Both the phase currents and zero-sequence current are used for the detection. In the experiments, the false alarm probability is set to be $15/N_{KLD}$, where $N_{KLD} = 5184000$ is the number of cycles per day. This is to control the number of detected events to be around 15 per day on average. For different detection methods, the average numbers of events per day are shown in Table 3.2. Results show that the proposed method can detect more events than the other two methods from Dataset 1 and Dataset 2.

However, for Dataset 3, the differential waveform RMS method can detect more events than the proposed method and the MAVSA method. With a closer look, we found that there are a large number of automatic meter reading

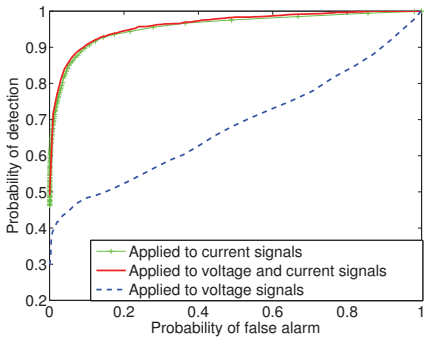

(a) Proposed method.

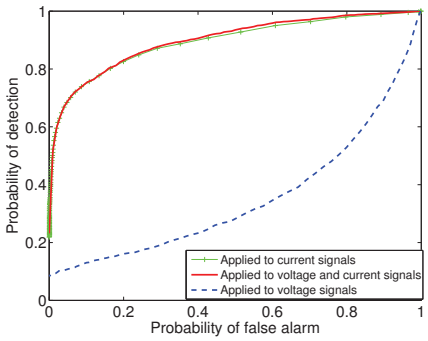

(b) Differential waveform RMS method.

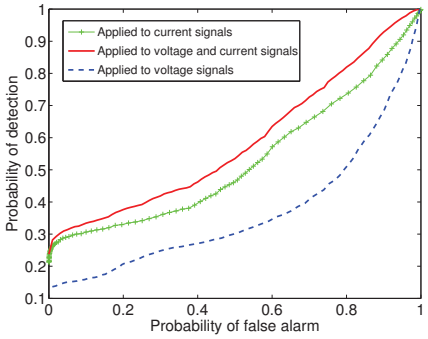

(c) MAVSA method.

Figure 3.12: Results after applying the three methods to different signals.

Table 3.2: Numbers of detected events per day.

Methods	Proposed method	Differential waveform RMS method	MVSVA method
Dataset 1	20	16	15
Dataset 2	22	14	13
Dataset 3	33	47	16

(AMR) signals in the data, as shown in Figure 3.13. The existence of AMR signals can affect the threshold selection of the proposed method by enlarging it. As a result, the proposed method misses some events. There are two ways to boost the sensitivity of the proposed method: one is to reduce the detection window if sampling frequency is large enough; the other one is to increase the false alarm probability used in the threshold selection.

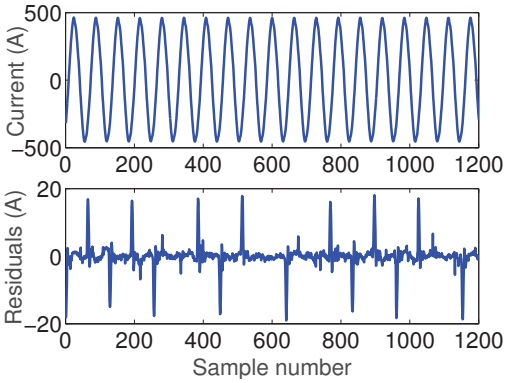

Figure 3.13: An example of AMR signals.

Since the number of real abnormalities is more useful in determining the detection performance, we checked the detected events manually and summarized the number of false alarms in Table 3.3 to reveal the number of abnormalities. We can know from Table 3.2 and Table 3.3 that the proposed method can detect more abnormalities that contain transient behavior than the other two methods for Dataset 1 and Dataset 2. But for Dataset 3, the differential waveform RMS method can detect more abnormalities.

Table 3.3: Numbers of false alarms.

Methods	Proposed method	Differential waveform RMS method	MVSVA method
Dataset 1	0	8	0
Dataset 2	12	8	4
Dataset 3	0	0	0

3.3.3 Performance of the Proposed Method With Simulated Data

As field data are limited, to further test the proposed methods, simulations with PSCAD are also conducted. The modified IEEE-13 bus system as shown in [42], which is derived from [43], is used for the simulation. The events used in the

simulation include high current arcing fault, low current (or high impedance) arcing fault, capacitor switching, constant impedance fault, and load switching. Load switching is seen as normal events, while others are abnormal events to be detected. Load switching events are common in distribution systems and account for many small variations in substation measured currents. These events are representative to test the performance of the proposed method in discriminating between normal variations and abnormalities corresponding to equipment failures. In our simulation, 1402 load switching events are simulated with varying load parameters. For faulty events, we simulate 54 cases of high current arcing fault, 485 cases of low current arcing fault, 252 cases of capacitor switching operation and 420 cases of constant impedance fault, all with varying fault duration, fault locations, fault starting instant, and fault resistance.

For both low and high current arcing faults, we fix the arcing parameters as follows [42]: arc time constant $\tau = 0.0002$, characteristic arc voltage $u_0 = 2900$, characteristic arc resistance $r_0 = 0.001$. The arcing fault starts at around the voltage peak. The occurrence of a constant impedance fault in a cycle is set to be random. For capacitor switching events, the compensated reactive power ranges from 100 kVAr to 300 kVAr per phase. For load switching events, the load current ranges from 10 A to 30 A. Other parameters such as fault location, fault duration and fault resistance can be found in Table 3.4, where the fault location is shown as node number of IEEE-13 node system. Random Gaussian noises are added in the simulation data where the signal-to-noise-ratio is set as 50dB.

Three sets of data are simulated at three different sampling frequencies, 3840 Hz, 7680 Hz and 15360 Hz corresponding to 64, 128, and 256 points per cycle, respectively. Intuitively, when the sampling frequency is too low, the number of sampling points in each cycle will be small. It is conceivable that the pdf estimation will be highly erroneous and the proposed method will have low performance [1]. With high enough sample frequency, we investigate

Table 3.4: Simulation setup.

Fault Type	Fault Location	Fault Duration (cycle)	Fault Resistance (ohm)
High Current Arcing Fault	633, 634, 645	0.25 to 1.25	0.003 to 0.005
Low Current Arcing Fault	680, 652, 692	0.25 to 1.25	100 to 800
Constant Impedance Fault	680, 652, 692	2 to 3.25	0.1 to 500
Capacitor Switching	680, 652, 675	N/A	N/A
Load Switching	675, 611, 646	N/A	N/A

the relationship between the performance and the sampling frequency. The P_D v.s. P_{FA} curves for the proposed method and differential waveform RMS method derived with the simulated data are shown in Figure 3.14 and Figure 3.15. We can see that the performance of the proposed method improves as the sampling frequency increases. However, the impact is not significant. For all sampling frequencies, the proposed method has considerably higher performance than the differential waveform RMS method and the MAVSA method.

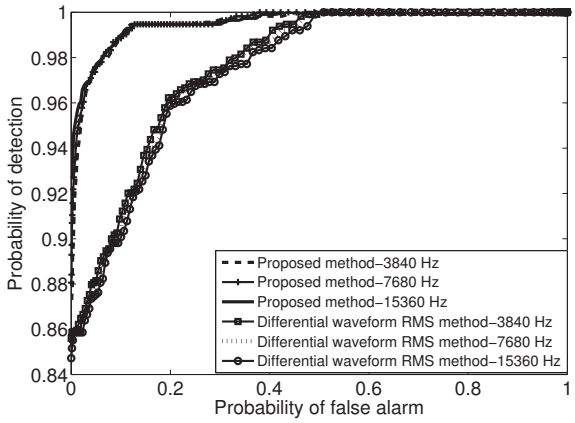

Figure 3.14: Performance comparison of proposed method and differential waveform RMS method under different sampling frequencies.

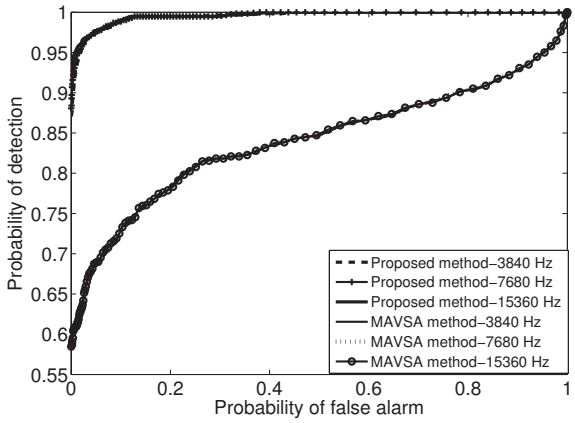

Figure 3.15: Performance comparison of proposed method and MAVSA method under different sampling frequencies.

3.3.4 Strength and Limitations of the Proposed Method

The advantage of the proposed detection method over the differential waveform RMS method and the MAVSA method results from two aspects. First, the KLD measure used in the proposed method is more sensitive to waveform abnormality and less sensitive to small load variations. Abnormal cases are usually signatured by waveform changes. Second, the KLD measure is more sensitive to asymmetrical abnormality. This is an appealing feature because many abnormalities are asymmetrical, such as the abnormalities in capacitor switching transients and cable incipient failures.

In the proposed method, the residual signals are obtained by subtracting the steady-state components derived from the previous cycle. Only one cycle of the residual data is used to construct the pdf. Therefore, the algorithm has very fast response. Experience shows that many industrial processes load fluctuations (except arc-furnace) are in the order of multi-cycles or even seconds. So the relative slow change of such loads is not expected to cause problems for the proposed algorithm. The algorithm as it stands now is not suitable for monitoring conditions such as aging. In reality, the available equipment failure cases have shown that the associated abnormalities may last several seconds to

minutes at most. If there are sudden activities such as arcing due to aging, the algorithm is expected to detect it.

The proposed method is very sensitive to abnormalities in the shape of the residual signals. But it may capture variations with very small magnitude, causing false alarm. A typical example is shown in Figure 3.7. In this case, there is a burst of noise-like current variation. Based on our knowledge of various creditable power disturbances, such a waveform is unlikely to contain useful information. So it is manually identified as a normal event. But the algorithm picked it up as an abnormal event. This is because the residual of a normal waveform contains unusual noise or alike that does not follow expected Gaussian distribution of normal waveforms.

This work establishes an automatic and adaptive threshold selection scheme which has theoretical foundation [38]. It proposes to use an easy-to-understand "probability of false alarm" parameter to select threshold. This is a step forward in comparison with traditional experience-based threshold selection. To improve this scheme further, more research on automatic threshold selection is desired, e.g. how to set the "probability of false alarm" in real application.

3.4 Summary

In this chapter, a new approach for the detection of generic and unknown abnormalities associated with utility equipment failures from the current signal has been presented. The problem is formulated as a binary hypothesis test. In finding a detection solution, first, the steady-state components which are common for both hypotheses are removed from the measured current signal. Under normal situation, the residual data are modeled as samples of a Gaussian random variable; while under abnormal situation, they are expected to largely deviate from Gaussian samples. The KLD from the residual data distribution to Gaussian distribution is used in the detection rule. The proposed method

is tested by field data and simulated data. Results show that it can effectively detect abnormality-containing data, and at the same time reduce false alarms. It performs significantly better than two existing methods.

Chapter 4

Soft Detection of Waveform Abnormality

Based on the novel detection method presented in Chapter 3, soft detection methods are proposed in this chapter. Instead of returning hard binary detection result (i.e., whether or not the data of interest contain a waveform abnormality), the soft detection method returns a numerical value in the interval [0,1] for the data of interest which reflects the credibility that the data contain a waveform abnormality [44].

4.1 Motivations for Soft Detection and Existing Literature

This section provides motivations for soft detection as well as existing literature on soft detection of waveform abnormality.

4.1.1 Motivations for Soft Detection

Performance of the binary detection method in Chapter 3 is affected by several critical parameters, for example, the KLD threshold value. The setting of these

parameters is inevitably affected by imprecision and imcomplete knowledge in waveform abnormality. As well, when the data of interest contain uncertainties introduced by inaccurate measurements and missing data, the binary detection method may have undesirable performance, especially for borderline events or at least may not adequately implement human knowledge to analyze data [45]. In viewing of such situation, this chapter proposes a soft detection method.

Soft detection method returns a numerical value between 0 and 1 which can reflect the credibility that the data of interest contain a waveform abnormality as well as the severity of a certain abnormality. When the returned value is big, it means the abnormality is more severe, and the corresponding incipient failure may be severe and close to final failure or permanent fault. Besides, it can also capture waveforms with relatively low abnormality credibility, which would be missed if binary detection is used. This is useful for systems with very high reliability requirement, e.g., high-impedance fault relay.

4.1.2 Review of Existing Literature on Soft Detection

The only found reference on soft detection of waveform abnormality is [44]. It deals with the detection of voltage sag which is an important type of power quality disturbance. Its detection procedure can be summarized in Figure 4.1.

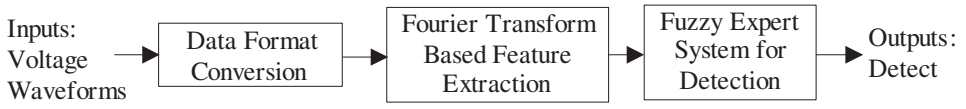

Figure 4.1: Detection flow chart for the soft detection in [44].

After data conversion of input voltage waveforms, the fundamental component, phase angle shift and total harmonic distortion of the signals are extracted by applying Fourier transform on the data. Then these features are sent to a fuzzy expert system for the detection of abnormality. A value between 0 and 1 is assigned to a variable "Detect", which reflects the credibility or degree that

certain abnormality exists. The output for the detection can be determined with the following equation,

$$Detect = max\{MF_1(THD_n), MF_2(PS_n), MF_3(V_n), MF_4(V_n)\} \tag{4.1}$$

where MF_1, MF_2, MF_3, MF_4 are membership functions, THD_n represents the total harmonic distortion of the data of interest, PS_n is the phase shift, V_n is the fundamental component, max represents the operation to get the maximum one among several values. The output is "Detect".

In (4.1), each input of the max operation corresponds to a fuzzy set which consists of elements and a membership function, e.g., V_n values and membership function MF_3 constitute a fuzzy set and are used to evaluate the abnormality in the magnitude of the fundamental component. $MF_3(V_n)$ is the membership degree in the fuzzy set and reflects the degree for V_n being abnormal. It lies in the range $[0, 1]$. The four membership degrees in (4.1) determine if a waveform abnormality exists and how severe it is.

4.2 Proposed Soft Detection Scheme

As illustrated in Chapter 3, the KLD value from the distribution of current residual data to the theoretical Gaussian distribution is sensitive and reliable in measuring the abnormality of waveform. Thus, KLD value can be used as a feature for the detection of abnormality. Thus, we propose to use KLD value and a membership function to conduct soft detection. When the membership degree of data of interest is larger than 0, an abnormality can be considered to be detected; then, the data and the membership degree will be saved for further analysis. The general structure of the soft detection scheme is illustrated in Figure 4.2.

Figure 4.3 shows an example of membership function. In this illustrative example, when the calculated KLD value is 20, it corresponds to an abnormality

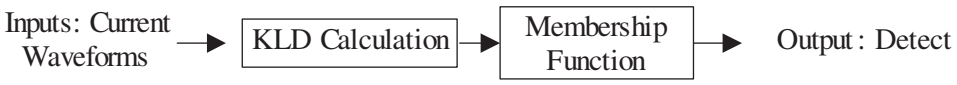

Figure 4.2: General structure of the proposed soft detection scheme.

to a degree of 0.5. The corresponding data of interest will be captured and saved.

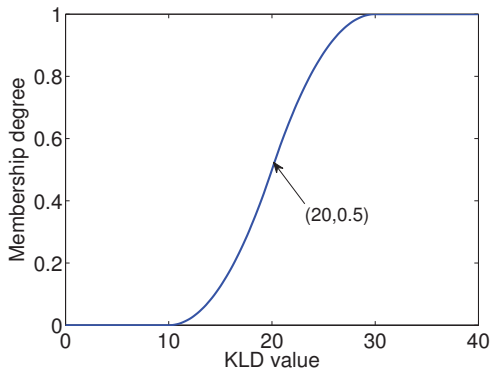

Figure 4.3: An illustrative example of membership function.

To implement the soft detection scheme, two problems need to be solved.

- Selection of membership function. Generally, the bigger the calculated KLD value, the more possible the data of interest contain abnormality. Thus, there should be a positive correlation between the input and output of the membership function.
- Determination of critical parameters of the selected membership function.

The following subsections discuss these aspects.

4.2.1 Selection of Membership Function

We choose the membership function from commonly used ones, including triangular membership function, trapezoidal membership function, S-shaped membership function, and Gaussian membership function. The graphical representation of these membership functions are shown in Figure 4.4. Their analytical

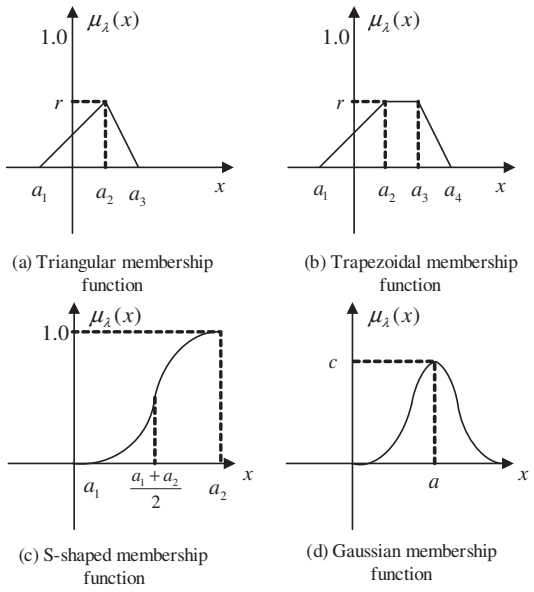

Figure 4.4: Typical membership functions [47][48].

representations are shown in (4.2)-(4.5), respectively.

$$\mu_\lambda = \begin{cases} \frac{x-a_1}{a_2-a_1}r, & if a_1 \le x \le a_2 \\ \frac{a_3-x}{a_3-a_2}r, & if a_2 < x \le a_3 \\ 0 & otherwise \end{cases} \tag{4.2}$$

$$\mu_\lambda = \begin{cases} \frac{x-a_1}{a_2-a_1}r, & if a_1 \le x \le a_2 \\ r, & if a_2 < x \le a_3 \\ \frac{a_4-x}{a_4-a_3}r, & if a_3 < x \le a_4 \\ 0, & otherwise \end{cases} \tag{4.3}$$

$$\mu_\lambda = \begin{cases} 0, & if x \le a_1 \\ 2(\frac{x-a_1}{a_2-a_1})^2, & if a_1 < x \le \frac{a_1+a_2}{2} \\ 1-2(\frac{a_2-x}{a_2-a_1})^2, & if \frac{a_1+a_2}{2} < x \le a_2 \\ 1, & if x > a_2 \end{cases} \tag{4.4}$$

$$\mu_\lambda = ce^{-\frac{(x-a)^2}{2\sigma^2}} \tag{4.5}$$

In our situation, the S-shaped function is a proper one since only this one shows the positive correlation between the inputs and outputs. In reality, a linear function as shown in Figure 4.5 can also be used because it is increasing on the interval $[a_1, a_2]$. However, the S-shaped function is smoother at corner points than this linear function [48, 49]. Thus, we choose to use the S-shaped function in this work.

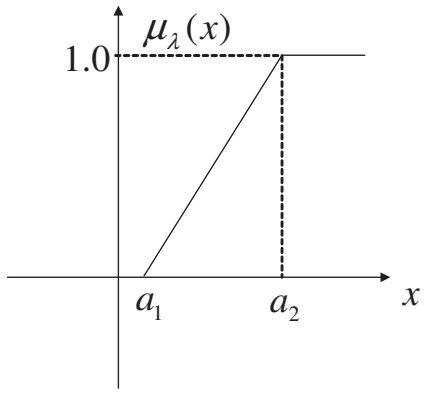

Figure 4.5: A linear membership function.

4.2.2 Determination of the Parameters of the S-shaped Function

There are two parameters (i.e., a_1 and a_2) we need to determine in using the S-shaped function for soft detection. The two parameters set the interval within which soft detection results need to be assigned. Technically, the KLD value whose corresponding false alarm rate is zero should be selected as the upper limit; the KLD value whose corresponding detection rate is one should be chosen as the lower limit. That is, the range should be the overlap KLD range of the two hypotheses. However, in real application, it is difficult to get theoretical KLD values that can be used to set the upper and lower limits.

Instead, we choose the parameters based on the binary detection scheme illustrated in Chapter 3. Let the threshold under the binary detection scheme be D_{th}. By using the D_{th} as the midpoint of the upper limit a_1 and lower limit

a_2, a_1 and a_2 can be simplified into $(1-\alpha)D_{th}$ and $(1+\alpha)D_{th}$, respectively. In this way, the number of parameters that need to be predefined reduces to one. As well, we can easily integrate the soft detection scheme into the detection procedure under binary detection scheme.

We need to study the impact of α on the performance and find its optimal value. An appropriate performance measure should be selected first. Let P_{FA} be the desired level of false alarm probability and D_{th} be the corresponding hard threshold of the binary detection scheme. For an arbitrary α, denote $\tilde{P}_{FA}(\alpha)$ and $\tilde{P}_D(\alpha)$ as the probability of false alarm and the probability of detection under soft detection scheme. In an experiment where the data contains m normal cycles and n abnormal cycles in the data of interest. $\tilde{P}_{FA}$ and $\tilde{P}_D$ can be calculated as follows,

$$\tilde{P}_{FA}(\alpha) = \frac{\sum_{i=1}^{m} MDN_i(\alpha)}{m} \tag{4.6}$$

$$\tilde{P}_D(\alpha) = \frac{\sum_{k=1}^{n} MDA_k(\alpha)}{n} \tag{4.7}$$

where $MDN_i(\alpha)$ represents the membership degree of the ith normal cycle, $MDA_k(\alpha)$ represents the membership degree of the kth abnormal cycle.

Following the Neyman-Pearson detection framework, we use $\tilde{P}_{FA}$ and $\tilde{P}_D$ as performance measures and formulate the α-optimization as follows,

$$\hat{\alpha} = \arg \max_{\alpha \in [0,1), \tilde{P}_{FA}(\alpha) \leq P_{FA}} \tilde{P}_D(\alpha). \tag{4.8}$$

This formulation means to maximize the detection probability while keeping the false alarm probability under P_{FA}.

(1) Determination of α with field data

In this part, the field data measured at one end of a transmission cable is

used to determine the proper range of α. 2991 events (they are also used in the Chapter 3) are selected from the data, consisting of 1069 normal events which do not contain abnormalities and 1922 abnormal events. Figure 4.6 shows the probability of false alarm v.s. different KLD values under binary detection scheme. The D_{th} value which corresponds to a given P_{FA} value are used to determine the S-shaped function of the soft detection scheme.

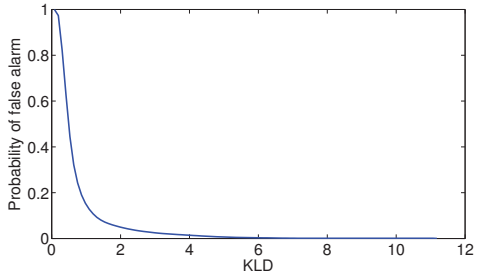

Figure 4.6: False alarm probability v.s. different threshold values for soft detection.

To get $\hat{\alpha}$, one-dimensional exhaustive search over its possible range $[0, 1)$ is conducted. The value which corresponds to the maximum detection probability $\tilde{P}_D$ while keeping the false alarm probability $\tilde{P}_{FA}$ under P_{FA} is selected as the optimal value. Results show that the optimal value $\hat{\alpha}$ mainly lies in the following range for all P_{FA} values. Specifically, optimal values for α of about 90% of all the cases fall in this range.

$$\hat{\alpha} \in (0, 0.3) \tag{4.9}$$

(2) Determination of α with simulated data

Since field data are limited, the KLD values used to determine α are limited and discontinuous. Thus, the results presented above may have bias in revealing the result. To overcome this disadvantage, we can simulate a large number of cases to mimic the field data. Based on the IEEE 13 bus system explained in Chapter 3, we simulate normal events (i.e., small loading switching events) and

abnormal events which includes high current arcing faults, low current arcing faults, constant impedance faults and capacitor switching events. The numbers of simulated normal and abnormal events are 1212 and 5088, respectively.

Based on (4.8), the optimal choices of α for different false alarm rates (different D_{th} values) lie in the same range as shown in (4.9).

Since the optimal α may vary with time and different datasets, the $\hat{\alpha}$ can be updated periodically in real applications.

4.2.3 Proposed Soft Detection Algorithm and Test Results

The integrated soft detection procedure is shown in Figure 4.7. To illustrate the advantage of soft detection over the binary detection explained in Chapter 3, the numbers of missing events for the binary detection and the soft detection with the optimal α are presented in Table 4.1. A missing event refers to an abnormal event that is not detected. We can clearly see from this table that for all desired false alarm probability levels, the numbers of missing events under soft detection are less than the situation under binary detection.

Two illustrative examples of missing events that are not detected with binary detection scheme but detected with soft detection scheme are presented in Figure 4.8. The soft detection results of the two cases are 0.0896 and 0.1622, respectively. Figure 4.9 presents an example that is detected by both binary detection and soft detection scheme. The oscillatory behavior in current residuals makes it a more severe abnormality compared with the examples in Figure 4.8. The returned numerical value under soft detection scheme is 1, which is much higher than the results of the examples in Figure 4.8. These three cases show that the soft detection results can be used as a reference in evaluating the severity of a certain abnormality. In other words, the returned values can reflect the credibility that the waveforms contain abnormality. As well, our proposed soft

detection scheme can capture waveforms with less abnormality which would be missed if binary detection is used.

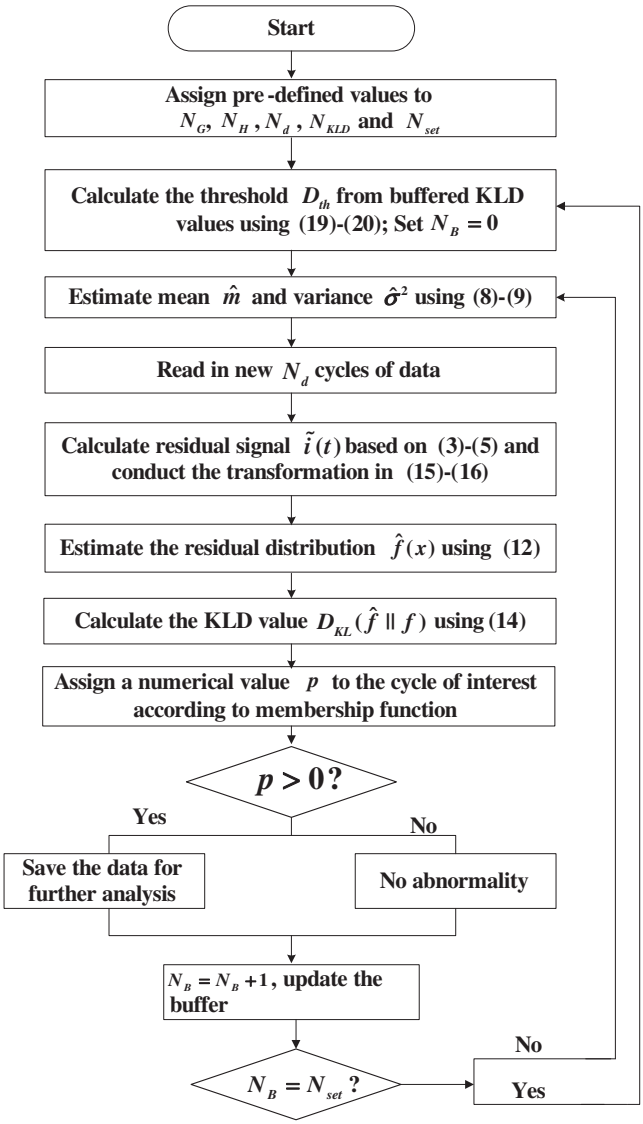

Figure 4.7: Procedure of the proposed soft detection scheme.

Table 4.1: Number of missing events under soft and binary detection scheme.

False alarm rate	Binary detection	Soft detection
0.2	120	71
0.4	64	64
0.6	40	0
0.8	18	0

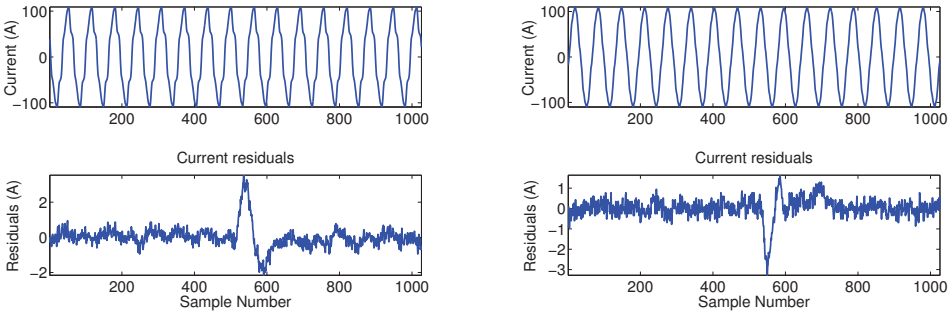

(a) Example 1 (b) Example 2

Figure 4.8: Two examples of missing events.

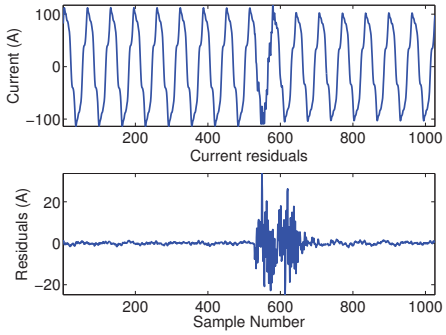

Figure 4.9: An example with severe abnormality.

4.3 Summary and Discussion

In this chapter, a soft detection scheme based on fuzzy set theory is proposed. This scheme is easy to implement and its output for a certain period of waveform data is a value between the interval [0, 1], which reflects the degree or

credibility for the data being abnormal. The S-shaped membership function is recommended and methods to determine its parameters are given. The proposed soft detection scheme is tested with transmission cable data. Results show that our proposed soft detection scheme can capture waveforms with less abnormality which would be missed if binary detection is used. Meanwhile, the soft detection results can be used as a reference in evaluating the severity of a certain abnormality.

Chapter 5

Conclusions and Future Work

Conclusions and possible future work are presented in this chapter.

5.1 Conclusions

This thesis dicsusses the detection of waveform abnormality aimed at power equipment condition monitoring. The major conclusions and contributions of this thesis are summarized as follows.

- An extensive survey was made to summarize the electrical signatures of various utility equipment failures and existing work on their detection. The main characteristics of equipment failure signatures include abnormal current response, diverse time scales, complexity in characterization and challenge in detection. The survey lays the foundation for the research presented in this thesis, which is to detect generic waveform abnormalities, expecially those associated with equipment failures.

- An improved detection method is proposed based on segment RMS values of differential waveform and half-cycle refreshed RMS values of original waveform. The signals used here include both phase voltage and phase current waveforms. Illustrative examples of detection results are

presented to show main types of abnormalities to be detected and the effectiveness of this method.

- A novel detection method based on probability density function of current residual waveform is proposed for the detection of generic waveform abnormality. The problem is formulated as a binary hypothesis test. After deriving residual data by removing steady-state components from the measured signal, the KLD from the residual data distribution to Gaussian distribution is used in the detection rule. The difficulty to set proper threshold due to large variations of current values is overcome through the adoption of KLD as the distance measure and a systematic threshold selection method. The proposed method is tested by field data and simulated data. Results show that it can effectively detect abnormality-containing data, and at the same time reduce false alarms due to small load changes. It performs significantly better than two existing methods.

- A soft detection scheme is proposed. Unlike traditional detection methods which determine if or not a certain period of data contain abnormality, the proposed detection schemes returns a numerical value in unit interval [0,1] for the data of interest, which represents the degree for the data being abnormal as well as the severity of a certain abnormality. Besides, it can capture abnormality with low severity, which would be missed with a binary detection scheme. Illustrative examples and results on miss detection numbers are used to show advantages of the soft detection scheme over binary detection method.

5.2 Suggestion for Future Work

The work in this thesis can be extended in the following three aspects:

- In Chapter 3, the KLD is used to measure distance between two distri-

butions. Other distance measures for distribution function or properties of distribution function can be investigated for their effectiveness in abnormality detection for equipment condition monitoring.

- The soft detection scheme proposed in Chapter 4 only considers KLD as a feature for the detection. Other features such as change in instantaneous power can be introduced to make better and more comprehensive decisions about the degree for a certain period of data being abnormal.

- It is useful to evaluate if the recurring abnormalities prior to equipment final failure correspond to similar soft detection results. If their soft detection results are close to each other, we may be able to use the results to classify captured abnormalities and then derive associated characteristics.

Bibliography

[1] J. A. Wischkaemper, C. L. Benner, B. D. Russell and K. Manivannan, "Application of waveform analytics for improved situation awareness of electric distribution feeders, *IEEE Trans. Smart Grid*, vol. 6, no. 4, pp. 2041-2049, Apr. 2015.

[2] S. Bhowmick and S. Nandi, "Online detection of an interturn winding fault in single-phase distribution transformers using a terminal measurement-based modeling technique, *IEEE Trans. Power Del.* vol. 30, no .2, pp. 1007-1015, Apr. 2015.

[3] P. Dutta, A. Esmaeilian and M. Kezunovic, "Transmission-line fault analysis using synchronized sampling, *IEEE Trans. Power Del.*, vol. 29, no. 2, pp. 942-950, Apr. 2014.

[4] Saurabh Kulkarni, Surya Santoso, and Thomas A. Short, "Incipient fault location algorithm for underground cables," *IEEE Trans. Smart Grid*, vol. 5, pp. 1165-1174, May. 2014.

[5] K. Saarinen, M. J. Mousavi, J. Stoupis, and J. J. McGowan, "Systems and methods for power line event zone identification", U.S. Patent Application No. 13/155,249, Jan. 5, 2012.

[6] Thomas E. Grebe, "Effective collection and management of power quality data for analysis and detection of incipient distribution system components

faults and identification of their locations" CEATI Report No. T124700-5159, Sep. 2013.

[7] Carl L. Benner and B. Don Russell, "Distribution fault anticipator: phase II: field data collection and algorithm development," EPRI Report 1010662, Nov. 2005 (This report can be downloaded from EPRI website free of charge).

[8] B. Kasztenny, I. Voloh, C. G. Jones and G. Baroudi, "Detection of incipient faults in underground medium voltage cables," in *Proc. of 61st Annual Conference on Protective Relay Engineers*, Apr. 1-3, 2008, pp. 349-366.

[9] Tarlochan S. Sidhu and Zhihan Xu, "Detection of incipient faults in distribution underground cables," *IEEE Trans. Power Del.*, vol. 25, no. 3, pp. 1363-1371, Jul. 2010.

[10] *IEEE Recommended Practice for Monitoring Electric Power Quality*, IEEE Std. 1159-2009, 2009.

[11] *Electromagnetic Compatibility (EMC)Part 4-30: Testing and Measurement Techniques-ower Quality Measurement Methods*, IEC Std. 61000-4-30, 2008.

[12] Saurabh Kulkarni, Alicia J. Allen, Shivaz Chopra, Surya Santoso and Thomas A. Short, "Waveform characteristics of underground cable failures," in *Proc. of the IEEE Power and Energy Society General Meeting*, Jul. 25-29, 2010, pp. 1-8.

[13] Jeffrey A. Wischkarmper, Carl L. Benner and B. Don Russell, "A new monitoring architecture for distribution feeder health monitoring, asset management, and real-time situational awareness," in *Proc. of Innovative Smart Grid Technologies Conference (ISGT)*, Jan. 16-20, 2012, pp. 1-7.

[14] DOE/EPRI National Database Repository of Power System Events, [Online]. Available: http://expertmonitoring.com/doelibrary/

[15] H. Hu, Q. Shi, Z. He, J. H, and S. Gao, "Potential harmonic resonance impacts of PV inverter filters on distribution systems," *IEEE Trans. Sustain. Energy*, vol.6, no.1, pp.151-161, Jan. 2015.

[16] Q. Shi, H. Hu, W. Xu, and J. Yong, "Low-order harmonic characteristics of photovoltaic inverters," *Int. Trans. Electr. Energ. Syst.*, vol. 26, no. 2, pp. 347364, Feb. 2016.

[17] C. Jiang, Q. Shi, Y. Tian, X. Li, S. Lin and Y. Liu, "Sensitivity study on the stray voltage of low voltage residential networks," in 2016 8th International Power Electronics and Motion Control Conf. (IMPEC-ECCE Asia), Hefei, China, pp. 1-6.

[18] Saurabh Kulkarni, Duehee Lee, Alicia J. Allen, Surya Santoso and Thomas A. Short, "Waveform characterization of animal contact, tree contact, and lightning induced faults," in *Proc. of the IEEE Power Energy Society General Meeting*, July. 25-29, 2010, pp. 17.

[19] Lance A. Irwin, "Real experience using power quality data to improve power distribution reliability," in *Proc. of 14th International Conference on Harmonics and Quality of Power*, Sep. 26-29, 2010, pp. 1-4.

[20] Carl L. Benner, B. Don Russell and Ashok Sundaram, "Feeder interruptions caused by recurring faults on distribution feeders: faults you don't know," in *Proc. of 61th Annual Conference on Protective Relay Engineers*, Apr. 1-3, 2008, pp. 584-590.

[21] M. B. Barbieri, R. E. Bianchi Lastra, P. L. Arnera and J. L. Aguero, "Transients due to multiple prestrike phenomenon when energizing capac-

itor banks with a vacuum circuit-breaker," in *Proc. of Transmission & Distribution Conference and Exposition*, Aug. 15-18, 2006, pp. 1-6.

[22] Yingyao Zhang, He Yang, Yingsan Geng, Zhiyuan Liu and Lijun Jin, "Effect of high-frequency high-voltage impulse conditioning on inrush current interruption of vacuum interrupters," *IEEE Trans. Dielectr. Electr. Insul.*, vol. 22, no. 2, pp. 1306-1313, Apr. 2015.

[23] Bogdan Kasztenny, Ilia Voloh, Alvin Depew and Joseph Wolete, "Re-strike and breaker failure conditions for circuit breakers connecting capacitor banks," in *Proc. of 61th Annual Conference for Protective Relay Engineers*, Apr. 1-3, 2008, pp. 180-195.

[24] S. Santoso and D. D Sabin, "Power quality data analytics: Tracking, interpreting, and predicting performance," in *Proc. of the IEEE Power and Energy Society General Meeting*, Jul. 22-26, 2012, pp. 1-7.

[25] Carl L. Benner and B. Don Russell, "Investigation of incipient conditions leading to failure of distribution system apparatus," in *Proc. of the Power Systems Conference and Exposition*, Oct. 10-13, 2004, pp. 703708.

[26] Carl L. Benner and B. Don Russell, "Distribution incipient faults and abnormal events: case studies from recorded field data," *in Proc. of 57th Annual Conference on Protective Relay Engineers*, Apr. 1-1, 2004, pp. 86-90.

[27] Karthick Muthu-Manivannan, Carl L. Benner, Peng Xu and B. Don Russell, "Arcing event detection," U.S. Patent No. 7,865,321, Jan. 2011.

[28] Mirrasoul J. Mousavi, John J. McGowan, James Stoupis and Vaibhav D. Donde, "Apparatus and method for adaptive fault detection in MV distribution circuits," U.S. Patent No. 8,390,302, Mar. 2013.

[29] Olivier Poisson, Pascal Rioual and Michel Meunier, "Detection and measurement of power quality disturbances using wavelet transform," *IEEE Trans. Power Del.*, vol. 15, no. 3, pp. 1039-1044, Jul. 2000.

[30] C. Benner, K. Butler-Purry and B. Russell, "Distribution fault anticipator," EPRI, Palo Alto, CA, Rep. 1001879, Dec. 2001.

[31] R. Torquato, Q. Shi, W. Xu, and W. Freitas, "A Monte Carlo simulation platform for studying low voltage residential networks," *IEEE Trans. Smart Grid*, vol.5, no.6, pp.2766-2776, Nov. 2014.

[32] S. Sriram, S. Nitin, K. M. M. Prabhu and M. J. Bastiaans, "Signal denoising techniques for partial discharge measurements," *IEEE Trans. Dielectr. Electr. Insul.*, vol. 12, no. 6, pp. 1182-1191, Dec. 2005.

[33] H. Zhang, T. R. Blackburn, B. T. Phung and D. Sen, "A novel wavelet transform technique for on-line partial discharge measurements part 1: WT de-noising algorithm," *IEEE Trans. Dielectr. Electr. Insul.*, vol. 14, no. 1, pp. 3-14, Feb. 2007.

[34] B. Yazici and S. Yolacan, "A comparison of various tests of normality," *Journal of Statistical Computation and Simulation*, vol. 77, no. 2, pp. 175-183, Feb. 2007.

[35] P. J. Brockwell and R. A. Davis, *Introduction to Time Series and Forecasting*. New York, USA: Springer Science & Business Media, 2006, pp. 28-30.

[36] B. W. Silverman, *Density Estimation for Statistics and Data Analysis*. London, UK: CRC press, 1986, pp. 9-48.

[37] C. M. Bishop, *Pattern Recognition and Machine Learning*. New York, USA: Springer Science & Business Media, 2006, pp. 55-56.

[38] B. C. Levy. *Principles of Signal Detection and Parameter Estimation*. New York, USA: Springer Science & Business Media, 2008, pp.16-18.

[39] IEEE Working Group on Power Quality Data Analytics. Draft report: Electric signatures of power equipment failures. [Online]. Available: http://grouper.ieee.org/groups/td/pq/data/

[40] Wilsun Xu, "Review and update of power quality measurement protocol," CEATI Report No. T034700-5119, Apr. 2004.

[41] IEEE Working Group on Power Quality Data Analytics. Download-1 day data from XLPE underground cable. [Online]. Available: http://grouper.ieee.org/groups/td/pq/data/

[42] W. Zhang, Y. Jing and X. Xiao, " Model-Based General Arcing Fault Detection in Medium Voltage Distribution System," *IEEE Trans. Power Del.*, DOI 10.1109/TPWRD.2016.2518738, Jan. 2016.

[43] W. H. Kersting, "Radial distribution test feeders," in *Proc. of Power Engineering Society Winter Meeting, 2001. IEEE*, Jan. 28-Feb. 1, 2001, pp. 908-912.

[44] Mladen Kezunovic and Yuan Liao, "A novel software implementation concept for power quality study," *IEEE Trans. Power Del.*, vol. 17, no. 2, pp. 544-549, Apr. 2002.

[45] K. Muthu-Manivannan, C. L. Benner, P. Xu and B. D. Russell, "Identification of power system events using fuzzy logic," U.S. Patent No. 8,370,285, Feb. 2013.

[46] Y. Bai and D. Wang, *Fundamentals of Fuzzy Logic Control-Fuzzy Sets, Fuzzy Rules and Defuzzifications*. Springer London, 2006, pp.23-24.

[47] R. A. Aliev and O. H. Huseynov, *Decision Theory with Imperfect Information*, World Scientific, 2014, pp.52.

[48] G. Klir and B. Yuan, *Fuzzy Sets and Fuzzy Logic*, Prentice hall New Jersey, 1995.

[49] L. X. Wang, *A Course in Fuzzy Systems.* Prentice-Hall press, USA, 1999. 1.5

Appendix A

Positive-Going Zero Crossing Point Detection and Frequency Variation Correction

When detecting disturbances using the proposed practical method, zero crossing point should be checked and frequency variation correction should be conducted. They are discussed in details below.

A.1 Positive-Going Zero Crossing Point Detection

The recommended zero-crossing point detection is explained as follows:

- Step 1: Take one cycle of the sampled waveform. If the sampling frequency is N points, this means take N points of the sample data $x(1)$, $x(2)$, ..., $x(N)$.
- Step 2: Find the sample that gives the minimum value among the N sampled values. The value should be negative. The corresponding sample number is recorded as, for example, k.

- Step 3: Check the values of $x(k+1)$, $x(k+2)$, ..., $x(N)$. The first data sample that has a positive value is the positive-going zero-crossing point.

It should be noted that if a waveform contains multiple zero-crossing points due to, for example, large harmonic distortions, the first positive-going zero-crossing point is considered as the correct point.

A.2 Frequency Variation Correction

The operating frequency of a power system normally fluctuates within a narrow range, and may not be always exactly constant at 60 Hz. This frequency variation will result in an error when two cycles of a waveform are subtracted. The error caused by frequency variation is illustrated in Figure A.1.

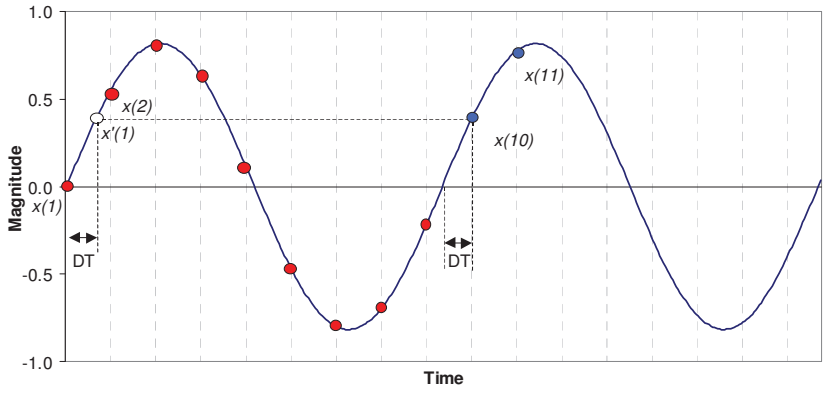

Figure A.1: Impact of frequency variation on sample locations

The waveform is sampled at a rate of approximately 9 samples per cycle ($N = 9$). If the second cycle is subtracted by the first cycle simplify according to the sample locations, we will get a differential waveform as:

$$\Delta x(k) = x(N+k) - x(k) \tag{A.1}$$

For example, if $k = 1$, the subtraction is done between $x(10)$ and $x(1)$. It can be clearly that $x(10)$ is not at the same phase as that of $x(1)$. As a result,

such a subtraction will cause errors; $\Delta x(k)$ will not be zero even if the two cycles are identical. The correct way to subtract the two cycles is:

$$\Delta x(k) = x(N+k) - x'(k) \tag{A.2}$$

where $x'(k)$ is the estimated sample value on the first cycle. The sample has the same phase angle as that of $x(N+k)$. $x'(k)$ can be estimated using linear interpolation on its two adjacent samples. In this example, the two adjacent samples are $x(1)$ and $x(2)$.

A more precise description of the above correction method and its implementation procedure are presented below. It assumes that the frequency is constant during the 5 to 10 cycles' period where the subtraction takes place. Figure A.2 shows the parameters associated with the method. The symbols and their meanings used in this figure are listed in Table A.1.

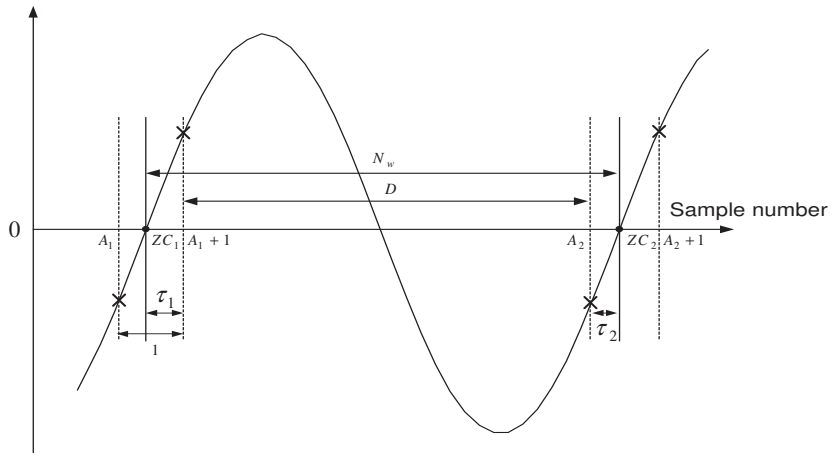

Figure A.2: Parameters for frequency variation correction

A reference cycle is the one that is used to subtract other cycles. For the example of Figure A.1, it is the first cycle. The procedure for the frequency variation correction is as follows:

1. Determine the exact zero-crossing point ZC_1 of the reference cycle. The location of ZC_1 lies between a sample with a negative value A_1 and the

Table A.1: List of symbols used in frequency variation correction

Symbol	Meaning
N	the number of samples per cycle
ZC_1	the first zero-crossing sample
ZC_2	the second zero-crossing sample
A_1	the sample closest to the ZC_1 and with a negative value
A_2	the sample closest to the ZC_2 and with a negative value
τ_1	the fraction difference between samples A_1+1 and ZC_1 $(0 \leq \tau_1 \leq 1)$
τ_2	the fraction difference between samples A_2 and ZC_2 $(0 \leq \tau_2 \leq 1)$
D	the sample difference between samples A_1+1 and A_2, $D = A_2-(A_1+1)$
N_w	the actual sample number of the reference cycle, $N_w = D+\tau_1+\tau_2$

next sample with a positive value $A_1 + 1$. These two values can be used to determine the exact ZC_1 location through linear interpolation. The result is the fraction difference between samples $A_1 + 1$ and ZC_1, which is labeled as τ_1.

2. A similar procedure can be used to find the next zero-crossing point ZC_2. The value of ZC_2 lies between sample points A_2 and $A_2 + 1$. The result is the fraction difference between samples A_2 and ZC_2.

3. The precise period of the waveform, i.e. T_w, can then be calculated from the following equation.

$$T_w = [A_2-(A_1+1)+\tau_1+\tau_2]\times\Delta T = [D+\tau_1+\tau_2]\times\Delta T = N_w\times\Delta T \quad \text{(A.3)}$$

where $\Delta T = \frac{1}{N\times 60}$. In other words, the precise frequency of the waveform is equal to $\frac{1}{T_w} = \frac{60\times N}{N_w}$. If $N_w > N$, the actual frequency is less than 60 Hz and if $N_w < N$, the actual frequency is greater than 60 Hz.

4. With the above parameters, the subtracted waveform can then be calculated. For example, if we want to compute the subtracted value for any

sample, the equation is as follows,

$$\Delta x(k) = x(k) - x'_{ref}(k) \tag{A.4}$$

where $x'_{ref}(k)$ is the value of the reference cycle that shall be used to subtract $x(k)$.

5. The first step to find $x'_{ref}(k)$ is to compute the time difference between $x(k)$ and the exact zero crossing point of the reference cycle, ZC_1, as follows,

$$T_{diff} = k - ZC_1 \tag{A.5}$$

The number of cycles separating the two instants is:

$$N_{diff} = \frac{(k - ZC_1)\Delta T}{T_w} = \frac{(k - ZC_1)}{N_w} \tag{A.6}$$

Note that N_{diff} is not an integer. Its remainder, denoted as N_R, represents the sample location where $x'_{ref}(k)$ should be calculated. N_R resides between 0 and 1. If $N_R = 0.5$, it means that $x'_{ref}(k)$ is located at the exact mid-point of the reference cycle.

6. The N_R value can then be used to find the two adjacent samples of x_{ref} that should be used to calculate $x'_{ref}(k)$. To do this, we first compute N'_R as follows,

$$N'_R = N_R \times N - \tau_1 + 1 \tag{A.7}$$

The value of N'_R will reside between two integers. These two integers are recorded as K_1 and K_2. The remainder of N'_R is recorded as τ. For example, if $N'_R = 5.34$, we have $K_1 = 5, K_2 = 6$ and $\tau = 0.34$. The value of $x'_{ref}(k)$ is computed from linear interpolation of $x_{ref}(K_1)$ and $x_{ref}(K_2)$

as shown in Figure A.3. The equation is as follows,

$$x'_{ref}(k) = x_{ref}(K_1) + \tau[x_{ref}(K_2) - x_{ref}(K_1)] \tag{A.8}$$

If $K_1 = 0$, the first point is the ZC_1 so the value of $x_{ref}(K_1) = 0$, if K_2 is the last sample of the reference cycle, the interpolation should take place between K_2 and ZC_2.

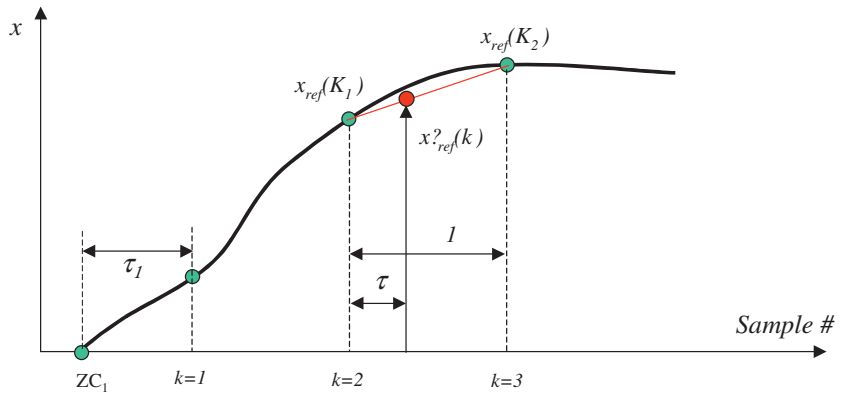

Figure A.3: Determining the value of $x'_{ref}(k)$

Appendix B

Sensitive Study and Performance Comparison Using Phase-B and Phase-C of Field Data

This appendix presents the parameter selection results and performance comparison of the proposed method with differential waveform RMS method and MAVSA method derived with Phase-B and Phase-C data.

The sensitive study on N_d, N_G, N_H are presented in Figure B.1 to Figure B.3. Based on the sensitive study results and the need to detect short-duration abnormalities, the optimal choices of these parameters are $N_d = 1$, $N_G = 10$ and $N_H = 1$. The performance comparison of Phase B and Phase C shows that the proposed method performs better than the differential waveform RMS method and MAVSA method. The results are consistent with those presented in Chapter 3.

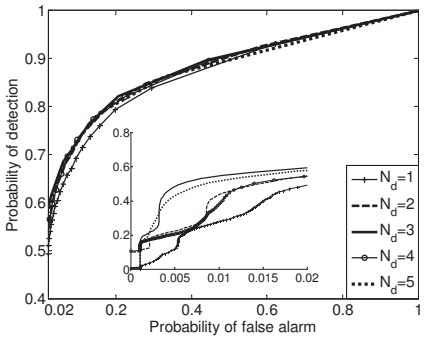

(a) Phase-B results.

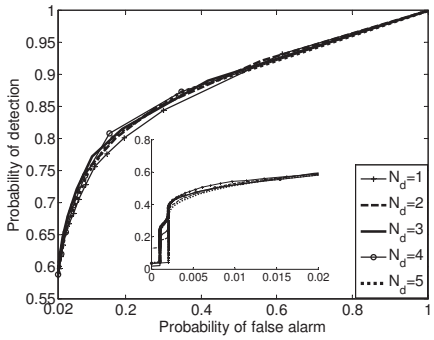

(b) Phase-C results.

Figure B.1: Detection performance for different N_d derived with Phase-B and Phase-C data.

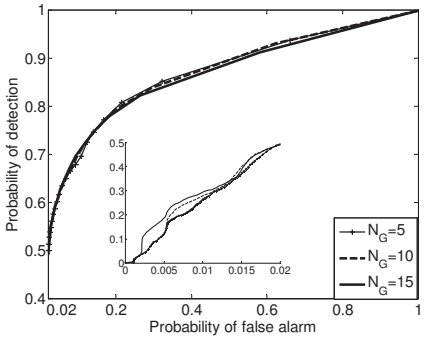

(a) Phase-B results.

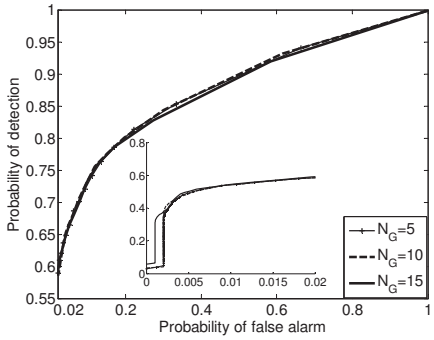

(b) Phase-C results.

Figure B.2: Detection performance for different N_G derived with Phase-B and Phase-C data.

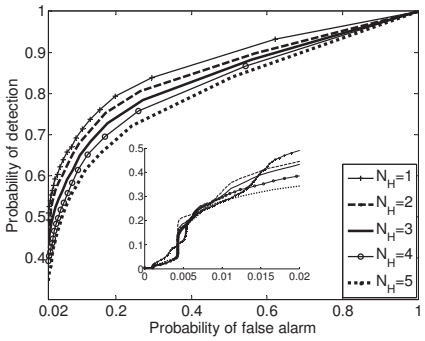

(a) Phase-B results.

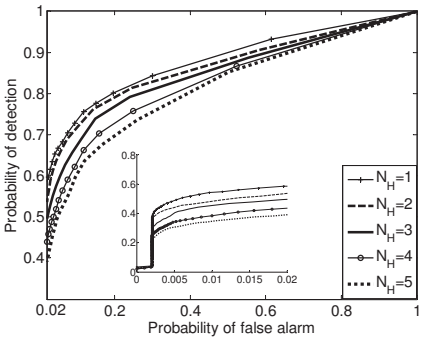

(b) Phase-C results.

Figure B.3: Detection performance for different N_H derived with Phase-B and Phase-C data.

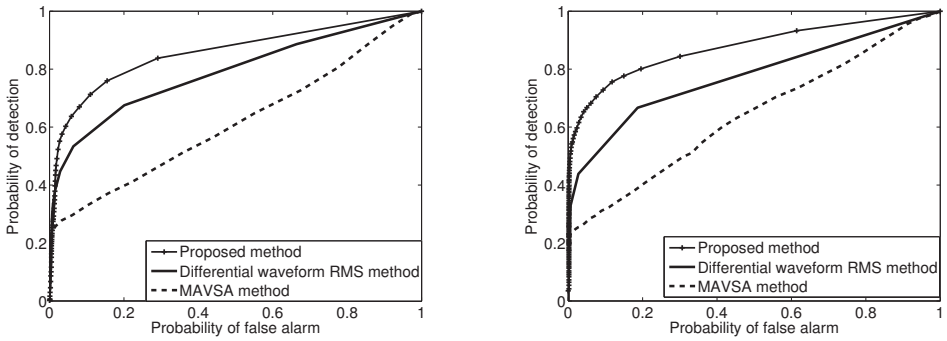

(a) Phase-B results.

(b) Phase-C results.

Figure B.4: Detection performance comparison derived with Phase-B and Phase-C data.